From Cells to Canopies: Reconstructing Vegetation Structure and its Response to Climate Change in the Middle Cenozoic of Patagonia Using Phytolith Morphology

Regan Elizabeth Dunn

A dissertation

submitted in partial fulfillment of the

requirements for the degree of

Doctor of Philosophy

University of Washington

2013

Reading Committee.

Caroline A.E. Strömberg, Chair

Roger del Moral

Gregory P. Wilson

Program Authorized to Offer Degree:

Department of Biology

University of Washington

Abstract

From cells to canopies: Reconstructing vegetation structure and its response to climate change in the middle Cenozoic of Patagonia using phytolith morphology

Regan Elizabeth Dunn

Chair of the Supervisory Committee:

Associate Professor Caroline A.E. Strömberg

Department of Biology

Reconstructing ancient ecosystems to answer outstanding questions in paleoecology requires a multidisciplinary approach. This dissertation research integrates geochronology and conventional phytolith analysis, with a new method for reconstructing vegetation structure (Leaf Area Index) based on the response of epidermal cell (and phytolith) morphology to light. First, a highly resolved U-Pb dated chronology provides precise ages for a densely sampled phytolith record of fossil samples ranging from 42-18 Ma. Second, two experiments were conducted to examine epidermal cell response to varying levels of light. Based on the observation that epidermal cells of shade leaves are more undulated and larger than those of sun leaves in several species of dicots, the first

study tested whether this same pattern occurs in grasses in a controlled growth experiment. We found that grass cell undulation is not affected by light, but their morphology changes in other ways. For instance, grass cells tend to have longer epidermal cells in the shade treatments, though this pattern was not found in all species.

The second experiment tests the same idea, but uses a different approach. Instead, it tests whether non-grass phytolith assemblages extracted from soils vary with canopy complexity, measured as Leaf Area Index (LAI). We hypothesized that phytoliths from soils under denser canopies will be larger and more undulated than phytoliths growing in more open habitats. Soils were collected across an LAI gradient in Costa Rican habitats and phytoliths were extracted and measured. We found that mean phytolith undulation and mean phytolith area are highly correlated to LAI. We constructed a robust model to predict LAI and using this model, we reconstructed LAI (rLAI) from 44 fossil phytolith assemblages from Patagonia. The synthesis of this research is a long deep-time record of environmental change that relates to climate in southern South America spanning from 50-11 Ma. The results reveal new details about the environmental history of temperature and rainfall, and how LAI responds to these variables. Additionally, the rLAI record may track Patagonian habitat response to major climatic changes associated with the opening of the Drake Passage.

TABLE OF CONTENTS

LIST OF FIGURES

LIST OF TABLES

Acknowledgements

I wish to express my sincere gratitude to Caroline Strömberg for her enthusiasm, intellect, support, and understanding throughout the course of this dissertation research. Caroline is an excellent mentor who shows unfailing dedication to her students, she is a friend and an excellent role model, and I thank her for ensuring my growth as an independent scientist. Additionally, I would like to thank my committee members Roger del Moral, Gregory Wilson and Jody Bourgeois for their insights, experience and advice.

I would like to thank the many people who contributed to projects presented in this dissertation including Matt Kohn, Mark Schmitz, and Jim Crowley at Boise State University, and Guillermo Ré at the University of Buenos Aires. Fredy Carlini and Martín Ciancio were critical in all aspects of this project involving field and museum work in Argentina. I am indebted to them for their hospitality, generosity and knowledge gained. Also, thank you to Javier Gelfo, Guiomar Vucetich and Melanie Conner who all aided in fieldwork.

For work in Costa Rica, I would like to thank the Organization for Tropical Studies and the Area de Conservación de Guanacaste. In particular, I would like to thank Deedra McClearn, Gilberto Murillo, Ronald Vargas, Ernesto Alvarado, Rafael Ramirez and Roger Blanco Segura. All of these individuals helped greatly to insure that I was properly permitted, oriented in the field and that soil samples were properly imported.

I would also like to thank the staff in the UW Biology department including the Greenhouse staff, especially Doug Ewing and Jeanette Milne, David Giblin in the UW Herbarium, Karen Bergeron, Rodney Dungo, Judy Farrow, Alex Chung, Dave Hurley, Marissa Heringer and Eileen O'Conner who made everything about working at UW easy.

Also, I'd like to thank Ron Eng at the Burke Museum and the entire PaleoLunch Group for stimulating paleoconversations each week, including Estella Leopold, Chris Sidor, Liz Nesbitt, Greg Wilson, Patricia Kramer and Caroline Strömberg.

I am indebted to the several undergraduate researchers that worked dutifully on my dissertation projects including Darshi Banan, Terry Huang, Ross Fletcher Hill, Tony Jijina, Josh Johnson, Aidan Loeser and especially Thien-Y Le. As well as others in the Strömberg Lab including Julie Nicol, Marijana Surkovic, Avery Shinneman, Sutapa Dutta, and Stephanie Zaborac-Reed.

Also to my fellow graduate students, Elisha Harris, Brandon Peecook, Adam Huttenlocker, Lauren DeBay, Dave Demar, Matt McElroy, Pat Lu-Irving, Emily Palm, Daril Vilhena, Susan Waters all offered enlightening discussion about research topics.

Funding for this project was provided by the National Science Foundation DDIG (DEB-1110354), and from grants: EAR-0819910, EAR-0819842, EAR-0819837, the Ben Hall Plant Systematics Fellowship, the Melinda Denton Writing Fellowship, the Giles Award, UW Graduate School, the Evolving Earth Foundation, Geological Society of America Graduate Student Award, and Burke Museum travel funds.

Lastly, I wish also thank my parents, Bruce and Heather Dunn for their unwavering support and to Rick Madden for his awe-inspiring and never ending source of ideas, his passion for discovery and his love.

CHAPTER I. Introduction

Vegetation is the context in which terrestrial biotas exist and evolve. Knowing the structure of vegetative communities through space and time is key for understanding how modern biotic communities have evolved to their present form and how climate has influenced and continues to influence these communities (Kay and Madden, 1997; Kay et al., 1997; Cramer et al., 2001). The preservation of phytoliths, microscopic silica bodies in the tissues of many types of plants including palms, dicots, conifers, ferns, mosses and most notably, grasses, provides a unique record of vegetation different from all other types of paleobotanical evidence such as pollen and macrofloras.

This is so because, first, phytoliths provide a record of local, more or less *in situ* vegetation (that may include upland soil source areas). In contrast, pollen is often transported long distances and disproportionately represents wind-pollinated species (Erdtman, 1943) and macrofloras preferentially represent material transported by rivers and riparian species (Burnham, 1989). Second, the evolution of grasses and grass-dominated habitats in deep time (pre-Quaternary records) is best-studied using phytoliths. Grasses are abundant accumulators of silica and the grass subfamilies produce diagnostic types of phytoliths that can be used to reconstruct grass phylogenies and the degree of habitat openness (Strömberg and Feranec, 2004; Prasad et al., 2005; Bremond et al., 2005; Prasad et al., 2011). Third, because phytoliths are often preserved with vertebrate remains, direct associations between animal diet and habitat (vegetation type) can be made, and hypotheses about co-evolutionary relationships can be tested directly (Strömberg, 2006; Strömberg et al., 2013). Fourth, in geologic sequences containing stacked paleosols, phytoliths can be preserved at nearly every stratigraphic interval, and

thus can provide a high-resolution record of vegetation change over long time intervals (Strömberg, 2004; Strömberg et al., 2007; Strömberg et al., 2013).

For those studying the evolution of grasses, grasslands and their associated faunas, understanding habitat type and canopy structure is especially important. Until phytolith records became available in deep time paleoecology (Strömberg, 2004; Strömberg, 2005; Strömberg, 2006; Strömberg, 2011; Strömberg et al., 2007; Strömberg et al., 2013), paleontologists relied on the Cenozoic trend towards progressively higher cheek teeth (hypsodonty, where tooth crowns evolve to extend far above the gum line) to infer the expansion of grassland biomes. Implicit with this scenario, is the idea that hypsodonty confers a selective advantage where abrasive materials in the diet produce excess tooth wear. Since modern grass-eating herbivores have hypsodont cheek teeth and since grasses are fibrous and rich in abrasive silica phytoliths, the expansion of grass-dominated habitats from the late early Miocene onwards has long been suspected to be an example of plant-animal co-evolution and grasses as a driver in the evolution of hypsodonty (Osborn, 1921; Stirton, 1947; Simpson and others, 1951; Webb, 1977; Jacobs et al., 1999).

The idea that hypsodonty evolved in response to the expansion of open grass-dominated systems has recently been tested through comparison of phytolith records in North America and Asia. In these regions, several groups of ungulate taxa demonstrate hypsodonty by 18 and 11 Ma, respectively. The phytolith record confirms that open-habitat grasslands were present by at least 24 Ma in North America and in Asia by 20 Ma (Strömberg, 2004; Strömberg, 2005; Strömberg, 2006; Strömberg et al., 2007). In both cases the occurrence of open-habitat grasslands predates the evolution of hypsodonty by

several million years and confirms that hypsodonty evolved in the context of grasslands in the Northern Hemisphere at least.

Building on this history of work that has used phytoliths to decipher plant-mammal co-evolution, this dissertation sets out reconstruct a history of vegetation in Southern South America (Patagonia) where endemic ungulate herbivores achieved hypsodonty as early as 38 Ma, 20 million years earlier than on any other continent (Madden et al., 2010). In 2009, Drs. Caroline Strömberg, Matt Kohn (Boise State University), Richard Madden (University of Chicago), and Alfredo Carlini (Museo de La Plata) and I set out to test the "early grassland hypothesis" for the evolution of precocious hypsodonty at South America's most continuous and faunally complete stratigraphic section, an area known as Gran Barranca (S45°42', W68°44'), the "Great Cliff" in the Chubut Province of Argentina. This work centered on outcrops of the Sarmiento Formation, which span from ~42–18 Ma. The interval of time preserved at Gran Barranca spans several climatic events including the Middle Eocene Climatic Optimum (41.5 Ma), the Eocene-Oligocene Transition (33.9 Ma), the Late Oligocene Warming (~24 Ma) and the beginning of the Middle Miocene Climatic Optimum around 18 Ma.

The specific aims of this dissertation were to 1) develop a highly precise age model for the strata at Gran Barranca; and 2) reconstruct vegetation structure using phytoliths to test the "open habitat hypothesis" as an alternative to the "early grassland hypothesis" for the evolution of hypsodonty, and to track how climate change influenced vegetation through the middle Cenozoic.

To establish precise ages of important climatic and biotic events at Gran Barranca, an improved age model was needed. In Chapter 2, entitled *A New Chronology*

for Middle Eocene–Early Miocene South American Land Mammal Ages, I detail the development of such a model for strata at Gran Barranca based on nine new ID-TIMS U/Pb radioisotopic ages from single zircon crystals extracted from volcanic tuffs. The nine new ages were used to calibrate the existing magnetostratigraphy at Gran Barranca (Ré et al., 2010) to the global polarity timescale of Pälike et al. (2006) (Pälike et al., 2006). The new ages at Gran Barranca provide a regional framework to correlate and date other middle Cenozoic South American Land Mammal Ages (SALMAs) based on biostratigraphy. I used the new age model to assign precise ages to our collection of phytolith samples throughout the entire section (Dunn et al., 2013; Strömberg et al., 2013). The newly constructed age model for the Sarmiento Formation at Gran Barranca is among the most precise and highly resolved of any section for the middle Cenozoic in the Southern Hemisphere. This combined with the occurrence of at least 74 faunal levels assignable to six distinctive SALMAs, and well-preserved phytoliths, makes Gran Barranca the ideal location to study biotic change from the Eocene to the Miocene in South America.

To test the "early grassland hypothesis", Dr. Strömberg and I analyzed 50+ samples using traditional phytolith analysis from samples collected at Gran Barranca (Strömberg et al., 2013). We found that grasses occurred in low abundances between 42–18 Ma, with very low abundances during the Eocene (< 6% of the total phytolith counts). In the late Oligocene and early Miocene samples, grasses never exceed 25% of any assemblage. Grass-dominated habitats should typically have relative abundances of at least 50% grass phytolith abundances, given their prolific production in grasses (Hodson et al., 2005). Hence, we interpreted the environments as closed forest habitats dominated

by palms and other woody taxa. Although they occurred only in low abundances, open-habitat grasses persisted from the middle Eocene onwards. The presence of moisture loving plants such as bamboos and palms, and in some cases, gingers lead us to the interpretation that the ancient ecosystems of Gran Barranca represented mostly warm, humid forests with open areas for grass colonization on forest edges or near water ways. Based on the general sparsity of open-habitat grass phytoliths, we rejected the early grassland hypothesis for the evolution of hypsodonty in South America, and instead suggested that hypsodonty evolved for other reasons such as dietary abrasives in other silica rich plants such as palms, or the presence of extrinsic abrasives resulting from dust and/or volcanic ash adhering to leaf surfaces (Strömberg et al., 2013).

Our interpretation of "closed forest" habitats for Gran Barranca is based on traditional phytolith quantification techniques that depend on the occurrence of open-habitat grasses to reconstruct openness. However, there are circumstances where open habitats lack grasses. For instance, extant dry shrublands have low abundances of grass phytoliths (Bremond et al., 2004) and in some open deciduous forests, understory grasses are unable to geminate due to shading from leaf litter (Sydes and Grime, 1981). Also, disturbance from ash falls >20 cm in depth can preferentially damage understory and herbaceous plant communities in fields, shrubland and forests communities (Eggler, 1948; Clarkson, 1990; del Moral and Grishin, 1999). Hence, we needed a different method to determine habitat openness, a taxon-independent method based on phytolith morphology.

Chapters 3 and 4 both address the question: How can habitat openness be reconstructed in the fossil record using phytolith morphology? To construct a

morphology-based proxy for habitat openness a phenotypically plastic trait that varies with an environmental variable corresponding to habitat openness is needed; and such trait must be expressed in plant cells that produce phytoliths. Light interception by plants varies tremendously with vegetation structure and the amount of light filtering through a canopy is exponentially dependent on the amount (total surface area) of leaves in the canopy (Waring, 1983). Specifically, plants in open habitats receive more direct solar radiation than plants in shaded forested environments. Therefore amount of solar radiation is a physical variable that can be used to track habitat openness. The shape and size of epidermal cells on leaf surfaces is determined by the amount of irradiance received by a leaf during development. This pattern was first detected in studies comparing leaf epidermal morphology in sun and shade leaves (Anheisser, 1900) and has been further investigated in the field and in controlled growth experiments in eudicotyledonous taxa such as ivy (Watson, 1942), oaks (Kurschner, 1997) and tobacco (Thomas et al., 2003), but not in monocotyledons such as grasses. Epidermal cells of both grasses and non-grasses are targets for silica deposition hence they meet the criteria needed for the development of a morphologically based proxy for habitat structure.

In Chapter 3, *Light Environment and Cell Morphology in Grasses*, I investigate differences in cell morphology across a light gradient in a greenhouse experiment to test whether the same phenotypic plasticity observed in eudicotyledons also occurs in grass epidermal cells. The study involved growing grasses under different light quantities to determine the effect of irradiance (light exposure) on epidermal cell size and cell shape (undulation of the cell wall). I hypothesized that plants grown in shade would have larger and more undulated epidermal cells, as observed in eudicotyledons. I grew five species of

grasses under four different light regimes (20, 60, 100 and 120% light) in the UW Botany Greenhouse. With the help of seven undergraduate research assistants, I measured size and undulation in over 12,000 grass epidermal cells. Discussion of the results includes a dialog about the applicability of grass cell morphology as a potential indicator of ancient light environment.

In Chapter 4, entitled *Major habitat change in Patagonia pre-dates Eocene-Oligocene Transition: A record of Leaf Area Index based on a new proxy from phytoliths*, I present a new method to reconstruct Leaf Area Index (LAI), a measure of habitat complexity and openness based on morphological variation in non-grass leaf epidermis (dicotyledons, non-herbaceous monocotyledons and potentially ferns). The method is based on a calibration study of modern soil phytolith assemblages collected in Costa Rican habitats where a robust relationship between mean phytolith undulation and area with LAI was found. The calibration study allowed for the construction of a model to predict LAI in the fossil record. Using the statistical model, I present a record of reconstructed LAI for the middle Cenozoic of Patagonia from 44 stratigraphic levels ranging from 49–11 Ma from Gran Barranca and surrounding areas.

The reconstructed LAI values add a previously unknown, spatial component to vegetation reconstructions previously unknown and this record is the first of its kind for any paleolandscape reconstruction. I then compare LAI values to records of global climate to determine the timing and nature of Cenozoic habitat change in Patagonia, and to records of hypsodonty to test alternative hypotheses for the evolution of this mammalian trait, including the "open-habitat hypothesis".

LITERATURE CITED:

Anheisser, R., 1900, Über die aruncoide Blattspreite: Flora 87, p. 64–94.

Bremond, L., Alexandre, A., Hély, C., and Guiot, J., 2005, A phytolith index as a proxy of tree cover density in tropical areas: calibration with Leaf Area Index along a forest--savanna transect in southeastern Cameroon: Global and Planetary Change, v. 45, no. 4, p. 277–293.

Bremond, L., Alexandre, A., Véla, E., and Guiot, J., 2004, Advantages and disadvantages of phytolith analysis for the reconstruction of Mediterranean vegetation: an assessment based on modern phytolith, pollen and botanical data (Luberon, France): Review of Palaeobotany and Palynology, v. 129, no. 4, p. 213–228.

Burnham, R.J., 1989, Relationships between standing vegetation and leaf litter in a paratropical forest: Implications for paleobotany: Review of Palaeobotany and Palynology, v. 58, no. 1, p. 5–32.

Clarkson, B.D., 1990, A review of vegetation development following recent (< 450 years) volcanic disturbance in North Island, New Zealand: New Zealand journal of ecology, v. 14, no. 1954, p. 59–71.

Cramer, W., Bondeau, A., Woodward, F.I., Prentice, I.C., Betts, R.A., Brovkin, V., Cox, P.M., Fisher, V., Foley, J.A., Friend, A.D., Kucharik, C., Lomas, M.R., Ramankutty, N., Sitch, S., et al., 2001, Global response of terrestrial ecosystem structure and function to CO 2 and climate change: results from six dynamic global vegetation models: Global Change Biology, v. 7, no. 4, p. 357–373.

Dunn, R.E., Madden, R.H., Kohn, M.J., Schmitz, M.D., Strömberg, C.A.E., Carlini, A.A., Ré, G.H., and Crowley, J., 2013, A new chronology for middle Eocene--early Miocene South American Land Mammal Ages: Geological Society of America Bulletin, v. 125, no. 3-4, p. 539–555.

Eggler, W. a., 1948, Plant Communities in the Vicinity of the Volcano El Paricutin, Mexico, After Two and A Half Years of Eruption: Ecology, v. 29, no. 4, p. 415.

Erdtman, G., 1943, An introduction to pollen analysis: Waltham, Mass., the Chronica Botanica Co.; London, WIW Dawson and Sons, Ltd.

Hodson, M.J., White, P.J., Mead, a, and Broadley, M.R., 2005, Phylogenetic variation in the silicon composition of plants.: Annals of botany, v. 96, no. 6, p. 1027–46.

Jacobs, B.F., Kingston, J.D., and Jacobs, L.L., 1999, The Origin of Grass-Dominated Ecosystems Source: Annals of the Missouri Botanical Garden, v. 86, no. 2, p. 590–643.

Kay, R.F., and Madden, R.H., 1997, Mammals and rainfall: paleoecology of the middle Miocene at La Venta (Colombia, South America).: Journal of human evolution, v. 32, no. 2-3, p. 161–199.

Kay, R.F., Madden, R.H., Van Schaik, C., and Higdon, D., 1997, Primate species richness is determined by plant productivity: implications for conservation: Proceedings of the National Academy of Sciences of the United States of America, v. 94, no. 24, p. 13023–7.

Kürschner, W.M., 1997, The anatomical diversity of recent and fossil leaves of the durmast oak (*Quercus petraea* Lieblein / *Q. pseudocastanea* Goeppert) - implications for their use as biosensors of palaeoatmospheric CO_2 levels: Review of Palaeobotany and Palynology, v. 96, p. 1–30.

Madden, R.H., Kay, R.F., and Guiomar, M., 2010, Gran Barranca: A 23-million-year record of middle Cenozoic faunal evolution in Patagonia: The Paleontology of Gran Barranca: Evolution and Environmental Change through the Middle Cenozoic of Patagonia, p. 423–439.

Del Moral, R., and Grishin, S.Y., 1999, Volcanic Disturbances and Ecosystem Recovery, *in* Walker, L.R. ed., Ecosystems in Disturbed Ground, Elsevier, p. 137–155.

Osborn, H.F., 1921, The age of mammals in Europe, Asia and North America: The Macmillan Co.

Pälike, H., Norris, R.D., Herrle, J.O., Wilson, P. a, Coxall, H.K., Lear, C.H., Shackleton, N.J., Tripati, A.K., and Wade, B.S., 2006, The heartbeat of the Oligocene climate system: Science, v. 314, no. 5807, p. 1894–1898.

Prasad, V., Strömberg, C.A.E., Leache, A.D., Samant, B., Patnaik, R., Tang, L., Mohabey, D.M., Ge, S., and Sahni, A., 2011, Late Cretaceous origin of the rice tribe provides evidence for early diversification in Poaceae: Nature communications, v. 2, p. 480.

Prasad, V., Strömberg, C.A.E., Alimohammadian, H., and Sahni, A., 2005, Dinosaur coprolites and the early evolution of grasses and grazers: Science, v. 310, no. 5751, p. 1177–1180.

Ré, G.H., Geuna, S.E., and Vilas, J.F., 2010, Paleomagnetism and magnetostratigraphy of Sarmiento Formation (Eocene-Miocene) at Gran Barranca, Chubut, Argentina: The Paleontology of Gran Barranca: Evolution and Environmental Change through the Middle Cenozoic of Patagonia, p. 32–45.

Simpson, G.G., 1951, Horses. The story of the horse family in the modern world and through sixty million years of history: New York: Oxford University Press Inc.

Stirton, R.A., 1947, Observations on evolutionary rates in hypsodonty: Evolution, v. 1, no. 1/2, p. 32–41.

Strömberg, C.A.E., 2005, Decoupled taxonomic radiation and ecological expansion of open-habitat grasses in the Cenozoic of North America: Proceedings of the National Academy of Sciences, v. 102, no. 34, p. 11980–11984.

Strömberg, C.A.E., 2011, Evolution of Grasses and Grassland Ecosystems: Annual Review of Earth and Planetary Sciences, v. 39, no. 1, p. 517–544.

Strömberg, C.A.E., 2006, Evolution of hypsodonty in equids: testing a hypothesis of adaptation: Paleobiology, v. 32, no. 2, p. 236–258.

Strömberg, C.A.E., 2004, Using phytolith assemblages to reconstruct the origin and spread of grass-dominated habitats in the great plains of North America during the late Eocene to early Miocene: Palaeogeography, Palaeoclimatology, Palaeoecology, v. 207, no. 3, p. 239–275.

Strömberg, C.A.E., Dunn, R.E., Madden, R.H., Kohn, M.J., and Carlini, A.A., 2013, Decoupling the spread of grasslands from the evolution of grazer-type herbivores in South America: Nature communications, v. 4, p. 1478.

Strömberg, C.A.E., and Feranec, R.S., 2004, The evolution of grass-dominated ecosystems during the late Cenozoic: Annual Review of Earth and Planetary Sciences, v. 207, p. 199–201.

Strömberg, C.A.E., Werdelin, L., Friis, E.M., and Saraç, G., 2007, The spread of grass-dominated habitats in Turkey and surrounding areas during the Cenozoic: phytolith evidence: Palaeogeography, Palaeoclimatology, Palaeoecology, v. 250, no. 1, p. 18–49.

Sydes, C., and Grime, J., 1981, Effects of tree leaf litter on herbaceous vegetation in deciduous woodland: II. An experimental investigation: The Journal of Ecology, v. 69, no. 1, p. 249–262.

Thomas, P.W., Woodward, F.I., and Quick, W.P., 2003, Systemic irradiance signalling in tobacco: New Phytologist, v. 161, p. 193 –198.

Waring, R., 1983, Estimating forest growth and efficiency in relation to canopy leaf area: Advances in Ecological Research, v. 13, p. 327–354.

Watson, R.W., 1942, the Effect of Cuticular Hardening on the Form of Epidermal Cells: New Phytologist, v. 41, no. 4, p. 223–229.

Webb, S.D., 1977, A history of savanna vertebrates in the New World. Part I: North America: Annual Review of Ecology and Systematics, v. 8, p. 355–380.

CHAPTER II: A new chronology for middle Eocene–early Miocene South American Land Mammal Ages[1]

ABSTRACT

Cenozoic South American Land Mammal Ages (SALMAs) have historically been correlated to the geologic time scale using $^{40}Ar/^{39}Ar$ dating and magnetostratigraphy. At Gran Barranca (68.7˚W, 45.7˚S)—one of South America's key areas for constraining SALMAs—existing radioisotopic ages have uncertainties of up to 4 Myr. To better constrain the ages of mammalian assemblages we employed high precision (± <40 kyr) U-Pb dating using single zircon crystals. We dated 9 tuffs from the Sarmiento Formation containing middle Eocene–early Miocene faunas (Barrancan, Mustersan, Tinguiririca n, Deseadan, Colhuehuapian and "Pinturan").

The new dates span from 39.861 ± 0.037 Ma to 19.041 ± 0.027 Ma. The La Cancha Tuff, occurring within the Tinguiririca n faunal level yielded an age of 33.581 ± 0.015 Ma, confirming that the Vera Member contains the only fossiliferous geologic section encompassing the Eocene–Oligocene Transition in the Southern Hemisphere. The pre-Deseadan fauna, La Cantera is ≤30.77 Ma, the age of the Colhuehuapian is expanded to 21.1–20.1 Ma, and the Pinturan may be as old as ~19 Ma.

The new U-Pb dates confirm that atmospheric temperatures and vegetation remained constant across the EOT in Patagonia and that hypsodonty occurred in South American ungulates much earlier than on any other continent. Additionally, refinement of the SALMA boundaries will eventually provide the context necessary to compare faunal

[1] This article was first published in the GSA Bulletin: Dunn, R.E., Madden, R.H., Kohn, M.J., Schmitz, M.D., Strömberg, C.A.E., Carlini, A.A., Ré, G.H., and Crowley, J., 2013, A new chronology for middle Eocene--early Miocene South American Land Mammal Ages: Geological Society of America Bulletin, v. 125, no. 3-4, p. 539–555.

transitions across continents, although currently too much data are missing to allow such comparisons. Finally, the new ages provide a high-resolution age model from which hypotheses about rates of environmental and evolutionary change at Gran Barranca can be tested.

INTRODUCTION

South America was an island continent for most of the middle Cenozoic from about 40 Ma when it lost its former connection to Antarctica, to 9-7 Ma when the first waif immigrants arrived from North America (Woodburne, 2010; Campbell et al., 2001; 2010; Verzi & Montalvo, 2008) and ~3 Ma when the Panamanian Land Bridge formed and wholesale faunal exchange occurred (Marshall et al., 1983). As a result, endemic faunas of South America including the meridiungulates (e.g., notoungulates, litopterns, astrapotheres, pyrotheres), metatherians (marsupials) and xenarthrans (armadillos and sloths) evolved and radiated largely in geographic isolation. The extinct endemic mammalian faunas from South America, particularly in Patagonia, have been extensively studied for over a century and have pivotally influenced the evolutionary thinking of many paleontologists and biologists (Darwin, 1859; Ameghino, 1906; Patterson and Pascual, 1968; Simpson, 1980).

Although the notoungulates are taxonomically unrelated to ungulates of North America and Europe, they convergently evolved similar dental and post-cranial morphologies, but at different times. A striking pattern in the evolution of the notoungulates is the early and progressive lengthening of tooth crowns, known as hypsodonty, at a time long before ungulates elsewhere (Jacobs et al., 1999). While

several North American ungulate lineages (e.g., the equids and camelids) evolved hypsodonty by ~18 Ma (Janis et al., 2002), South American ungulates show increases in tooth crown height beginning much earlier, ~38 Ma (Madden et al., 2010). Hypsodonty has long been assumed to be an adaptation to the opening of habitats and the spread of grassland biomes and has been used to infer the timing of such habitat change across continents (Jacobs et al., 1999; Strömberg, 2011). Therefore South America, specifically Patagonia, has been hypothesized as the cradle of grassland evolution (Stebbins, 1981; Jacobs et al., 1999; Zucol et al., 2010), although recent paleobotanical work has challenged this notion (Strömberg and Stidham, 2001; Barreda and Palazzesi, 2007; Strömberg et al., 2010; review in Strömberg, 2011).

Gran Barranca, the "great cliff" in central Patagonia, Chubut, Argentina, preserves the most complete and continuous record of middle Cenozoic terrestrial climatic and biotic evolution in South America and likely the entire Southern Hemisphere. Spanning ~42–18.5 Ma, the Sarmiento Formation at Gran Barranca preserves over 80 faunal levels encompassing assemblages from six successive South American Land Mammal Ages (SALMAs; Madden et al., 2010). From oldest to youngest the SALMAs represented at Gran Barranca are: the Barrancan, Mustersan, Tinguiririca n, Deseadan, Colhuehuapian and Pinturan. A faunal assemblage intermediate between Tinguiririca n and Deseadan is also preserved. The faunal sequence at Gran Barranca, documents the progressive and episodic increase in tooth crown heights among many lineages of notoungulates, and it preserves an extraordinary record of vegetation in the form of phytoliths (Mazzoni, 1979; Zucol et al., 2007; 2010; Sanchez et al., 2010; Strömberg et al., 2010). Additionally, the Sarmiento Formation provides a distal record

of volcanism along the Andean Arc beginning in the middle Eocene (Ardolino et al., 1999).

Gran Barranca is the only location in South America that contains six land mammal ages in superposition and it is the type locality for the several of the SALMAs, including the Barrancan, Mustersan and Colhuehuapian. Therefore, Gran Barranca is widely considered to be the most important sequence for mammalian biostratigraphy in all of South America (Madden et al., 2010).

Much stratigraphic and geochronologic work has recently been compiled for Gran Barranca (Ré et al., 2010a; 2010b; Madden et al., 2010; Bellosi, 2010a; 2010b). The geochronologic framework is based on magnetostratigraphy, calibrated by ten $^{40}Ar/^{39}Ar$ radioisotopic dates (Ré et al., 2010b). Due to the fine-grained texture of ashes from Gran Barranca, sanidine separates were not recovered. Therefore, Ré et al. (2010b) used step-heating age spectrum methods on bulk plagioclase and bulk glass separations, laser fusion methods for bulk plagioclase samples, and plateau and integrated ages for basalts. In some cases, their methods yielded large age discrepancies. For example, Ré et al. (2010b) report 0.33 Ma to 4 million year age differences between glass and plagioclase separates from the same samples (see Figs. 4–6). The authors attributed the age discrepancies between the bulk samples to argon loss from glass minerals and xenocrystic contamination due to sediment reworking. To address the problem, they calculated arithmetic mean ages using different combinations of preferred results from the glass plateau, plagioclase laser fusion mean ages and the plagioclase plateau ages (see Table 4.1 in Ré et al. 2010b). Error ranges for the arithmetic mean calculations were not

reported. For on-going high-resolution studies of paleoclimate and its effect on vegetation and mammalian evolution at Gran Barranca, a more precise geochronology is needed.

The aim of the current work is to refine the geochronology of Gran Barranca using high precision U-Pb geochronology of single zircon crystals. Zircon is ideal for this study as the crystals are abundant in the distal tuffs at Gran Barranca, and they can be dated individually allowing for better control over reworking. For simple volcanic populations, chemical abrasion isotope dilution thermal ionization mass spectrometry (CA-TIMS) techniques can produce ages with uncertainties of less than 0.1% even for relatively young volcanic tuffs (Schmitz and Bowring, 2001). In the current study, we present U-Pb ages obtained from new collections of four tuffs previously dated by $^{40}Ar/^{39}Ar$ (Simpson's Y, Rosado, Kay, and Big Mammal) and six new tuffs, not previously dated (Bed 10, La Cancha, La Cantera, Carbon, and CHW01-24.5).

In combination with existing magnetostratigraphy, our new geochronology provides a highly resolved age model for ongoing paleoecological studies in the Gran Barranca section. Additionally, the new dates (a) provide clarification on the ages of the six members of the Sarmiento Formation at Gran Barranca and the duration of hiatuses in the section, (b) highlight areas of the section spanning the Eocene-Oligocene Transition (EOT), (c) confirm the age of the important, transitional "pre-Deseadan" La Cantera fauna, and (d) provide age constraints for the middle Cenozoic SALMAs that can be applied more broadly across the continent.

SALMAs

While regions of Patagonia preserve a rich record of fossil vertebrates, the exposures and fossil localities are often distant from one another, and they lack the geologic context to be placed in a regional stratigraphic framework. Historically, fossil sites were assigned a rough age and stratigraphic position based on the content and evolutionary stage of the fossil mammal assemblages (Ameghino, 1906).

Florentino Ameghino first described the South American faunas of the middle Cenozoic and placed them into an evolutionary sequence (Ameghino 1897; 1901; 1906), relying heavily on superpositional relationships of fossils found at Gran Barranca. Later, Simpson (1933; 1940) officially distinguished the names of the unique mammalian assemblages based on geographic and geologic criteria. These names form the basis of the middle Cenozoic South American Land Mammal Ages (SALMAs) used broadly today.

While SALMAs are considered merely informal biochronologic units, they have proven useful in temporal correlation in South America (Kraglievich, 1934, 1930; Stirton, 1953; Hoffstetter, 1969; Villarroel, 1974). Consequently, efforts have been made to constrain the ages of the SALMAs by applying chronostratigraphic techniques (magnetostratigraphy and radioisotopic dating) to particular fossil localities (Madden et al., 1997). Flynn and Swisher (1995) present a correlated geochronology for the Cenozoic South American Land Mammal Ages using the geomagnetic timescale of Berggren et al. (1995). Their correlation is based on a compilation of the magnetostratigraphy, $^{40}K/^{40}Ar$, $^{40}Ar/^{39}Ar$, and fission track geochronology available at that time from multiple fossil localities.

Since 1995, refinements in several of the SALMA ages have been made. For instance Flynn et al. (2003) refined age estimates of the Tinguiririan fauna in the Chilean Andes to ~31.5 Ma. Deseadan faunas have also been dated at Salla, Bolivia (29.4 to 25.65 Ma; Kay et al, 1998) and Moquegua, Peru (26.25 ± 0.10 Ma; Shockey et al., 2009). $^{40}Ar/^{39}Ar$ radioisotope dating and magnetostratigraphic correlation at Gran Barranca, however, provide the most recent and major refinements to the geochronology of these SALMAs (Ré et al., 2010a; 2010b; Madden et al, 2010).

Ré et al. (2010a; 2010b) correlated the SALMA durations to the GPTS (Geopolarity Timescale) of Gradstein et al. (2004). Here, we suggest refinements in the ages of the SALMAs at Gran Barranca using the magnetostratigraphic sequence of Ré et al. (2010b), but calibrated using new, more precise and accurate $^{238}U/^{206}Pb$ isotopic dates. We correlate the new age model for Gran Barranca to the astronomically age-calibrated magnetic polarity record of Ocean Drilling Program (ODP) Leg 199, Site 1218 (equatorial Pacific) of Pälike et al. (2006, see their supplementary data) herein referred to as Pälike06. Site 1218 contains a well-constrained record of calcareous nanoplankton and magnetostratigraphy that has resulted in a highly resolved age model for the late Eocene through the early Miocene. For comparison purposes, we show the magnetic timescales of Gradstein et al. (2004) and Cande and Kent (1992) in addition to the Pälike et al. (2006), but age durations for the rock units and corresponding SALMAs presented here are based on correlation to the Pälike06.

The Sarmiento Formation

Gran Barranca exposes fine-grained, distally deposited volcaniclastic rocks and stretches for 7 km along the southern shore of Lake Colhue-Huapi in Chubut Province, Argentina (S45º42'49", W68º44'16", Fig.1). Strata are mapped as the superposed Koluel Kaike and Sarmiento formations. The Sarmiento Formation is an entirely terrestrial unit that was deposited in the San Jorge Basin between 43 and 18.5 Ma (Kay et al., 1999; Ré et al., 2010a; 2010b). It measures 320 meters in total thickness (Bellosi, 2010a) and contains mostly pyroclastic material, both primary and secondarily reworked through fluvial and pedogenic processes (Spaletti and Mazzoni, 1979). The Sarmiento Formation represents a distal record of Plinian style volcanic eruptions from the Andean volcanic arc in central Patagonia (Mazzoni, 1985).

The Sarmiento Formation consists of six members: in ascending order they are the Gran Barranca, Rosado, Lower Puesto Almendra, Vera, Upper Puesto Almendra and the Colhue-Huapi (Fig. 2.2). The members are primarily composed of fine-grained tuffaceous siltstones, mudstones and fine-grained sandstones. Individual horizons likely represent single or sequences of paleosols of various stages of development as rooting and other forms of bioturbation are evident (Bellosi, 2010a; 2010b; 2010c; 2010d). Within the Upper Puesto Almendra Member are lenticular basalt flows occurring in Profiles A, H, I and N (Fig. 2.2a).

Notable compositional and evolutionary differences between superposed mammalian faunal assemblages along with the presence of distinct and more or less continuous erosional surfaces indicate that several hiatuses occurred during deposition of the Sarmiento Formation (Windhausen, 1924; Simpson, 1940; Feruglio, 1949; Spalletti and Mazzoni, 1979; Legarrata and Uliana, 1994). These hiatuses may have resulted from

tectonic uplift and/or local deformation (Simpson, 1940) or changes in base level and accommodation space relating to sea-level fluctuations (Leguarreta and Uliana, 1994). Based on field observations at Gran Barranca, 10 discontinuities (numbered 1–10 from bottom to top, see Fig. 2.2) have been identified (Bellosi, 2010a). The discontinuities are characterized by degree of erosion and include: Type A) pronounced erosive unconformities; Type B) paraconformities with moderate to slight erosive surfaces; and Type C) non-erosive unconformities consisting of stacked paleosols. Type A discontinuities mark distinctive contacts between the members including Discontinuities 5 and 6, which represent deep erosional episodes before the deposition of the Vera and Upper Puesto Almendra members respectively. Discontinuity 10 is also a Type A erosive episode between the deposition of the Upper Puesto Almendra and the Colhue-Huapi members. Type B discontinuities occur at the lower contacts of the Simpson's Y tuff, the Rosado Member, and Bed 10 tuff (Discontinuities 1, 2 and 4 respectively), the irregular surface at the base of the lenticular basalt flows in the Upper Puesto Almendra (Discontinuity 7), the eroded surface at the top of the basalt flows which includes deposits of coarse-grained conglomerates containing basalt clasts (Discontinuity 8), and the slightly irregular base of the Upper Channel Series of the Upper Puesto Almendra Member (Discontinuity 9). Type C discontinuities occur at the top of the Gran Barranca Member in Profiles A, H and N and within a calcrete horizon at the top of the Rosado Member within Profiles J and M (Discontinuity 3). Using the geochronology of Ré et al. (2010b), Bellosi (2010a) estimated temporal gaps at the discontinuities to range between "negligible" to as long as 3.48 million years in duration.

Previous Geochronologic Studies at Gran Barranca

Four $^{40}K/^{40}Ar$ radioisotopic ages for basalt flows exposed in the Upper Puesto Almendra member of the Gran Barranca section range from 28.8 ± 0.9 to 24.3 ± 0.5 Ma, and broadly correlate with magmatic activity at Scarritt Pocket in the Meseta de Canquel ~100 km north of Gran Barranca (Marshall et al., 1986). Four $^{40}Ar/^{39}Ar$ ages for the same basalts range from 28.87 ± 0.13 Ma to 26.34 ± 0.32 Ma (Ré et al., 2010b) and were interpreted as separate flows during a hiatus implicated by Discontinuity 7 (Fig. 2.2).

Kay et al. (1999) presented a geochronology for the Gran Barranca section based on an early paleomagnetic section that was calibrated by a laser fusion $^{40}Ar/^{39}Ar$ date for plagioclase from the Mazzoni Tuff (MZ-7) of 36.01 ± 0.67 Ma. This key study confirmed that the Casamayoran SALMA was at least 18-20 million years younger than previously assumed. More recently, Ré et al. (2010b) presented ten $^{40}Ar/^{39}Ar$ radioisotopic dates from glass and plagioclase, calibrated using a Fish Canyon Tuff age standard of 28.27 Ma (according to Kwon et al., 2002). Their dates range in age from 41.27 to 18.5 Ma and include a revised age of the Mazzoni Tuff of 39.08 Ma. They present a chronostratigraphy based on the new dates correlated to a 6-profile composite magnetostratigraphy (Ré et al., 2010a), which constrains durations of the deposition of different members and of their corresponding SALMA (Madden et al., 2010).

RESULTS: THE TUFFS AND THEIR U-PB AGES

Tuff samples (~5 kg each) were collected from all members of the Sarmiento Formation at Gran Barranca (Fig. 2.1) along well-established measured sections where previous paleomagnetic and $^{40}Ar/^{39}Ar$ dating efforts were concentrated (Bellosi, 2010a;

Kay et al., 1999; Ré et al., 2010a; 2010b). Geographic coordinates for the tuff samples are listed in Table A1.1 in Appendix 1. Concordant U-Pb dates (considering decay constant errors) were obtained from 96 individually analyzed zircon grains from the 9 dated samples (Table 2.1) using chemical abrasion isotope dilution thermal ionization mass spectrometry (Mattinson, 2005; Davydov et al., 2010; full analytical methods, data and images of sample locations and zircon separates may be found in Appendix 1), and are illustrated as concordia diagrams in Figure 3. Five samples yielded majority clusters of equivalent single zircon $^{206}Pb/^{238}U$ dates, which we interpret as the igneous crystallization age of the zircons and the eruption and deposition age of the tuff. Dates that are older than the majority cluster at 95% confidence are interpreted as basement-derived xenocrysts or antecrysts from an earlier magmatic episode, and are ignored. By contrast five samples (including two samples of the Cantera Tuff) yielded arrays of non-equivalent analyses presumably resulting from mixed populations of volcanic and detrital zircon grains. In these cases we conservatively interpret the maximum depositional age of each tuff layer from the youngest grain(s) of the sample.

Gran Barranca Member

The Simpson's Y Tuff is the principal marker horizon in the Gran Barranca Member. It is 4–5 meters thick, very light gray, and massive. The basal contact is sharp, slightly undulating and erosive forming the Discontinuity 1 surface (Bellosi, 2010a). It entombs Barrancan faunas and occurs about 40 meters above the lowest Barrancan faunal level, 37 meters above the VRS tuff (dated via $^{40}Ar/^{39}Ar$ on plagioclase at 41.7±0.4 Ma; Ré et al., 2010b), and 7 meters below the highest Barrancan level (see Appendix 1 for a

list of fossil occurrences by member). From a sample collected at the base of the Simpson's Y tuff at Profile MMZ (Fig. A1.1, Appendix 1), a large population of elongate prismatic zircon crystals was recovered (Fig. A1.2, Appendix 1). Excluding 2 older grains, 7 zircons indicate a depositional age of 39.861 ± 0.037 Ma, (Fig. 2.3).

Rosado Member

The Rosado Tuff occurs approximately 4 meters above the base of the Rosado Member, within a zone of Mustersan faunas distributed throughout the member. The tuff is light gray and massive, measuring 1–2 meters in thickness. Our sample was collected just west of the Profile J axis, along an old road cut (Fig. A1.1, Appendix 1). The tuff sample yielded an array of non-equivalent zircon grains including three Mesozoic xenocrysts and eight grains ranging from 38.59 to 38.00 Ma (Fig. 2.3). A robust magmatic age for the Rosado Tuff cannot be calculated, however the maximum age of tuff deposition is estimated at ≤ 38.03 Ma from the weighted mean of the youngest two crystals. Ré et al. (2010b) calculated a tuff age of 38.66 Ma for the Rosado Tuff based on the mean of two glass plateau ages and one plagioclase laser fusion age.

Lower Puesto Almendra Member

The Bed 10 Tuff occurs about 25 meters above the base of the Lower Puesto Almendra Member, whose basal conglomerate hosts Mustersan fossils. Bed 10 forms a prominent marker horizon along Profiles A–H with a uniform thickness of around 4 meters. It consists of a poorly sorted basal conglomerate (0.5-m thick), a massive unit (2-m thick), capped by 1.5 meters of bioturbated tuff (Fig. A1.1, Appendix 1). The base is

slightly erosive and represents Discontinuity 4. Our sample was collected 1 meter from the base of the tuff in the massive zone. Excluding two clearly older xenocrysts, eight grains define a weighted mean date and interpreted eruptive age of 37.000 ± 0.014 Ma (Fig. 2.3).

The Kay Tuff occurs 0-3 meters above the Bed 10 Tuff and is similar in thickness and appearance, however it is less continuously exposed (Profiles A–J). Our sample was collected from the massive zone of the tuff, 1 meter from the base (Fig. A1.1, Appendix 1). The analysis of 14 zircons resulted in an array of non-equivalent dates ranging from 40.56 to 36.72 Ma (Fig 3). A maximum age of tuff deposition is estimated at ≤ 36.73 Ma based on the weighted mean of the youngest two crystals. The U-Pb age for the Kay Tuff is slightly younger but consistent with the mean $^{40}Ar/^{39}Ar$ age of 37.045 Ma (Ré et al., 2010b).

Vera Member

The La Cancha Tuff is a thin, light gray tuff (0.3 m thick) occurring within a 3 meter-thick zone containing Tinguiririca fossils, about 55 meters above the base of the Vera Member (Fig. A1.1, Appendix 1). The La Cancha Tuff occurs 1–3 meters above the Carlini Tuff which was dated by Ré et al. (2010b) at ~34 Ma. Ten zircons from the La Cancha Tuff indicate a depositional age of 33.581 ± 0.015 Ma, excluding 1 older grain (Fig. 2.3).

Upper Puesto Almendra Member

The La Cantera Tuff forms the basal stratum (Unit 3) of the Upper Puesto Almendra Member, and entombs taxa intermediate between Tinguiririca n and Deseadan type faunas. It is a massive unit, 8 meters thick consisting of pale-gray tuffaceous mudstone (Fig S1). The base of the tuff was deposited on an erosional surface (Discontinuity 6) cutting into the Bed 10 Tuff in Profile A-2 (Fig. 2.2a). Two separate samples, SGB09-093 (base of tuff) and SGB09-099 (5-m above the base), yielded similar arrays of non-equivalent dates ranging from 61.8 to 30.7 Ma. We interpret the weighted mean of the two youngest grains as the maximum age of tuff deposition near 30.77 Ma.

The Carbon Tuff occurs about 4 meters above the base of the Upper Puesto Almendra Member in Profile MMZ, and 1.5 meters above major unconformities associated with basalt pebbles and Deseadan faunas (Discontinuity 8). The tuff is pale-gray, massive and ranges from 2–4 meters in thickness (Fig S1). A maximum age of 23.13 Ma is inferred from the youngest zircon in an array of 8 non-equivalent ages (Fig. 2.3).

Colhue-Huapi Member

The Big Mammal Tuff occurs ~6 meters above the base of the Colhue-Huapi Member, within a zone of Colhuehuapian faunas that extends from 2 to 30 meters above the member base. The tuff is pale gray, massive and has a poorly sorted basal conglomerate that forms an erosive contact (Fig S1). Five zircon crystals indicate a depositional age of 20.890 ± 0.033 Ma, excluding 5 older grains (Fig. 2.3). This age is over 1 million years older than the $^{40}Ar/^{39}Ar$ mean age of 19.75 Ma presented by Ré et al. (2010b).

The CHW01-24.5 Tuff occurs ~51 meters above the base of the member, and 8 meters below a 3-meter thick zone of "Pinturan" faunas. The tuff is 8 meters above the MMZ24.5 Tuff dated as 19.295 Ma by Ré et al. (2010b). It is a pale-gray, massive unit, around 4-m thick. Five zircons indicate a depositional age of 19.041 ± 0.027 Ma, excluding two slightly older grains (Fig. 2.3). The U-Pb age is younger than the Ar/Ar age of the MMZ 24.5 Tuff, which occurs 8 below our sample, consistent with stratigraphic positioning.

The Monkey Tuff, 22 meters from the base of the Colhue-Huapi section, was dated by Ré et al. (2010b) as 19.81 Ma (Fig. 2.6). We made no attempt to date this level, but considering sedimentation rates of ~16 m/Myr calculated using the U-Pb ages for Big Mammal Tuff and the CHW01-24.5 Tuff, the Ar/Ar date for the Monkey Tuff is consistent with what would be expected at this stratigraphic level.

DISCUSSION

Gran Barranca Section-Comparison of $^{206}Pb/^{238}U$ to $^{40}Ar/^{39}Ar$ Dates

Our new accurate, high-precision (<0.1%) dates from the Gran Barranca section generally agree with published arithmetic mean ages of the combined bulk plagioclase and bulk glass $^{40}Ar/^{39}Ar$ ages of Ré et al. (2010b). Of the re-dated tuffs (Simpson's Y, Rosado, Kay and Big Mammal Tuff), our results differed from the $^{40}Ar/^{39}Ar$ calculated means by 0.011 Ma for the Simpson's Y Tuff, 0.63 Ma for the Rosado Tuff, 0.315 Ma for the Kay Tuff, and 1.14 Ma for the Big Mammal Tuff. However, the greater precision of the U-Pb ages dramatically increases our confidence in magnetostratigraphic correlation.

Paleomagnetic Correlation: Ages of the Members and Durations of Hiatuses

Through correlation of the magnetostratigraphic section to Pälike et al (2006), we propose the following maximum and minimum durations of deposition for the six members and durations of the major discontinuities (see also Table 2.2). Except for the Big Mammal Tuff, our dated tuffs and magnetic signals correlate with Pälike06. The rarity of reversed magnetic intervals in the upper Gran Barranca, Rosado and Lower Puesto Almendra members causes ambiguities in the durations of deposition and hiatuses, as discussed for each member below.

Gran Barranca Member

Based on our dates and the new magnetic correlation, we estimate that the Gran Barranca Member spans minimally from 41.7 (age of VRS Tuff) to >38.45 Ma (top of C18n.1n), or maximally from 42.11 (base of C19r) to ~38.16 Ma (bottom of C17n.3n). These ranges more or less agree with the previous estimate of Ré et al (2010b) of 41.6–38.7 Ma. The minimum base age is constrained by the $^{40}Ar/^{39}Ar$ mean age of 41.7 ± 0.38 Ma for the VRS Tuff (Ré et al, 2010b). If the VRS Tuff is in C19r, then, assuming there are no discontinuities below DS1, the normal polarity zone just under DS1 would correlate to C19n (Fig. 2.4). The age of Simpson's Y Tuff indicates that the normal polarity zone above DS1 is C18n.2n, so DS1 could represent removal of reversed polarity rocks corresponding to C18r which is ~1.2 Myr long. The normal polarity zone at the top of the Gran Barranca Member would probably correlate to C18n.1n which is supported by the (somewhat unreliable) mean age of 39.08 Ma determined by Ré et al. (2010b) for the Mazzoni Tuff, which occurs in a reversed polarity zone which could correlate to C18n.1r.

Ages for the top of the Gran Barranca Member are maximally constrained by the age of the Rosado Tuff in the overlying Rosado Member at ≤38.03 Ma, which occurs in a normal polarity zone correlated to C17n.3n (38.16 Ma).

Rosado Member

There is a single normal polarity site for the Rosado Member at Profile M (Site MI12, Ré et al., 2010a). The Rosado Tuff age correlates to chron C17n.3n (38.159-37.956 Ma; Fig. 2.4). However, given the coarse resolution of the Ré et al. (2010a) magnetostratigraphic record for the Rosado Member, which could have potentially missed some of the short reversed intervals within C17 and the presence of discontinuities above and below the member, it is difficult to reliably estimate its duration.

Lower Puesto Almendra Member

Because the Lower Puesto Almendra is entirely normal in polarity, a lower bounding age is ambiguous. However, Bed 10 and the overlying Kay Tuff ages both correspond to chron C17n.1n (37.520-36.668 Ma; Fig. 2.4). Therefore we estimate a maximum age duration of the Lower Puesto Almendra from the top of the Rosado Tuff to the top of chron C17n.1n (~38.03–36.67 Ma). The minimum duration is defined by the base of chron C17n.1n (37.52 Ma) and the youngest zircon from the Kay Tuff (36.73 Ma).

Vera Member

The Vera Member, measuring ~90 meters in thickness, represents the thickest unit at Gran Barranca, but it was deposited in a relatively short interval. The section is uniform in composition and no major unconformities have been identified within the member. The La Cancha Tuff age (33.58 Ma) correlates to chron C13n (33.705-33.232 Ma). There are two possible interpretations of the age of the Vera when correlating to the Pälike06. Because the lowest part of the Vera is also of normal polarity, it could correlate to C15n (35.254-35.126 Ma) or to C13r.1n (34.285-34.151 Ma; Fig. 2.5). The existence of chron C13r.1 is controversial, as it has not been recorded in high-resolution records elsewhere, including the Eocene-Oligocene boundary sections in Italy (Lowrie & Lanci, 1994), or ODP Site 1220 in the equatorial Pacific (Parés & Lanci, 2004). However, Channell et al. (2003) found chron C13r.1n in cores from ODP site 1090 in the South Atlantic Ocean. Due to the presence of the C13r.1n in both the equatorial Pacific and the South Atlantic records, this chron may also occur in the paleomagnetic record for Gran Barranca. This has important implications for the duration of the Vera Member. Excluding chron C13r.1n from the correlation, the Vera Member could span from 35.254–33.232 Ma (C15n–C13n). With inclusion of C13r.1n, the Vera could span from 34.285–33.232 Ma (C13n–C13n.1n), a difference of 1 million years.

The La Cancha Tuff (33.58 Ma) is ~ 10m above the base of C13n (33.71 Ma) which would indicate accumulation rates on the order of 80 m/Myr. This is more or less consistent with the deposition of an additional 30 m of normal polarity rock above the La Cancha Tuff, and would place the top of the Vera member around 33.2 Ma, but still within C13n. Correlation of the lower normal polarity zone within the Vera Member to C13r.1n is also consistent with this sedimentation rate. In contrast, correlation to C15

would require a tenfold decrease in accumulation rates during the deposition of the reversed polarity zone of the Vera Member. Potentially, there was a hiatus in deposition during the reversal, however, no such unconformity has as yet been identified in the section. A radioisotopic date is needed at the base of the Vera to select between the two alternatives. Given our estimate for the minimum upper age of the Lower Puesto Almendra Member (36.7 Ma) and the two interpretations for the base of the Vera Member, we estimate that either 1.4 or 2.4 Myr elapsed at Discontinuity 5.

Upper Puesto Almendra Member

We estimate a total duration of the Upper Puesto Alemendra Member (UPA) from ≤30.77 to at least 22.06 Ma and perhaps as young as 21.11 Ma. This extends the upper age estimate of Ré et al. (2010b) by 2-3 Myr (30.6–24.2 Ma). The lower bound is based on the Cantera Tuff age (≤30.77 Ma; Fig. 2.5) at the base of the UPA where it occurs in Profile A-2. An upper age for the UPA is estimated by calibrating the magnetic section using the maximum U-Pb age for the Carbon Tuff (≤23.13 Ma). The Carbon Tuff has normal polarity, whereas its maximum numerical age falls within a magnetically reversed interval (chron C6C.2r). Since the numerical age is a maximum, the oldest likely age corresponds with the next youngest normal chron, C6Cn.2n (23.026-22.854 Ma, Fig. 2.6). Using this as a calibration point, assuming there are no hiatuses in deposition (at least below Disconformity 9), the top of Unit 4 would fall within chron C6Bn.2n (22.299 – 22.062 Ma). Since Unit 5 is of normal polarity, and must be older than the Big Mammal Tuff (20.89 Ma), it may correlate to any of the normal intervals occurring between chron C6Bn.2n and the top of chron C6AAn (22.299–21.114 Ma).

The Cantera Tuff at the base of this unit is of normal polarity, and correlates to chron C12n (Figs. 5 and 6). The top of chron C12n is 30.617 Ma, limiting deposition of tuffaceous strata between 30.77 and 30.617 Ma. Therefore, sedimentation below the basalts must have been of short duration, probably no more than 160 ka (Cantera Tuff age to top of chron C12n). Under this scenario, the duration of Discontinuity 7 could span from 1.44 Myr (30.617 to 29.18 Ma, the age of the oldest basalt flow), to 4.28 Myr (30.617 Ma to 26.34 Ma, age of the youngest basalt, see Fig. 2.7). Unit 4 of the UPA Member was deposited between 23.13–22.062 Ma. Therefore, Discontinuity 8, above the basalts, spans anywhere from 3.21 Myr (26.34 to 23.13 Ma), to 6.05 Myr (29.18 Ma to 23.13 Ma).

Colhue-Huapi Member

Deposition of the Colhue-Huapi Member spanned at least 1.9 Myr (≥20.89 to ≤19.04 Ma) and no more than 2.5 Myr (≤21.11 to ≥18.62 Ma). The lowermost dated tuff in the Colhue-Huapi Member, the Big Mammal Tuff (20.890 ± 0.033 Ma) is reported by Ré et al (2010b) as normal in polarity. All recent paleomagnetic timescale compilations (Pälike et al., 2006, Gradstein et al., 2004; Cande and Kent, 1992; 1995), however, indicate reversed polarity (C6An.2r) for this time. The paleomagnetic signal from the tuff collection site is considered an oblique virtual magnetic pole—a result intermediate between normal and reversed polarity. Because other paleomagnetic samples at the base of the Colhue-Huapi are reversed, we infer that the bottom of the section, including the Big Mammal Tuff, occurs in chron C6An.2r (21.114-20.652 Ma). Thus, initiation of sediment emplacement must have occurred by 21.11 Ma, but no later than 20.89 Ma. The

CHW01-24.5 Tuff occurs in an upper normal interval. Its age (19.041 ± 0.027 Ma) correlates with Chron 6n, which terminated at 18.616 Ma, suggesting that deposition of the Colhue-Huapi Member ceased sometime between 19.0 and 18.6 Ma.

Our dates extend the age of the Colhue-Huapi Member estimated by Ré et al., (2010b) slightly (0.1 to 0.7 Myr). Given our revised age for the top of the Upper Puesto Almendra Member (between 22.06 and 21.11 Ma), the hiatus indicated by Discontinuity 10, between deposition of the UPA and Colhue-Huapi members may have been negligible or as long as 1.17 Myr.

Calibration and Correlation of the Eocene-Miocene Paleontologic Record – South American Land Mammal Ages

Because Gran Barranca is the only section in South America that contains six successive SALMA associations, the ages of their occurrences at Gran Barranca in combination with known ages of other localities help constrain the age durations of these SALMAs. The following discussion considers all recent radioisotopic constraints for the SALMA durations (see also Table 2.3 and Fig. 2.7). Details about the lowest and highest mammal fossil occurrences and a list of pertinent index taxa per SALMA at Gran Barranca are described in Appendix 1.

Barrancan SALMA

The original Casamayoran SALMA proposed by Simpson (1933, 1940) was split into an older Vacan and younger Barrancan subage by Cifelli (1985) and, because their faunas are so distinct, we refer to them each as separate SALMAs. Therefore the age of

the Barrancan SALMA corresponds to the age of the Gran Barranca Member which we estimate to begin ~41.7 Ma. The highest occurrence of Barrancan faunas at Gran Barranca is 8 m above the base of Simpson's Y Tuff, and 7 m above a reversed polarity zone (site MI06, Ré et al., 2010a) that may correspond to chron C18n.2r. Therefore, the highest Barrancan fossil occurrences likely fall within C18n.1n (39.554–38.449 Ma), and above the Mazzoni Tuff, dated as 39.08 Ma (Ré et al., 2010b). Therefore, we estimate the Barrancan to span from 41.7–39.0 Ma. Barrancan fossils are known from at least three other locations in Patagonia that have not been dated (see Cifelli, 1985). Dating tuffs from these other areas may help to refine the lower and upper age limits of the Barrancan.

Mustersan SALMA

The Mustersan SALMA occurs at Gran Barranca throughout the Rosado Member and in the Lower Puesto Almendra Member, below the Bed 10 Tuff (Bond and Deschamps, 2010). Therefore, the duration of the Mustersan mammal age is equivalent to the age of the Rosado and part of the Lower Puesto Almendra. Because the Rosado stratigraphic level is all of normal polarity, the Mustersan at Gran Barranca cannot be older than the base of chron C17n.3n (38.159 Ma), but Mustersan assemblages from the Lower Puesto Almendra Member (Coley's Quarry, Simpson's #64) have not been relocated. Therefore, the highest occurrences of Mustersan faunas at Gran Barranca are uncertain, but can be no younger than 37 Ma based on the age of Bed 10. Other Mustersan localities in Patagonia have not been dated (Bond and Deschamps, 2010). In northwestern Argentina, a putative Mustersan faunal assemblage in the Geste Formation

(López, 1997; Goin et al, 1998, Pasqual, 1983; Reguero et al., 2008) is associated with detrital zircon ages between 37 and 35 Ma (DeCelles et al, 2007). Based on the oldest dated assemblages from Gran Barranca, and the youngest faunas in northwestern Argentina, the Mustersan may range from ~38.2–35 Ma, but we suggest a conservative estimate of 38.2–38.0 Ma based on the well-defined Mustersan levels at Gran Barranca.

Tinguiririca SALMA

The Tinguiririca SALMA is defined by faunas from the Chilean Andes (Wyss et al., 1990) and helps fill a long interval in the South American fossil record between late Eocene (Mustersan) and late Oligocene (Deseadan) faunas. Other Tinguiririca assemblages have also been described from northern Patagonia (e.g., Rocas Bayas, Vucetich et al., 2010a) and at Gran Barranca (Madden et al., 2010). The only assuredly Tinguiririca fauna at Gran Barranca is found within the La Cancha Tuff, here dated at 33.58 Ma. In the type area in the Chilean Andes Tinguiririca faunas are associated with tuffs with $^{40}Ar/^{39}Ar$ dates of 31.65 ± 0.32 Ma and 31.34 ± 0.17 Ma (Wyss et al., 1993; Flynn et al., 2003; Fig. 2.7). These ages imply that the Tinguiririca spans at least 33.6–31.3 Ma.

La Cantera faunas

The La Cantera Tuff in Unit 3 of the Upper Puesto Almendra Member contains a unique assemblage of taxa transitional between Tinguiririca and Deseadan faunas referred to as "pre-Deseadan" (Madden et al., 2010). The unique faunal assemblage includes one of the oldest occurrences of rodents in Argentina (Vucetich et al., 2010a),

the first appearance of large carnivorous borhyaenid marsupials, and the oldest record of Toxodontidae in South America (Madden et al., 2010). Ré et al., (2010a) could not correlate the normal polarity signal of the La Cantera tuff to a specific chron, but did constrain it to chrons C12n, C11n.2n, or C11n.1n spanning from 31.1–29.5 Ma. Despite evidence of sediment reworking, our U-Pb dates suggest a maximum age of 30.77 Ma. This date correlates to chron C12n, suggesting that the La Cantera fauna is older than the top of this magnetic zone, 30.617 Ma. Therefore, the pre-Deseadan assemblage of La Cantera is likely between 30.77–30.617 Ma.

Deseadan SALMA

Past ages estimates for the Deseadan SALMA have ranged from 37.5 Ma to 21 Ma (see Flynn and Swisher, 1995). The oldest dated fossil of Deseadan age is a *Pyrotherium* mandible from Valle Hermoso between 29.9 and 32.1 Ma (Madden and Carlini, unpublished data). The age of *Pyrotherium* at Salla ranges from 29.4–25.8 Ma (Kay et al., 1998). A recent $^{40}Ar/^{39}Ar$ date of a Deseadan site in Moquegua, Peru of 26.25 ± 0.10 Ma falls within this range (Shockey et al., 2009). The pre-Deseadan fossil mammal assemblage at La Cantera is now known to be ≤30.77 Ma. On this basis, a basal age for the Deseadan SALMA can be established at about 30 Ma.

At Gran Barranca, Deseadan mammals occur along the erosional surfaces atop the basalts. If the tops of all the basalts were weathered at the same time (i.e., a single Discontinuity 8), then the Deseadan assemblages at Gran Barranca must be younger than 26.34 Ma, the age of the youngest basalt (Ré et al., 2010b). If instead there were multiple erosional discontinuities associated with the tops of several basalt flows of different ages,

then some of the Deseadan mammals at Gran Baranca could be as old as 28.9 Ma. Both scenarios are consistent with chronologic constraints from Bolivia and Peru. Another possibility is that these fossils from the base of Unit 4, are likely ~23.0 Ma, but possibly as young as ~22.6 Ma (Fig. 2.7), which would extend the Deseadan age range considerably. The beds are not sufficiently well exposed nor the faunas of Deseadan aspect well enough preserved to select among these alternatives.

The age of the Cerro Poco Poconi Ash at Salla (24.2 ± 0.6 Ma; Kay et al., 1998) provides the youngest securely dated fossil mammal assemblage of Deseadan age with *Pyrotherium*. However, $^{40}K/^{40}Ar$ ages as young as 23.4 and 21.6 Ma have been reported from Scarritt Pocket (Marshall et al., 1986). Confirming these young occurrences of Deseadan mammals will require more accurate $^{40}Ar/^{39}Ar$ or $^{206}Pb/^{238}U$ methods. Taking all of the current information into account, we estimate a minimum age range of 29.4–24.2 Ma for the Deseadan SALMA, possibly extending from 30 to 23 Ma.

Colhuehuapian SALMA

Colhuehuapian mammal-bearing strata at Gran Barranca span a reversed polarity zone correlated to chron C6An.2r (21.114–20.652 Ma) and below the Big Mammal Tuff (20.89 Ma) nearly to the top of a normal polarity zone correlated to chron C6An.2n (20.652–20.425 Ma). Given this correlation, we estimate that the Colhuehuapian fauna occurs between about 21.0 and 20.5 Ma at Gran Barranca.

Other Colhuehuapian faunas from Argentina have not been dated (see Vucetich et al., 2010b), but a Colhuehuapian assemblage from the Abanico Formation in the Chilean Andes is dated by $^{40}Ar/^{39}Ar$ at 20.09 ± 0.27 Ma (Flynn et al., 1995). Altogether we

estimate the duration of the Colhuehuapian SALMA of ~1 million years, 21.0–20.1 Ma, slightly expanding the proposed duration of Madden et al. (2010) of 20.2–20.0 Ma.

Pinturan SALMA

The Pinturan is recognized as a distinct assemblage between Colhuehuapian and Santacrucian faunas (see Kramarz et al., 2010) and we refer to it here as a SALMA. At Gran Barranca, vertebrate faunas characteristic of Pinturan assemblages occur ~8 m above the CHW01-24.5 Tuff (19.04 Ma) within the same magnetically normal interval, C6n. Because C6n terminates at 18.616 Ma, Pinturan faunas at Gran Barranca are bracketed between 19.04 and 18.62 Ma.

In the type area of the Pinturan, in NW Santa Cruz Province, a $^{40}Ar/^{39}Ar$ age from the base of the vertebrate levels is 17.5 Ma, whereas a $^{40}Ar/^{39}Ar$ date from above the faunal levels is 16.5 Ma (Kramarz et al., 2010). Thus, the maximum duration for the "Pinturan" is 19.04 to 16.5 Ma. This interval overlaps recently published bracketing $^{40}Ar/^{39}Ar$ ages of 18.79 ± 0.11 and 17.5 ± 0.4 Ma (Croft et al, 2007) for a Santacrucian fauna from Chucal, Chile (Croft et al., 2004; 2007). These data imply a smaller maximum span for the Pinturan, from 19.04 to 17.5 Ma.

EOCENE–OLIGOCENE TRANSITION AND HYPSODONTY EVOLUTION

Previous $^{40}Ar/^{39}Ar$ age determinations for the La Cancha Tuff, a massive tuff embedded within the La Cancha faunal horizon, have been problematic. Despite an arithmetic mean age of 33.995 Ma for the bulk glass and plagioclase samples (Ré et al., 2010b), high uncertainties in the age determination of this tuff limited interpretation of

the significance of the Vera Member with respect to the Eocene–Oligocene climatic transition (EOT). Pälike et al. (2006) present an interpolated age for the Eocene–Oligocene boundary of 33.79 Ma based on magnetostratigraphy of C13r(.14) which predates the Oi-1 excursion. The new precise La Cancha Tuff age of 33.581±0.015 clearly post-dates the EOT. Magnetostratigraphy of lower strata, however, imply initial deposition no later than ~34.1 Ma, well before the EOT. These data confirm that the Vera Member preserves the only documented terrestrial fossil-bearing EOT section in the Southern Hemisphere.

The new date for the La Cancha fauna of Gran Barranca verifies its occurrences as the oldest Tinguiririan fauna. Additionally, the new date adds temporal certainty to work showing that no major atmospheric temperature change occurred across the EOT at Gran Barranca based on oxygen isotopes in tooth enamel (Kohn et al., 2004). In agreement with the apparently stable atmospheric temperatures at Gran Barranca surrounding the EOT, a record of phytoliths shows that vegetation apparently did not change significantly during this episode of major global climatic change (Strömberg et al, 2010). These patterns suggest that the terrestrial, local climatic and biological consequences of the global climate changes at the EOT were complex and that substantially more work is needed to fully understand this climatic event.

The improved age correlation also provides firm dates for the successive changes in faunal hypsodonty in Patagonia, corroborating the longstanding notion that hypsodonty evolved at least 20 Myr earlier in Southern South America than elsewhere (Stebbins, 1981; Jacobs et al., 1999; Madden et al., 2010). The earliest faunas with several hypsodont members occurred at 38 Ma at Gran Barranca, whereas faunas with equivalent

prevalence of hypsodonty did not appear in North America, Western Eurasia, and Africa until after 18 Ma (Damuth and Janis, 2011; Jacobs et al., 1999; Janis et al., 2002; Jernvall and Fortelius et al., 2002; Strömberg, 2011). Hypsodonty evolution in mammalian herbivores was therefore not a uniform, direct response to global, climatic events; rather, the factors influencing it have to be sought on a continent-by-continent basis (Strömberg, 2011). South America remains a strikingly unique case, but one that is vital for fully understanding the controls of adaptation and convergent evolution.

DID FAUNAL EVOLUTION TRACK CLIMATE CHANGE?

The new ages may help advance research on climate change as a catalyst for mammalian evolution. This concept "…has pervaded the paleontological literature for nearly two centuries…" (Alroy et al., 2000), but remains hotly debated (e.g., Vrba, 1995; Webb and Opdyke, 1995; Prothero, 1999; Alroy et al., 2000; Barnosky, 2001; Woodburne et al., 2009; Figueirido et al., 2011), and different studies have reached nearly diametrically opposed conclusions. Most studies emphasize North American faunal change, because the faunal record and chronologies are generally more complete. Many of the major faunal turnover events in North America, however, were influenced strongly by immigration from other continents, and were not necessarily the direct result of climate change (but see Woodburne et al., 2009). Consequently, isolating the effects of climate change remains problematic. Because South America was largely (albeit not completely) isolated from other continents through much of the Cenozoic, it may provide a clearer perspective on this subject. Since land mammal ages by their construction are based on evolutionary trends in indigenous taxa, there is no reason that a biochron from

one continent should correlate to another. However, if global climate change drives patterns of evolutionary faunal change, then we might expect some correspondence between SALMA boundaries and either climate trends or mammal-based biostratigraphies on other continents, such as the North American Land Mammal Ages (NALMA) or the European Land Mammal Ages (ELMA). That is, direct intra- or inter-continental correlation could provide an important test of the climate-faunal evolution hypothesis. Here, we discuss the potential of such comparisons, but also remaining problems.

It is important to remember that the mammalian groups that made up the mid-Cenozoic faunas of South America, most of which are completely extinct, were only distantly related to the clades (e.g., Perissodactyla, Artiodactyla) that inhabited other parts of the world. Two notable exceptions include caviomorph rodents, which arrived by the middle Eocene (Antoine et al., 2011), and platyrrhine primates, present by the late Oligocene (Hoffstetter, 1969; MacFadden et al., 1985). This major phylogenetic disjunct limits direct, taxonomic comparisons among continents. Nevertheless, evaluation of the timing of turnover events across continents, signaled by respective Land Mammal Age boundaries may be just as useful. Specifically, it provides a means to explore whether extinction, origination, or immigration events in mammalian faunas were globally synchronized during certain periods of the Cenozoic.

The largest obstacle to comparing in detail the SALMAs to other Land Mammal Ages relates to the persisting uncertainty in the exact dates for SALMA boundaries, illustrated in Fig. 2.7. Often, the uncertainty, that is, the gap between well-dated faunal levels, is on the order of several million years. This makes it impossible in many cases to

reject (or support) a hypothesis of coincidence. To illustrate this point further, we provide a comparison between SALMAs as temporally revised herein and the seven NALMAs that occur during the mid-Cenozoic (Woodburne, 2004; Albright et al., 2008) (Fig. 2.7). The comparison shows that, in most cases, because of missing data from South America, we simply cannot say whether the boundaries occur simultaneously. For example, whereas the lower and upper boundary of the Tinguiririca falls within the Orellan and Whitneyan, respectively (Fig. 2.7), more research might show that the Tinguiririca boundaries do coincide with the base of the Orellan and the top of the Whitneyan. In other cases boundaries appear coincident at our current state of knowledge, such as the start of the Pinturan and Hemingfordian (Fig. 2.7), but because of a gap in the fossil record, the Pinturan might have started a million years earlier. Conversely some turnover events are clearly disjoint between continents. The Orellan-Whitneyan boundary falls in the middle of the Tinguiririca SALMA, and the Uintan-Duschesnean boundary falls within the Barrancan.

Another problem when directly comparing Land Mammal Age boundaries on different continents is the lack of consistent criteria for defining them. Therefore, it might be necessary to take a more detailed look at faunal evolution to test inter-continental patterns. For example, a recent study used factor analysis to discover "evolutionary faunas", which only in part corresponded to traditionally defined NALMAs, and argued that global climate helped control the dynamics of these faunas (Figueirido et al., 2011). Such a detailed comparison is not yet possible in South America, but we offer one example intercomparing faunal change dynamics between North and South America. The Uintan-Duchesnean boundary occurs at ~39.74 Ma (Prothero & Swisher, 1992) and

corresponds approximately to the Simpson's Y Tuff (39.861 Ma) level at Gran Barranca, during the Barrancan land mammal age. The Duchesnean NALMA marks the first appearances of *Hyaenodon*, *Duchesneodus*, *Duchesnehippus intermedius*, *Amynodontopsis*, *Eotylopus* (Robinson et al., 2004), *Pterodon*, Leptomerycidae, and Anthracotheriinae (Robinson et al., 2004; Woodburne, 2004). Half of these first appearances are Asian or European immigrants into North America, but many others probably mark *in situ* evolution. There are no identified dispersal events in Patagonia during the Barrancan nor do faunal compositions change across the numeric age of the Uintan–Duchesnean boundary, i.e. faunal turnover in North America is countered by faunal stasis in South America.

Finally, we find no direct evidence as yet for changes to SALMAs in response to global climate change. Late Oligocene warming occurred within the Deseadan, and late Eocene cooling occurred with no obvious change to faunas during the Barrancan. On the other hand, it is possible that Tinguiririan faunas evolved in response to the EOT – a hypothesis that can be tested with fossiliferous strata of the lower Vera member that assuredly predate the EOT.

Although we find little support for the climate-faunal evolution hypothesis in South America, we reiterate that additional chronologies and paleontological investigations could provide superior datasets for testing it, either across the continent or in targeted strata such as the lower Vera member. Conversely, further chronologic and faunal analysis of Pinturan strata elsewhere in South America might elucidate processes of faunal change during a time when global climate was nearly invariant. Such studies

will require, however, accurately-dated horizons whose stratigraphic and chronologic relationship to faunally distinctive strata is clear.

CONCLUSIONS

Our U-Pb dates combined with the magnetostratigraphic section of Ré et al. (2010a) and correlation to the timescale of Pälike et al. (2006) provide a precise age model for present and future high-resolution paleoecological studies testing hypotheses about rates of ecological and/or evolutionary change in South America. Additionally, since Gran Barranca is the reference section for the middle Cenozoic SALMAs for all of South America and Western Antarctica, the dates help refine the ages of the SALMA occurrences and their durations. To this end, latitudinal differences in faunal occurrences can be studied in more detail.

The analysis of tuffs from the Sarmiento Formation at Gran Barranca yielded weighted $^{206}Pb/^{238}U$ mean ages of: 39.861 ± 0.037 Ma (Simpson's Y Tuff); 37.000 ± 0.014 Ma (Bed 10 Tuff); 33.581 ± 0.015 Ma (La Cancha Tuff); 20.890 ± 0.033 Ma (Big Mammal Tuff); and 19.041 ± 0.027 Ma (CHW01-24.5 Tuff). Maximum ages for four other tuffs were determined from the youngest 1-2 zircon ages: 38.03 Ma (Rosado Tuff); 36.73 Ma (Kay Tuff); 30.77 Ma (Cantera Tuff); and 23.13 Ma (Carbon Tuff).

These dates combined with the magnetostratigraphic correlation indicate the following maximum and minimum durations for the members of the Sarmiento Formation: Gran Barranca: 42.11–38.16 Ma and 41.7–38.45 Ma; Rosado: 38.16–37.96 Ma and 38.03–37.96 Ma; Lower Puesto Almendra: 38.03–36.73 Ma and 37.52–36.73

Ma; Vera: 35.25–33.23 and 34.15–33.58 Ma; Upper Puesto Almendra: 30.77–21.11 Ma and 30.77–22.06 Ma; Colhue-Huapi: 21.11–18.62 Ma and 20.89 to 19.04 Ma.

Because the Sarmiento Formation at Gran Barranca contains the type sections of the Barrancan, Mustersan, and Colhuehuapian SALMAs, refinement of these and the age boundaries of the Vacan, Tinguiririca, Deseadan and Pinturan SALMAs are best addressed in this succession. By compiling the new dates from Gran Barranca with other dated vertebrate assemblages in South America, we propose the following durations for the middle Cenozoic SALMAs: 41.7–39.0 Ma (Barrancan); 38.2–38.0 Ma (Mustersan); 33.6–31.3 Ma (Tinguiririca); 29.4–24.2 Ma (Deseadan); 21.0–20.1 Ma (Colhuehuapian); and 19.0–17.5 Ma (Pinturan).

The pre-Deseadan, post-Tinguiririca faunas found at the La Cantera site, Gran Barranca, are between 30.77 and 30.62 Ma. This new age constraint is significant because it shows that this fauna, distinctive from either Tinguirriica or Deseadan faunas post-dates the Tinguiriirrica and pre-dates the Deseadan. Thus, it is reasonable that the La Cantera Fauna could be proposed as its own SALMA if similar faunal assemblages where found elsewhere in Patagonia. But, to date, the La Cantera fauna is unique to Gran Barranca.

The Vera Member preserves the only known fossil-bearing, terrestrial record of the Eocene–Oligocene Transition in the southern hemisphere. The record at Gran Barranca during this interval indicates that atmospheric temperatures remained constant across the climatic event, and that vegetation, based on a record of phytoliths, did not change substantially in composition. In addition, the faunal record at Gran Barranca shows that taxonomic turnover postdates the EOT event. Finally, our dates confirm the

longstanding hypothesis that hypsodonty increases seen at Gran Barranca occur significantly earlier than on other continents.

Although precise dating of biostatigraphically important beds will eventually allow inter-continental comparisons of turnover events, we conclude that the current state of knowledge of the boundaries of SALMAs does not permit such studies except in a few cases. Work seeking to fill in the gaps in the faunal record will be necessary before such a comparison is possible.

ACKNOWLEDGMENTS

Funding for this project was provided by the National Science Foundation grant numbers EAR-0819910 to Caroline Strömberg, EAR-0819842 to Richard Madden and EAR-0819837 to Matthew Kohn; and Proyecto de Investigación en Ciencias y Técnicas 1860 of the Fondo Nacional de Ciencia y Tecnología (FONCyT). We thank Guiomar Vucetich and Martin Ciancio for field assistance during this project and Pan American Energy for field support. Also we would like to thank Michael O. Woodburne, Bradly S. Singer and 3 anonymous reviewers for their comprehensive and thorough reviews of the manuscript.

LITERATURE CITED

Albright, B.L., III, Woodburne, M.O., Fremd, T.J., Swisher, C.C.III., MacFadden, B.J., and Scott, G.R., 2008, Revised chronostratigraphy and biostratigraphy of the John Day Formation (Turtle Cove and Kimberly members), Oregon, with implications for updated calibration of the Arikareean North American Land Mammal Age: Journal of Geology, v. 116, p. 211–237.

Alroy, J., Koch, P.L., and Zachos, J.C., 2000, Global climate change and North American mammalian evolution: Paleobiology, v. 26, p. 259–288.

Amehgino, F., 1897, Mammifères crétacés de l'Argentina Deuxième contribution à la connaisasance de la faune mammalogique des couches à Pyrotherium: Boletín del Instituto Geográfico Argentina, v. 18, p. 406–521.

Ameghino, F., 1901, Notices preliminaries sur des ongulés nouveaux des terrains crétacés de Patagonie, Boletin de las Academin Nacional de Ciencias en Córdoba, v. 16, p. 349–426.

Ameghino, F., 1906, Les formations sedimentaires du Crétacé supérieur et du tertiaire de Patagonie avec un parallele entre leurs faunes mammalogiques et celles de 1'ancien continent: Anales del Museo Nacional de Buenos Aires, Série 3, v. 15, p. 1–568.

Antoine, P., Marivaux, L., Croft, D.A., Billet, G., Ganerød, M., Jaramillo, C., Martin, T., Orliac, M.J., Tejada, J., Altamirano, A.J., Duranthon, F., Fanjat, G., Rousse, S., Gismondi, R.S., 2011, Middle Eocene rodents from Peruvian Amazonia reveal the pattern and timing of caviomorph origins and biogeography: Proceedings of the Royal Society B, v. 279, p. 1319–1326.

Ardolino, A., Franchi, M., Remesal, M. and Salani, F., 1999, El volcanismo en la Patagonia extraandina, *in* Geología Argentina. Caminos, R. (ed.), Servicio Geológico Nacional Anales, v. 29, p. 579–612.

Barnosky, A.D., 2001, Distinguishing the effects of the Red Queen and Court Jester on Miocene mammal evolution in the northern Rocky Mountains: Journal of Vertebrate Paleontology, v. 21, p. 172–185.

Barreda, V., and Palazzesi, L., 2007, Patagonian vegetation turnovers during the Paleogene–early Neogene: Origin of arid-adapted floras: The Botanical Review, v. 73, p. 31–50.

Bellosi, E.S., 2010a, Physical stratigraphy of the Sarmiento Formation (Middle Eocene–Lower Miocene) at Gran Barranca, central Patagonia, *in* Madden, R.H., Carlini, A.A., Vucetich, M.G., and Kay, R.F., *eds.,* The Paleontology of Gran Barranca: Evolution and Environmental Change through the Middle Cenozoic of Patagonia: Cambridge, UK, Cambridge University Press, p. 19–31.

Bellosi, E.S., 2010b, Loessic and fluvial sedimentation in Sarmiento Formation pyroclastics, middle Cenozoic of central Patagonia, *in* Madden, R.H., Carlini, A.A., Vucetich, M.G., and Kay, R.F., *eds.,* The Paleontology of Gran Barranca: Evolution and Environmental Change through the Middle Cenozoic of Patagonia: Cambridge, UK, Cambridge University Press, p. 278–292.

Bellosi, E.S., 2010c, Paleosols of the middle Cenozoic Sarmiento Formation, central Patagonia, *in* Madden, R.H., Carlini, A.A., Vucetich, M.G., and Kay, R.F., *eds.,* The Paleontology of Gran Barranca: Evolution and Environmental Change through the Middle Cenozoic of Patagonia: Cambridge, UK, Cambridge University Press, p. 293–305.

Bellosi, E.S., 2010d, Ichnofacies analysis of the Sarmiento Formation (middle Eocene–early Miocene) at Gran Barranca, central Patagonia, *in* Madden, R.H., Carlini, A.A., Vucetich, M.G., and Kay, R.F., *eds.,* The Paleontology of Gran Barranca: Evolution and Environmental Change through the Middle Cenozoic of Patagonia: Cambridge, UK, Cambridge University Press, p. 306–316.

Berggren, W.A., Kent, D.V., Swisher, C.C., Aubry, M.-P., 1995, A revised Cenozoic geochronology and chronostratigraphy, *in* Berggren, W.A., Kent, D.V., Aubry, M.-P., and Hardenbol, J. eds., Geochronology, Time Scales and Stratigraphic Correlation: SEPM Special Publication No. 54, p. 129–212.

Bond, M., and Deschamps, C.M., 2010: The Mustersan age at Gran Barranca: A review, *in* Madden, R.H., Carlini, A.A., Vucetich, M.G., and Kay, R.F., *eds.,* The Paleontology of Gran Barranca: Evolution and Environmental Change through the Middle Cenozoic of Patagonia: Cambridge, UK, Cambridge University Press, p. 255–263.

Campbell, K. E., Heizler, M. Frailey, C.D., Romero-Pittman, L., and Prothero, D.R., 2001, Upper Cenozoic chronostratigraphy of the southwestern Amazon Basin: Geology, v. 29, p. 595–598.

Campbell, K.E., Prothero, D.R., Romero-Pittman, L., Hertel, F., and Rivera, N., 2010, Amazonian magnetostratigraphy: Dating the first pulse of the Great American Faunal Interchange, v. 29, p. 610–626.

Cande, S.C., and Kent, D.V., 1995, Revised calibration of the geomagnetic polarity timescale for the Late Cretaceous and Cenozoic: Journal of Geophysical Research, v. 100, p. 6093–6095.

Cande, S.C., and Kent, D.V., 1992, A new geomagnetic polarity time scale for the Late Cretaceous and Cenozoic: Journal of Geophysical Research, v. 97, p. 13917–13951.

Channell, J.E.T., Galeotti, S., Martin, E.E., Billups, K., Scher, H.D. and Stoner, J.S., 2003, Eocene to Miocene magnetostratigraphy, biostratigraphy, and chemostratigraphy at ODP Site 1090 (sub-Antarctic South Atlantic): GSA Bulletin, v. 11, p. 607–623.

Cifelli, R.L., 1985, Biostratigraphy of the Casamayoran, Early Eocene, of Patagonia: American Museum Novitates, v. 2820, p. 1–16.

Croft, D.A., Flynn, J.J, and Wyss, A.R., 2004, Notoungulata and Litopterna of the Early Miocene Chucal Fauna, northern Chile: Fieldiana, Geology, v. 50, p. 1–52.

Croft, D.A., Flynn, J.J, and Wyss, A.R., 2007, A new basal glyptodontid and other Xenarthra of the early Miocene Chucal Fauna, northern Chile: Journal of Vertebrate Paleontology, v. 27, p. 781–797.

Damuth, J., and Janis, C.M., 2011, On the relationship between hypsodonty and feeding ecology in ungulate mammals, and its utility in paleoecology: Biological Reviews, v. 86, p. 733–758.

Darwin, C., 1859, On the Origin of Species by Means of Natural Selection. John Murray, London.

Davydov, V.I., Crowley, J.L., Schmitz, M.D., and Poletaev, V.I., 2010, High-precision U-Pb zircon age calibration of the global Carboniferous time scale and Milankovitch-band cyclicity in the Donets Basin, eastern Ukraine: Geochemistry, Geophysics, Geosystems, v. 11, Q0AA04, doi:10.1029/2009GC002736.

DeCelles, P.G., Carrapa, B., and Gehrels, G.E., 2007, Detrital zircon U-Pb ages provide provenance and chronostratigraphic information from Eocene synorogenic deposits in northwestern Argentina: Geology, v. 35, p. 323–326.

Feruglio, E., 1949, Descripción geológica de la Patagonia, Yacimientos Petrolíferos Fiscales, v. 2., p. 1–349.

Figueirido B., Janis, C.M., Pérez-Claros, J.A., De Renzi, M., and Palmqvist, P., 2012, Cenozoic climate change influences mammalian evolutionary dynamics: Proceedings of the National Academy of Sciences, v. 109, p. 722–727.

Fleagle, J.G., Bown, T.M., Swisher, C.C., and Buckley, G., 1995, Ages of the Pinturas and Santa Cruz Formations: Actas VI Congreso Argentino de Paleontología y Bioestratigrafía, p. 129–135.

Flynn, J.J., Wyss, A.R., Croft, D.A., and Charrier, R., 2003. The Tinguiririca Fauna, Chile: biochronology, paleoecology, biogeography, and a new earliest Oligocene South American Land Mammal ‘Age’: Palaeogeography, Palaeoclimatology, Palaeoecology, v. 195, p. 229–259.

Flynn, J.J, Wyss, A.R., Charrier, R., Swisher, C.C. III, 1995, An Early Miocene anthropoid skull from the Chilean Andes: Nature, v. 373, p. 603–607.

Flynn, J.J. and Swisher, C.C. III, 1995, South American Land Mammal Ages: Correlation to Global Geochronologies, *in* Berggren, W.A. ed., Geochronology, Time Scales and Global Stratigraphic Correlation, SEPM (Society for Sedimentary Geology) Special Publication 54, p. 317–333.

Goin, F.J., Candela, A.M., Lopez, G.M., 1998, Middle Eocene marsupials from Antofagasta de la Sierra, Northwestern Argentina: Geobios, v. 31, p. 75–85.

Gradstein, F.M., J.G. Ogg and A. Smith, eds., A Geological Time Scale 2004, Cambridge University Press, Cambridge, UK, pp. 384–408.

Hoffstetter, R., 1969. Un primate de l'Oligocène inferieur sudamericain, *Branisella boliviana*, gen. et sp. nov.: Comptes Rendus de l'Académie des Sciences, Paris, sér. D, v. 269, p. 434–437.

Jacobs, B.F., Kingston, J.D., and Jacobs, L.L., 1999, The Origin of Grass-Dominated Ecosystems: Annals of the Missouri Botanical Garden, v. 86, p. 590–643.

Janis, C.M., Damuth, J., Theodor, J.M., 2002, The origins and evolution of the North American grassland biome: the story from the hoofed mammals: Palaeogeography, Palaeoclimatology, Palaeoecology, v. 177, p. 183–198.

Jernvall, J, and Fortelius, M., 2002, Common mammals drive the evolutionary increase of hypsodonty in the Neogene: Nature, v. 417, p. 538–540.

Kay, R.F., MacFadden, B.J., Madden, R.H., Sandeman, H., and Anaya, F., 1998, Revised age of the Salla Beds, Bolivia, and its bearing on the age of the Deseadan South American Land Mammal "Age": Journal of Vertebrate Paleontology, v. 18, p. 189–199.

Kay, R.F, Madden, R.H., Vucetich, M.G., Carlini, A.A., Mazzoni, M.M., Ré, G.H., Heizler, M., and Sandeman, H., 1999, Revised geochronology of the Casamayoran South American Land Mammal Age: climatic and biotic implications: Proceedings of the National Academy of Sciences, v. 96, p. 13235–13240.

Kramarz, A.G., Vucetich, M.G., Carlini, A.A., Ciancio, M.R., Abello, M.A., Deschamps, C.M., and Gelfo, J.N., 2010, A new mammal fauna at the top of the Gran Barranca sequence and its biochronological significance, *in* Madden, R.H., Carlini, A.A., Vucetich, M.G., and Kay, R.F., *eds.,* The Paleontology of Gran Barranca: Evolution and Environmental Change through the Middle Cenozoic of Patagonia: Cambridge, UK, Cambridge University Press, p. 182–192.

Kraglievich, L., 1930, La formación Friaseana del Río Frías, Río Fénix, Laguna Blanca, etc. y su fauna de mamíferos: Physis, v.10, p. 127–161.

Kraglievich, L., 1934, La antigüedad pliocena de las faunas de Monte Hermoso y Chapadmalal, deducidas de su comparación con las que le pocedieron y sucedieron: Imprenta El Siglo Ilustrado, Montevideo, pp. 1–136.

Kohn, M.J., Josef, J.A., Madden, R., Kay, R., Vucetich, G. Carlini, A.A., 2004, Climate stability across the Eocene–Oligocene transition, southern Argentina: Geology, v. 32, p. 621–624.

Kwon, J, Min, K., Bickel, P., and Renne, P.R., 2002, Statistical methods for jointly estimating decay constant of ^{40}K and the age of a dating standard: Mathematical Geology, v. 34, p. 457–474.

Legarreta, L., and Uliana, M.A., 1994, Asociaciones de fosiles y hiatos en el supracretacico-neogeno de Patagonia: una perspeciva estratigrafico-secuencial: Ameghiniana, v. 31, p. 257–281.

López, G.M., 1997, Paleogene faunal assemblages from Antofagasta de La Sierra, Catamarca province, Argentina: Palaeovertebrata, v. 26, p. 61–81.

Lowrie, W., Lanci, L., 1994, Magnetostratigraphy of the Eocene-Oligocene boundary sections in Italy: no evidence for short subchrons within chrons 12r and 13r Earth and Planetary Science Letters, v. 126, p.247–258.

MacFadden, B.J., Campbell, K.E., Cifelli, R.L, Siles, O., Johnson, N.M, Naeser, C.W., and Zeitler, P.K., 1985, Magnetic polarity stratigraphy and mammalian fauna of the Deseadan (late Oligocene–early Miocene) Salla Beds of northern Bolivia: Journal of Geology, v. 93, p. 223–250.

Madden, R.H., J. Guerrero, R.F. Kay, J.J. Flynn, C.C. Swisher III, & A.H. Walton, 1997. The Laventan Stage and Age. In Kay, R.F., R.H. Madden, R.L. Cifelli & J.J. Flynn eds., Vertebrate Paleontology in the Neotropics. Smithsonian Institution Press, Washington DC, pp. 499–519.

Madden, R.H., Kay, R.F., Vucetich, M.G., and Carlini, A.A., 2010, Gran Barranca, a twenty-three million year record of middle Cenozoic faunal evolution in Patagonia, *in* Madden, R.H., Carlini, A.A., Vucetich, M.G., and Kay, R.F., *eds.,* The Paleontology of Gran Barranca: Evolution and Environmental Change through the Middle Cenozoic of Patagonia: Cambridge, UK, Cambridge University Press, p. 423–439.

Marshall, L.G., Hoffstetter, R., and Pascual, R., 1983, Mammals and stratigraphy: Geochronology of the continental mammal-bearing Tertiary of South America: Palaeovertebrata, Mémoire Extraordinaire, p. 1–93.

Marshall, L.G., Cifelli, R.L., Drake, R.E., and Curtis, G.H., 1986, Vertebrate paleontology, geology, and geochronology of the Tapera de Lopez and Scarritt Pocket, Chubut Province, Argentina: Journal of Paleontology, v. 60, p. 920–951.

Mattinson, J.M., 2005, Zircon U-Pb chemical abrasion ("CA-TIMS") method: combined annealing and multi-step partial dissolution analysis for improved precision and accuracy of zircon ages: Chemical Geology, v. 220, p. 47–66.

Mazzoni, M.M., 1979, Contribución al conocimiento petrográfico de la Formación Sarmiento, Barranca Sur del Lago Colhué-Huapí, Provincia de Chubut: Revista de la Asociación Argentina de Mineralogía Petrología y Sedimentología, v. 10, 33–53.

Mazzoni, M.M., 1985, La Formación Sarmiento y el vulcanismo paleogeno: Revista de la Asociación Geológica Argentina, 40(1-2):60–68.

Pälike, H., Norris, R.D., Herrle, J.O., Wilson, P.A., Coxall, H.K., Lear, C.H., Shackleton, N.J., Tripati, A.K., and Wade, B.S., 2006, The heartbeat of the Oligocene climate system: Science, v. 314, p. 1894–1898.

Parés, J.M., and Lanci, L., 2004, A Middle Eocene-Early Miocene magnetic polarity stratigraphy in equatorial Pacific sediments (ODP Site 1220). *In* Channell, J.E.T., Kent, D.V., Lowrie, W. and Meert, J.G., eds. Timescales of the paleomagnetic field: Geophysical Monograph Series, v. 145, p. 131–140.

Pascual, R., 1983, Novedosos marsupiales paleógenos de la Formación Pozuelos (Grupo Pastos Grandes) de la Puna, Salta, Argentina: Ameghiniana, v. 20, p. 265–280.

Patterson, B., and Pascual, R., 1968, Evolution of the mammals on southern continents. V. The fossil mammal fauna of South America: Quarterly Review of Biology, v. 43, p. 409–451.

Prothero, D.R., 1999, Does climatic change drive mammalian evolution?: GSA Today, v. 9, p. 1–2.

Prothero, D.R., and Swisher, C.C.III, 1992, Magnetostratigraphy and geochronology of the terrestrial Eocene–Oligocene transition in North America, *in* Prothero, D.R. and Berggren, W.A., *eds.,* Eocene–Oligocene Climatic and Biotic Evolution, Princeton, Princeton University Press, p. 74–87.

Ré, G.H., Geuna, S.E., and Vilas, J.F., 2010a, Paleomagnetism and magnetostratigraphy of Sarmiento Formation (Eocene-Miocene) at Gran Barranca, Chubut, Argentina *in* Madden, R.H., Carlini, A.A., Vucetich, M.G., and Kay, R.F., *eds.,* The Paleontology of Gran Barranca: Evolution and Environmental Change through the Middle Cenozoic of Patagonia: Cambridge, UK, Cambridge University Press, p. 32–45.

Ré, G.H., Bellosi, E.S., Heizler, M., Vilas, J.F., Madden, R.H., Carlini, A.A., Kay, R.F., and Vucetich, M.G., 2010b, A geochronology for the Sarmiento Formation at Gran Barranca *in* Madden, R.H., Carlini, A.A., Vucetich, M.G., and Kay, R.F., *eds.,* The Paleontology of Gran Barranca: Evolution and Environmental Change through the Middle Cenozoic of Patagonia: Cambridge, UK, Cambridge University Press, p. 46–60.

Reguero, M.A., Croft, D.C., Lopez, G.M., Alonso, R.N., 2008: Eocene archaeohyracids (Mammalia: Notoungulata: Hegetotheria) from the Puna, nortwest Argentina: Journal of South American Earth Sciences, v. 26, p. 225–233.

Robinson, P., Gunnell, G.F., Walsh, S.L., Clyde, W.C., Storer, J.E., Stuckey, R.K., Froehlich, D.J., Ferrusquia-Villafranca, I., and McKenna, M.C., 2004, Wasatchian through Duchesnean biochronology, *in* Woodburne, M.O. *ed.* Late Cretaceous and Cenozoic Mammals of North America: Biostratigraphy and Geochronology, New York, Columbia University Press, p. 106–155.

Sánchez, M.V., González, M.G., and Genise, J.F., 2010, Phytolith analysis of Coprinisphaera, unlocking dung beetle behavior, herbivore diets and palaeoenvironments along the Middle Eocene–Early Miocene of Patagonia: Palaeogeography, Palaeoclimatology, Palaeoecology, v. 285, p. 224–236.

Schmitz, M.D., and Bowring, S.A., 2001, U-Pb zircon and titanite systematics of the Fish Canyon Tuff: an assessment of high- precision U-Pb geochronology and its application to young volcanic rocks: Science*, v.* 65, p. 2571–2587.

Shockey, B.J., Gismondi, R.S., Gans, P., Jeong, A., and Flynn, J.J., 2009, Paleontology and Geochronology of the Deseadan (late Oligocene) of Moquegua, Perú: American Museum Novitates, v. 3668, p. 1–24.

Simpson, G.G. 1940. Review of the Mammal-Bearing Tertiary of South America: Proceedings of the American Philosophical Society, v. 83, p. 649–709.

Simpson, G.G., 1933, Stratigraphic nomenclature of the early Tertiary of Central Patagonia: American Museum Novitates, v. 644, p. 1–13.

Simpson, G.G., 1980, Splendid Isolation: The Curious History of South American Mammals. Connecticut, Yale University Press, 275 p.

Spalletti, L.A., and Mazzoni, M.M., 1979, Estratigrafia de la Formacion Sarmiento en la barranca sur del Lago Colhue-Huapi, Provicia del Chubut: Asociación Geológica Argentina, Revista, 34, p. 271–281.

Stebbins, G.L., 1981, Coevolution of grasses and herbivores: Annals of the Missouri Botanical Garden, v. 68, p. 75–86.

Stirton, R.A.,1953, Vertebrate paleontology and continental stratigraphy in Colombia: Bulletin of the Geological Society of America, v. 64, p. 603–622.

Strömberg, C.A.E., 2011, Evolution of grasses and grassland ecosystems: Annual Reviews of Earth and Planetary Science, v. 39, p. 517–544.

Strömberg, C.A.E., and Stidham, T.A., 2001, Dung beetle brood balls and notoungulate diet: Journal of Vertebrate Paleontology, v. 21, p. 105A.

Strömberg, C.A.E, Dunn, R., Kohn, M., Madden, R., Carlini, A., 2010, Was the evolution of hypsodonty in South America a response to the spread of grassland vegetation?: New phytolith records from Gran Barranca, Argentina: Society of Vertebrate Paleonotology 2010 Program and Abstracts, p. 171A.

Verzi, D.H., and Montalvo, C.I., 2008, South American Cricetidae (Rodentia) and Mustelidae (Carnivora): Late Miocene faunal turnover in central Argentina and the Great American Biotic Interchange: Palaeogeography, Palaeoclimatology, Palaeoecology, v. 267, p. 284–291.

Villarroel, C., 1974, Les Mésothériinés (Notoungulata, Mammalia) du Pliocène de Bolivie; leurs rapports avec ceux d'Argentine: Annales de Paléontologie, Paris, v. 60, p. 245–286.

Vrba, E.S., 1995, On the connections between paleoclimate and evolution *in* Vrba, E.S., Denton, G.H., Partridge, T.C. and Burckle, L.H., *eds.*, Paleoclimate and evolution with emphasis on human origins: New Haven, Yale University Press, p. 24–48.

Vucetich, M.G., Vieytes, E.C., Pérez, M.E., and Carlini, A.A., 2010a, The rodents from La Cantera and the early evolution of caviomorphs In South America, *in* Madden, R.H., Carlini, A.A., Vucetich, M.G., and Kay, R.F., *eds.,* The Paleontology of Gran Barranca: Evolution and Environmental Change through the Middle Cenozoic of Patagonia: Cambridge, UK, Cambridge University Press, p. 193–205.

Vucetich, M.G., Kramarz, A.G., and Candela, A.M., 2010b, Colhuehuapian rodents from Gran Barranca and other Patagonian localities: the state of the art, *in* Madden, R.H., Carlini, A.A., Vucetich, M.G., and Kay, R.F., *eds.,* The Paleontology of Gran Barranca: Evolution and Environmental Change through the Middle Cenozoic of Patagonia: Cambridge, UK, Cambridge University Press, p. 206–219.

Webb, S.D., and Opdyke, N.D., 1995, Global climatic influence on Cenozoic land mammal faunas *in* Kennett, J., and Stanley, S., *eds.,* Effects of Past Global Change on Life: Washington D. C., National Academy Press, p. 184–208.

Windhausen, A., 1924, Líneas generales de la constitución geológica de la región situada al oeste del Golfo de San Jorge: Boletín Academia Nacional de Ciencias, v. 27, p. 167–320.

Woodburne, M.O., 2004, Global events and the North American mammalian biochronology *in* Woodburne, M.O. *ed.* Late Cretaceous and Cenozoic Mammals of North America: Biostratigraphy and Geochronology, New York, Columbia University Press, p. 315–343.

Woodburne, M.O., 2010, The Great American Biotic Interchange: Dispersals, tectonics, climate, sea level and holding pens: Journal of Mammalian Evolution, v. 17, p. 245–264.

Woodburne, M.O., Gunnell, G.F., and Stucky, R.K., 2009, Climate directly influences Eocene mammal faunal dynamics in North America: Proceedings of the National Academy of Sciences, v. 106, p. 133999–13403.

Wyss, A.R, Flynn, J.J., Norell, M.A., Swisher, C.C., Charrier, R., Novacek, M.J. and McKenna, M.C., 1993, South America's earliest rodent and recognition of a new interval of mammalian evolution: Nature, v. 365, p. 434–437.

Wyss, A.R, Norell, M.A., Flynn, J.J., Novacek, M.J., 1990, A new early Tertiary mammal fauna from central Chile: implications for Andean stratigraphy and tectonics: Journal of Vertebrate Paleontology, v. 10, p. 518–522.

Zucol, A.F., Brea, M., Bellosi, E, Carlini, A.A., and Vucetich, G., 2007, Preliminary phytolith analysis of Sarmiento Formation in the Gran Barranca (Central Patagonia, Argentina), *in* Madella, M. and Zurro, D. *eds*., Plants, People and Places. Recent Studies in Phytolith Analysis: Oxford, UK, Oxbow Books, p. 189–195.

Zucol, A. F., Brea, M., and Bellosi, E. S., 2010, Phytolith studies in Gran Barranca (central Patagonia, Argentina): the middle–late Eocene, *in* Madden, R.H., Carlini, A.A., Vucetich, M.G., and Kay, R.F., *eds.,* The Paleontology of Gran Barranca: Evolution and Environmental Change through the Middle Cenozoic of Patagonia: Cambridge, UK, Cambridge University Press, p. 317–340.

TABLE 2.1. SUMMARY OF VOLCANIC TUFF SAMPLES AND AGES

Tuff Name	Sample Number	Profile	Member	$^{206}Pb/^{238}U$ Age (Ma)*	MSWD†	probab. of fit	n
CHW01-24.5	SGB09-282	C-H West	Colhue-Huapi	19.041 ± 0.027 (0.035)	1.2	0.32	5 of 7
Big Mammal	SGB09-275	C-H West	Colhue-Huapi	20.890 ± 0.033 (0.040)	2.8	0.02	5 of 10
Carbon	RGB09-007	MMZ	U. Puesto Almendra	*≤ 23.13*			*1 of 8*
La Cantera	SGB09-093/099	A2	U. Puesto Almendra	*≤30.77*			*2 of 16*
La Cancha	SGB09-007	K	Vera	33.581 ± 0.015 (0.043)	2.1	0.03	10 of 11
Kay	RGB09-05	A	L. Puesto Almendra	*≤36.73*			*2 of 14*
Bed 10	SGB09-179	A	L. Puesto Almendra	37.000 ± 0.014 (0.046)	1.6	0.14	8 of 10
Rosado	SGB09-118	J	Rosado	*≤38.03*			*2 of 11*
Simpson's Y	SGB09-037	MMZ	Gran Barranca	39.861 ± 0.037 (0.060)	2.7	0.01	7 of 9

Notes: *All weighted mean ages with a probability of fit > 0.05 are reported with internal 2σ errors; those with a probability of fit < 0.05 are reported with the internal 2σ errors expanded by the square root of the MSWD and the Student's t multiplier for n-1 degrees of freedom (Ludwig, 2003). The second error in parentheses includes systematic uncertainties in tracer calibration (0.05%) and ^{238}U decay constant (0.106%). Maximum ages in italics are based upon the youngest grain(s) in tuff samples with abundant reworked zircon. †Mean Squared Weighted Deviation.

TABLE 2.2. SUMMARY OF MEMBER AND DISCONFORMITY MAXIMUM AND MINIMUM INTERVALS AND DURATIONS.

Formation	**Minimum Interval (Ma)**	**Maximum Interval (Ma)**
Gran Barranca	41.70 – 38.45	42.11 – 38.16
Rosado	38.03 – 38.03	38.16 – 37.96
LPA	37.52 – 36.73	38.03 – 36.67
Vera	34.15 – 33.58	35.25 – 33.23
UPA3	30.77 – 26.34	30.77 – 26.34
UPA4	23.13 – 22.30	23.13 – 22.06
UPA5	22.06 – 22.06	22.30 – 21.11
Colhue-Huapi	20.89 – 19.04	21.11 – 18.62
Disconformity	**Minimum Duration (Ma)**	**Maximum Duration (Ma)**
1 (Gran Barranca)	1.2	1.2
2 (Gran Barranca – Rosado)	0.00	0.20
3 (Rosado – LPA)	0.44	1.03
5 (LPA – Vera)	1.42	2.58
6 (Vera – UPA3)	2.46	2.96
7 (UPA3 – basalt)	1.44	4.28
8 (basalt – UPA4)	3.21	6.05
9 (UPA4 – UPA5)	0.00	0.24
10 (UPA5 – C-H)	0.00	1.17

Notes: LPA = Lower Puesto Almendra Member; UPA3, 4, 5 = units 3, 4, and 5 of the Upper Puesto Almendra Member; C-H = Colhue-Huapi Member. Disconformities 1 and 4 are viewed as representing negligible time (Ré et al., 2010). The maximum age for the Barranca Member is based on the relative durations of C19n vs. C19r and the absolute duration of C19n (Pälike et al., 2006). Ages from oldest to youngest are: 42.11 = age of base of C19r; 41.7 = age of VRS tuff; 38.45 = top of C18n.1n; 38.16 = base of C17n.3n; 37.96 = top of C17n.3n; 38.03 = maximum age of Rosado tuff; 37.52 = base of C17n.1n; 37.00 = age of Bed 10 tuff; 36.73 = maximum age of Kay tuff; 36.67 = top of C17n.1n; 35.25 = base of C15n; 34.15 = top of C13r.1n; 33.58 = age of La Cancha tuff; 33.23 = top of C13n; 30.77 = age of La Cantera tuff; 30.62 = top of C12n; 26.34 = age of youngest basalt; 23.13 = maximum age of Carbon tuff; 22.30 = base of C6Bn.2n; 22.06 = top of C6Bn.2n; 21.11 = top of C6AAn; 20.89 = age of Big Mammal tuff; 19.04 = age of CHW01-24.5 tuff; 18.62 = top of C6n; all chron ages from Pälike et al. (2006). Age of oldest basalt (needed for estimating durations of disconformities 7 and 8) = 29.18 Ma (Ré et al., 2010).

TABLE 2.3. PUBLISHED ISOTOPIC DATES FOR VERTEBRATE LOCALITIES

SALMA	Formation	Relation to fossils	Reference	Method (standard)	Age (Ma)
Mustersan	Geste	unclear	1	$^{238}U/^{206}Pb$ detrital zircons	37.3±1.5
	Geste	unclear	1	$^{238}U/^{206}Pb$ detrital zircons	35.4±0.55
Tinguiririan	Abanico	Within fossil zone	2, 3	$^{40}Ar/^{39}Ar$ (FCT 27.84 Ma)	31.65±0.32
	Abanico	Within fossil zone	2, 3	$^{40}Ar/^{39}Ar$ (FCT 27.84 Ma)	31.34±0.17
	Abanico	Below fossil zone	2, 3	$^{40}Ar/^{39}Ar$ (FCT 27.84 Ma)	31.5±1.0
	Abanico	Below fossil zone	2, 3	$^{40}Ar/^{39}Ar$ (FCT 27.84 Ma)	31.4±1.0
	Abanico	Below fossil zone	2, 3	$^{40}Ar/^{39}Ar$ (FCT 27.84 Ma)	34±1.3
	Abanico	Below fossil zone	2, 3	$^{40}Ar/^{39}Ar$ (FCT 27.84 Ma)	34.5±1.3
	Abanico	Below fossil zone	2, 3	$^{40}Ar/^{39}Ar$ (FCT 27.84 Ma)	36.22±0.19
	Abanico	Below fossil zone	2, 3	$^{40}Ar/^{39}Ar$ (FCT 27.84 Ma)	35.6±0.9
	Abanico	Below fossil zone	2, 3	$^{40}Ar/^{39}Ar$ (FCT 27.84 Ma)	37.67±0.31
	Abanico	Below fossil zone	2, 3	$^{40}Ar/^{39}Ar$ (FCT 27.84 Ma)	37.22±0.85
Deseadan	Salla beds	Buff Rubbly beds	4	$^{40}Ar/^{39}Ar$ (LP-6 & MAC-83)	26.4±0.4
	Salla beds	Nowhere ash (unit 2)	4	$^{40}Ar/^{39}Ar$ (LP-6 & MAC-83)	31.5±0.5
	Salla beds	Cerro Poco Poconi ash (1)	4	$^{40}Ar/^{39}Ar$ (LP-6 & MAC-83)	24.2±0.6
	Salla beds	Cerro Poco Poconi ash (2)	4	$^{40}Ar/^{39}Ar$ (LP-6 & MAC-83)	26.6±0.4
	Salla beds	Tapial Pampa West ash	4	$^{40}Ar/^{39}Ar$ (LP-6 & MAC-83)	25.4±0.3
	Salla beds	300m Upper White	4	$^{40}Ar/^{39}Ar$ (LP-6 & MAC-83)	26.5±0.4
	Moquegua	Within fossil zone	5	No analytical details provided	26.25±0.1
Colhuehuapian	Abanico	Within fossil zone	6	$^{40}Ar/^{39}Ar$ (FCT 27.84 Ma)	20.09±0.27
Pinturan	Pinturas	within fossil zone	7	unknown	17.7
	Pinturas	above fossil zone	7	unknown	16.5

References: 1. DeCelles et al. (2007); 2. Wyss et al. (1993); 3. Flynn et al. (2003); 4. Kay et al. (1998); 5. Shockey et al. (2009); 6. Flynn et al. (1995); 7. Fleagle et al. (1995)

Figure 2.1. Map of southern South America, showing study locations: Gran Barranca, Chubut Province, Argentina.

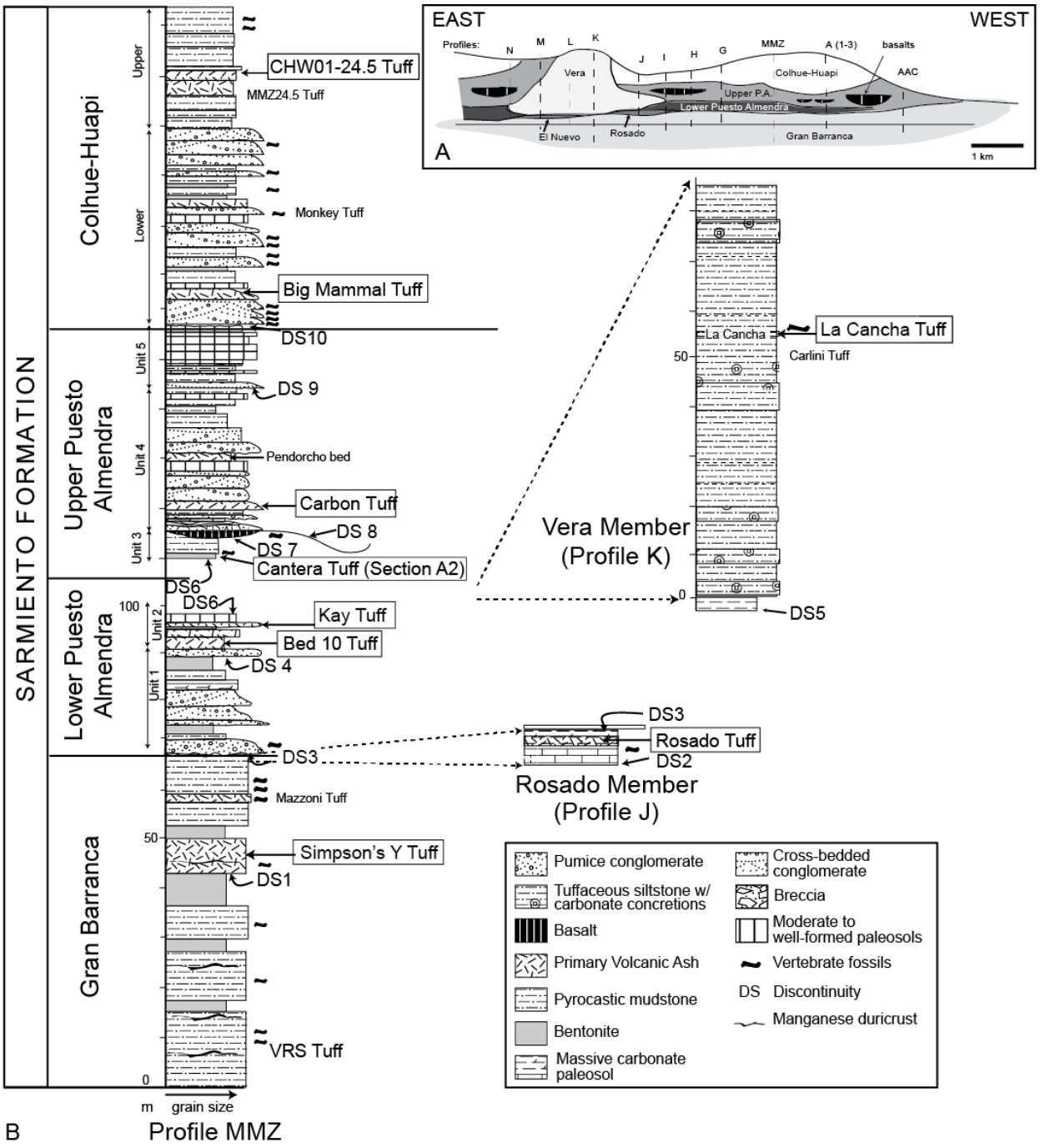

Figure 2.2. A. Schematic diagram looking south at the Gran Barranca showing lateral extent of the members of the Sarmiento Formation. Approximate locations of established stratigraphic profiles indicated by letter. B. Composite geologic section of Sarmiento Formation at Gran Barranca indicating member, lithostratigraphy, grain size, vertebrate fossil bearing levels, marker beds and volcanic tuff layers dated in this study.

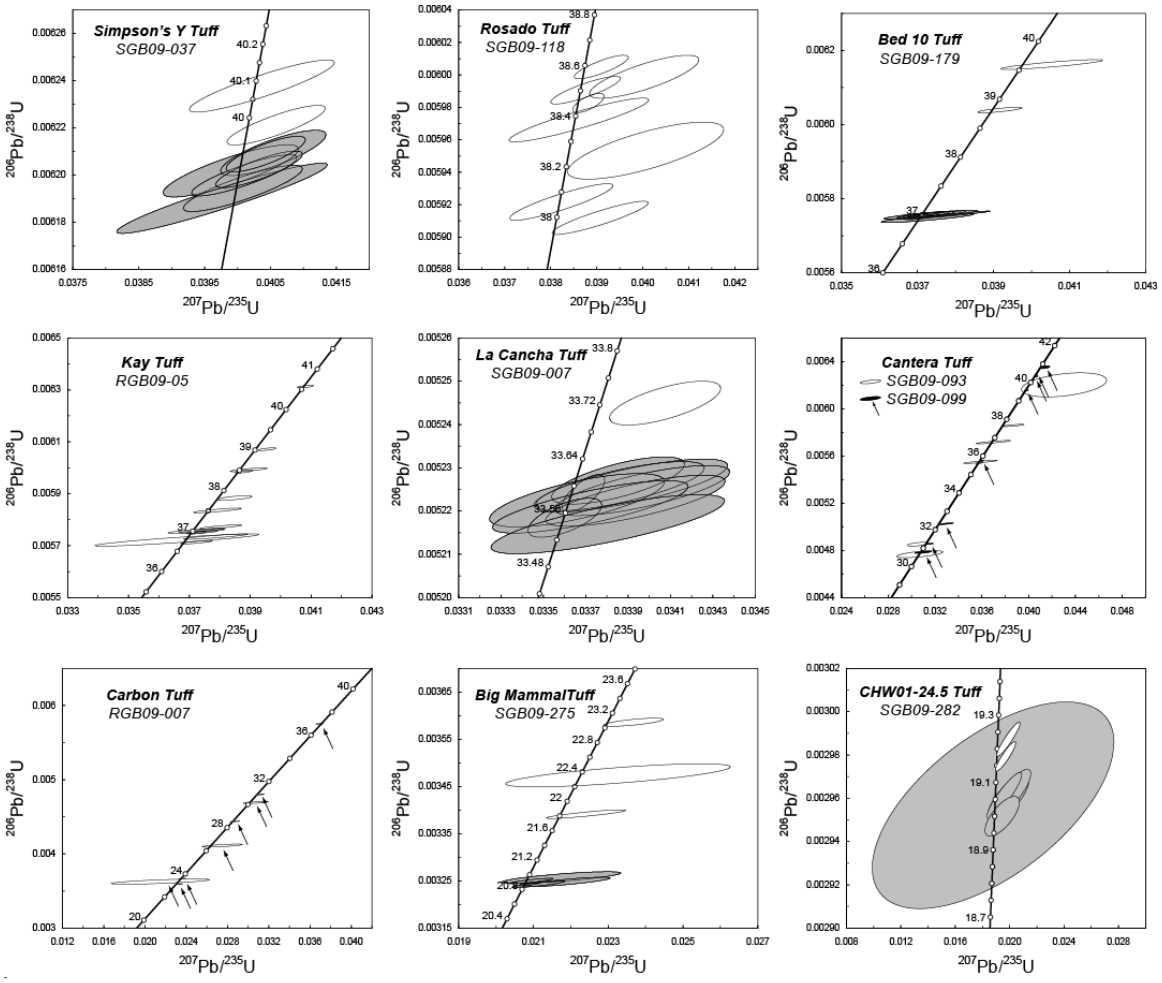

Figure 2.3. U-Pb concordia diagrams for zircon analyses from dated tuffs. All sample error ellipses are plotted at 2σ. Small ellipses are highlighted with arrows. Gray filled ellipses are included in weighted mean calculations. For the Cantera Tuff, two samples are plotted together as open versus filled ellipses.

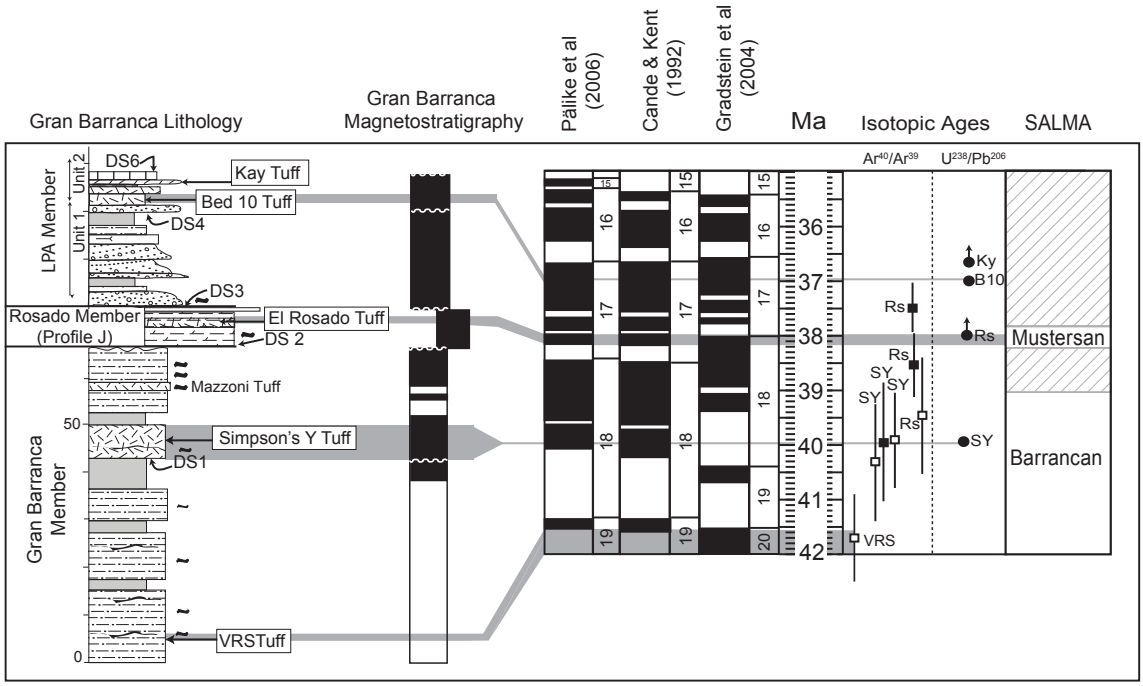

Figure 2.4. Geochronology for lower part of Sarmiento Formation. Member lithostratigraphy is plotted along with magnetostratigraphy of Ré et al. (2010). Gray bars demonstrate correlation of lithostratigraphy and magnetostratigraphy from Gran Barranca to global polarity time scales of Pälike et al. (2006, and their supplementary data). Cande and Kent (1992) and Gradstein et al. (2004) are shown for comparison. Isotopic age determinations are those from the 40Ar/39Ar dating from Ré et al. (2010b; open squares = best plagioclase dates; closed squares = best glass ages). Closed circles indicate U-Pb ages (this study). Abbreviations are: SY = Simpson's Y tuff; Rs = El Rosado Tuff; B10 = Bed 10; and Ky = Kay Tuff. For U-Pb dates, 2σ-error range is smaller than the symbol, thus error ranges are the widths of the gray horizontal lines. Black arrows on U-Pb dates indicate maximum ages for those samples. SALMA (South American Land Mammal Age) are also indicated. See Figure 2.2 legend for explanation of stratigraphic symbols.

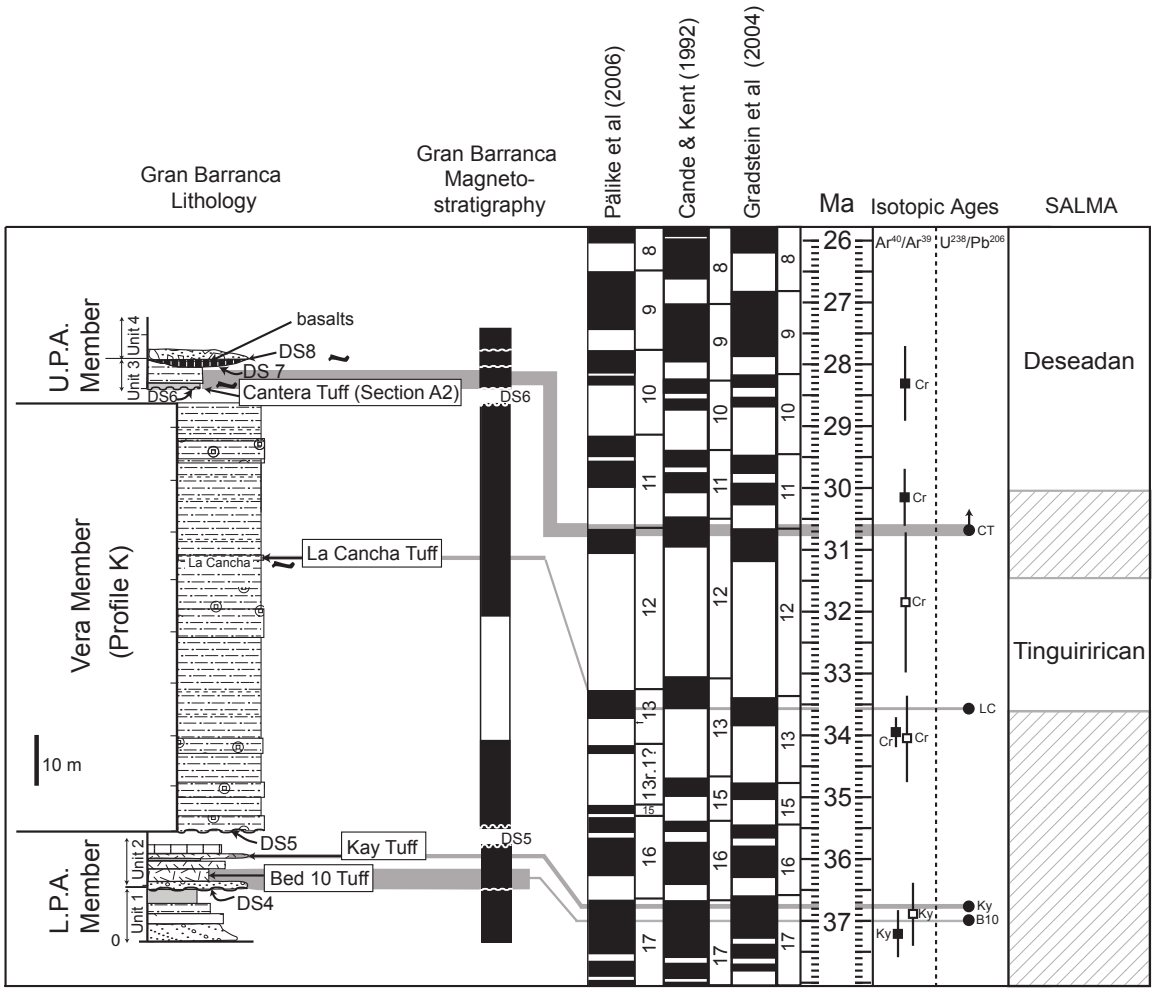

Figure 2.5. Geochronology for middle part of Sarmiento Formation. Symbols are the same as in Figure 2.4. Abbreviations are: B10 = Bed 10; Ky = Kay Tuff; Cr = Carlini Tuff; LC = La Cancha Tuff; and CT = Cantera Tuff. See Figure 2.2 legend for explanation of stratigraphic symbols.

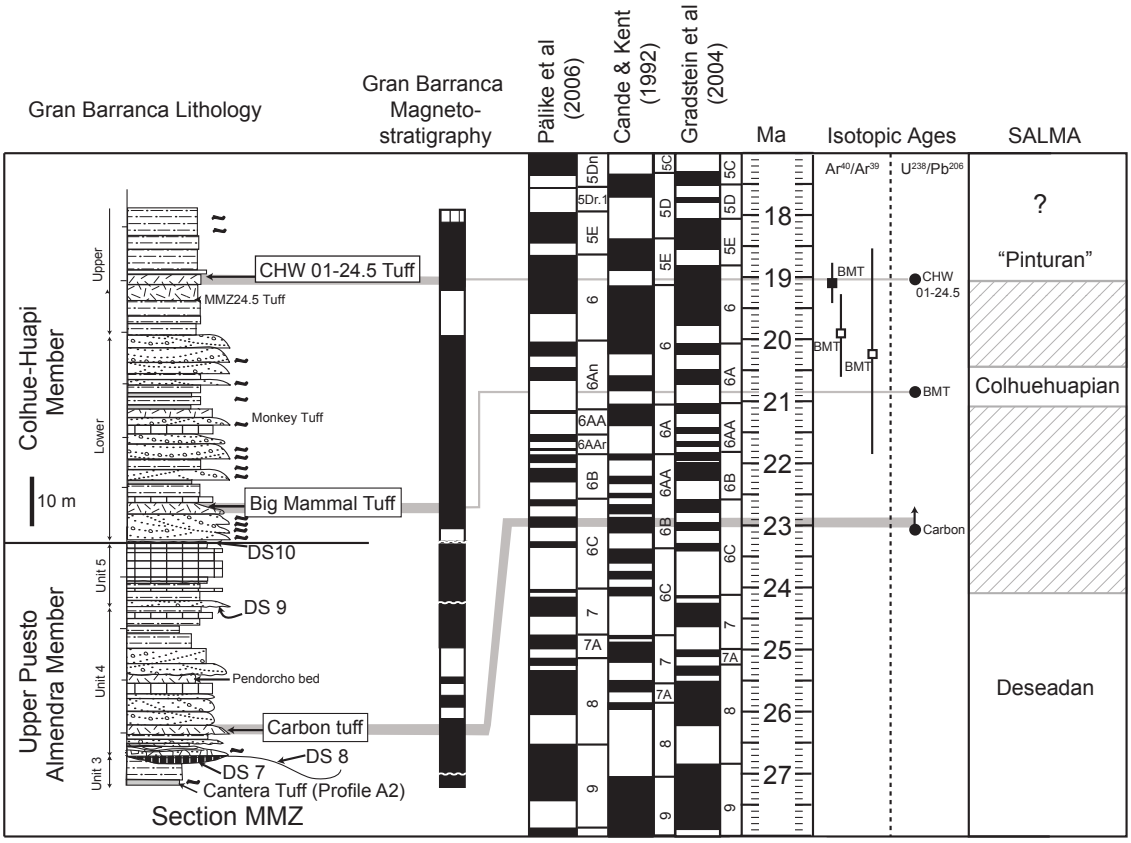

Figure 2.6. Geochronology for upper part of Sarmiento Formation. Symbols are the same as Figure 2.4. Abbreviations are: Carbon = Carbon Tuff; BMT = Big Mammal Tuff; and 01-24.5 = CHW01-24.5. See Figure 2.2 legend for explanation of stratigraphic symbols.

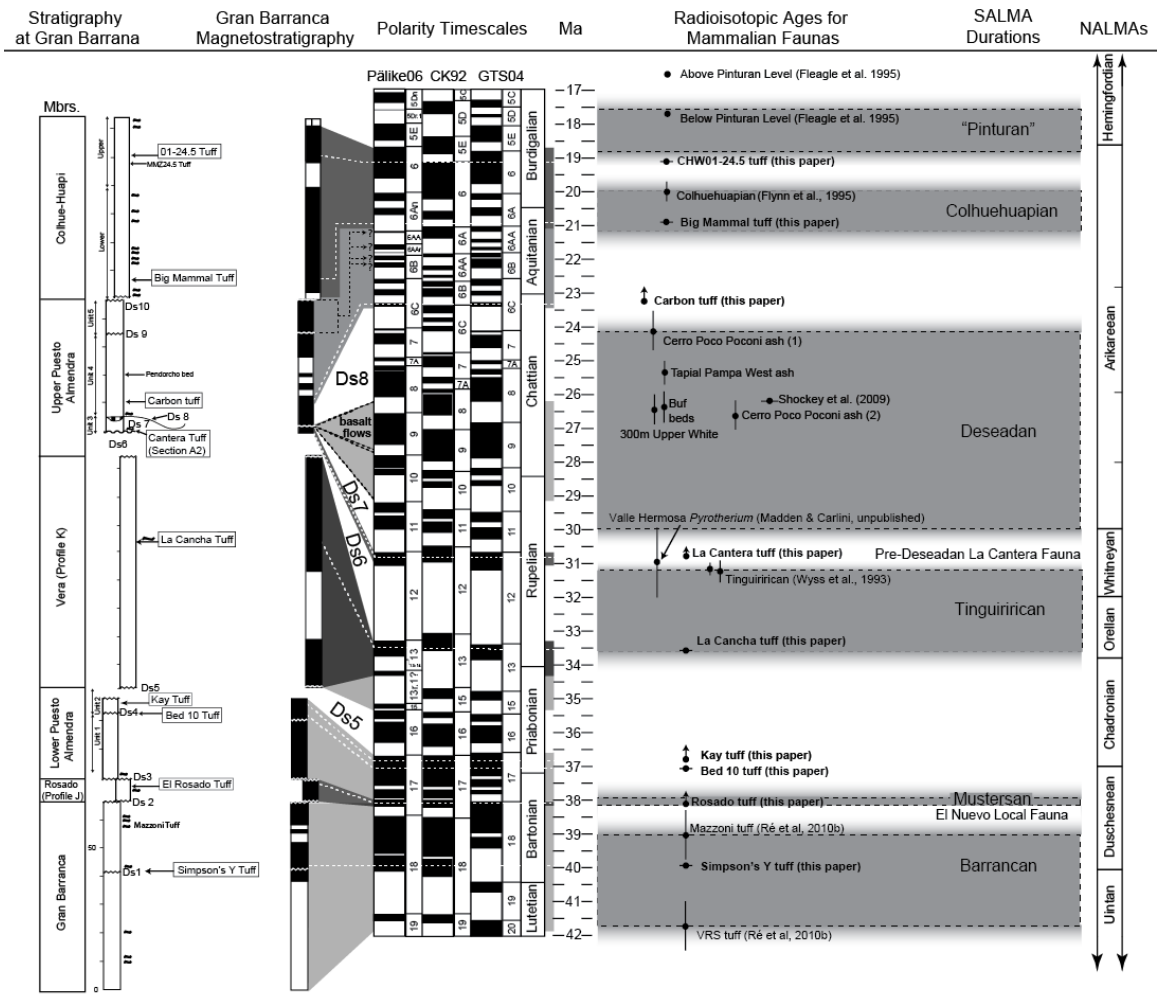

Figure 2.7. Summary geochronology for the Gran Barranca section showing timing of hiatuses and durations of the Sarmiento Formation members and SALMAs occurrences. Radioisotopic ages from other vertebrate localities in South America are plotted, and provide continent-wide age constraints for the SALMAs. Refer to Table 2.2 for references of radioisotopic dates. White dashed lines correlate U-Pb ages from this paper with the magnetostratigraphic section, bold black dashed lines show correlation of basalt ages, thin dashed black lines show possible chron correlation of rock units. NALMA durations and age boundaries from Woodburne (2004) and Albright et al. (2008).

CHAPTER III: Light environment and grass cell morphology in grasses

ABSTRACT

Premise of Study: Phytoliths (bio-opal) of grasses are preserved in the fossil record and constitute the best method to study the grasses and grassland evolution in deep time. However, methods currently used to reconstruct habitat openness based on grass phytolith abundance are potentially biased due to the prolific production of phytoliths in grasses compared to other plants, both herbaceous and woody (ferns and dicots). Based on relationships observed in eudicot epidermal cells, we hypothesize that shape (undulation) and size in epidermal cells (and phytoliths derived from them) will vary with irradiance levels. This variation could be used to develop a proxy for habitat openness in the fossil record.

Methods: We grew five species of grass under four irradiance levels, and measured epidermal cell parameters including undulation, area, length and width.

Key Results: With the exception of the shade-adapted *Chusquea*, grass species tested demonstrate increased cell length and cell area in shaded treatments irrespective of leaf dimensions; however there was no significant change in undulation for either long or short cells.

Conclusions: Grasses do not display changes in epidermal cell undulation with irradiance as documented in some dicotyledons. However, cell parameters such as cell length and

area for long cells and for crenate and polylobate short cells, do vary with irradiance and may be useful for determining ancient light regime and canopy cover from fossil phytolith assemblages.

INTRODUCTION

Reconstructing the evolutionary history of grasses and grassland ecosystems in the fossil record is most reliably done by studying silica microfossils, or phytoliths (e.g. Strömberg, 2004; 2005; 2006; 2007; 2011; Strömberg et al., 2013). All members of the Poaceae accumulate silica in their tissues. This silica can be deposited within cells or in extracellular spaces. In grass epidermis, silica accumulates in specialized cells, called Grass Silica Short Cells (GSSCs) as well as in, long cells, guard cells and trichomes (Fig. 3.1); typically the resulting phytoliths are casts (or molds) that preserve the original shape of the cells (e.g., Piperno 1988). When plants decay, these durable particles are deposited into soils and if preserved, provide a record of vegetation that can be millions of years old. GSSCs are diagnostic of the major grass clades and thus can be used to broadly interpret paleoecological settings. For instance, short cell phytoliths of the Bambusoideae and Pharoidae broadly indicate closed-habitats while short cells of the PACMAD and Pooideae clades can indicate open-habitats (Strömberg, 2004). In "traditional" phytolith analysis, the method for reconstructing the spread of grass-dominated and hence, presumably open habitats relies on the assumption that the proportion of grasses in assemblages also reflects how open the environment was (e.g., Alexandre et al., 1997; Piperno 2006; Bremond et al., 2005; Barboni et al., 2007; Mercader et al., 2011). As an example, the *FI-t* ratio uses the ratio between open habitat

grass phytoliths and "forest indicator" phytoliths (those from dicotyledons, non-grass monocotyledons [ie. Arecaceae, Zingerbales], ferns and conifers; Strömberg, 2005; Strömberg et al., 2007).

A fundamental problem with this approach, is that it may be unable to reliably reconstruct vegetation type when open-habitat grasses are absent or uncommon, as in a shrubland (Bremond et al., 2004), if open habitat grasses are growing under a forest canopy with low silica production, such as in many temperate forests (Hyland et al., 2013, Bozarth, 1993; Bremond et al., 2004; Strömberg, 2004), and in open environments where forbs and low-growing shrubs do not produce phytoliths (Thorn, 2004). Also, the *FI-t* ratio and other methods for reconstructing tree cover (e.g., Zucol et al., 2010) assumes that so-called open habitat grasses (Pooideae and PACMAD members) are chiefly, restricted to open environments (but see Osborne and Freckleton, 2009). Therefore, to reliably infer habitat openness using fossil phytolith assemblages, a taxon-free, morphological approach is needed. This study constitutes the first step towards such a proxy. In it, we perform a greenhouse experiment in which shade and enhanced light treatments are used to simulate canopy cover to test whether the morphology itself (cell dimensions and shape) of grass epidermal cells reflects light environment.

In nature, habitat openness (canopy openness) is determined by the amount of cover and vertical structure of vegetation. The canopy density determines the light regime of the understory, such that plants in open habitats receive more direct irradiation than those growing under a closed canopy. It is well known that leaf morphology and photosynthetic capacity are affected by light environment (e.g. Givnish, 1988). Sun leaves tend to be smaller, more deeply lobed, and have a higher leaf mass per area

(Hanson, 1917; Wylie, 1949; Talbert and Holch, 1957; Lichtenthaler, 1985; Bond et al., 1999). Additionally, sun leaves have higher vein and cell densities, thicker and more complex epidermis with higher stomatal densities, and if present, more papillae and hairs. (Bongers and Popma, 1988; Uhl and Walther, 2000 and references therein; Sack et al., 2003b). It has also been noted that irradiance levels affect the shape and size of individual epidermal cells. Specifically, studies have shown that cells of shade leaves are larger and more undulate than those of sun leaves in species such as oak (Kürschner, 1997), tobacco (Thomas et al., 2003), ivy (Watson, 1942), and goupie (*Goupia glabra*; Uhl and Walther, 2000).

This relationship between cell wall undulation and light has long been recognized in eudicots (Anheisser, 1900; Schramm, 1912; Watson, 1942; Metcalfe and Chalk, 1979; Kürschner, 1997; Thomas et al., 2003) and possibly ferns (Barbacka et al., 1998) however, similar observations are lacking for grasses. Grass epidermal ground mass cells consist of long cells and short cells (e.g., Metcalfe, 1960), both of which can have more or less sinuous/undulate shape. Are grass epidermal cell size and shape controlled by light environment in a similar way to other plants? If so, can the morphology itself of grass short and long cells, preserved in fossil soils, provide information about habitat structure of ancient environments?

The goal of this paper is to evaluate whether grass epidermal cell dimensions and shape are influenced by light environment. Specifically, we hypothesize that grass epidermal cells will be (1) larger and (2) more undulated under low light conditions than under high light conditions. To test these hypotheses, we grew five species of grasses under four lighting treatments and examined the effects of light quantity on both long and

short cell shape (degree of undulation) and size (surface area, length and width). We found that the morphologic response of epidermal cells to irradiance treatments is inconsistent among species but in most, a pattern of increased cell length and area with decreased irradiance is significant.

METHODS

Experimental treatments–The five species of grasses used in the experiment were chosen to cover a broad range of taxonomy, ecology, shade tolerance, GSSC type and photosynthetic pathway: *Chusquea culeo*, *Poa secunda*, *Sporobolus asper*, *Schizachyrium scoparium*, and *Stipa viridula*. *Chusquea culeo*, or Chilean feather bamboo, in the Bambusoideae subfamily of Poaceae, is a C3 evergreen, clump-forming bamboo. Natively, it grows in forest understories of *Nothofagus*-dominated temperate rainforests in Andean regions of south-central Chile and southwestern Argentina from elevations of 500-900 m (Veblin, 1982). It has predominately bilobate GSSCs, but also exhibits cross, and rare polylobate forms. *Poa secunda*, or Sandberg bluegrass in the Pooideae subfamily is a cool season (C3), perennial bunch grass with moderate shade tolerance that grows throughout western North America. It has crenate GSSCs. *Sporobolus asper*, or rough dropseed in the Chloridoideae subfamily, has characteristic chloridoid saddle shaped GSSCs, as well as occasional bilobate and cross-shaped forms. It is a perennial, warm season (C4) bunchgrass, native to North America that is shade intolerant. *Schizachyrium scoparium*, or little bluestem in the Panicoideae is a perennial warm season (C4) grass, with moderate shade tolerance and is one of the most widely distributed grasses native to North America. It has bilobate, panicoid-type GSSCs. *Stipa*

viridula (synonymous with *Nasella viridula*), or green needle grass in the Pooideae subfamily is a perennial, cool season (C3) bunch grass native to the Northern Great Plains as far south as Arizona. It is shade intolerant and has typical stipoid polylobate GSSCs (Strömberg, 2003).

Five replicates of four grass species [*Poa secunda* (PS)*, Schizachyrium scoparium* (SS)*, Sporobolus asper* (SA)*,* and *Stipa viridula* (SV)] to be dispersed among 4 treatments were germinated from commercially available seeds in 2.5-inch containers under ambient greenhouse conditions. Seedlings were grown for 30 days until each plant had produced two to three "true" leaves. The seedlings were divided randomly into four treatment groups (20% [deep shade], 60% [partial shade], 100% [control] and 120% [enhanced] light) and were placed into a randomized grid system within each treatment (Fig. A2.1, Appendix 2). The control was that of the ambient greenhouse environment and values of light percentage are relative to the control light level. Reduced light percentages were achieved using black-neutral density cloth (Hummert International, Earth City, MO USA) that reduced light by 80 and 40% for the 20 and 60% light treatments respectively. A 400-watt sodium light was placed above the enhanced light treatment to increase the amount of light to 120% relative to the control treatment. Photosynthetic Photon Flux Density (PPFD) was measured in each treatment using a LI-COR LI-250A light meter during cloudy, partly cloudy and sunny days to calibrate and confirm relative amounts of light received by each treatment. On sunny days at noon, PPFD values for the control treatment measured to be between 500-700 ($\mu mol\ s^{-1}m^{-2}$) and on cloudy days they were between 150-250 ($\mu mol\ s^{-1}m^{-2}$). PPFD measurements collected outdoors show that ambient greenhouse conditions received about 30-40% of the total

outdoor transmitted light. While irradiance values varied significantly on a daily basis, we were interested in how cell morphology changed relatively among the experimental light treatments. All treatments received consistent watering through capillary mats. The grasses grew from early March to June, 2010, at which time some species produced reproductive structures and all plants were harvested.

Due to difficulties in germinating bambusoid grasses, one-year old plants established from tissue culture of *Chusquea culeou* were purchased from BooShoot Gardens, LLC., Mt. Vernon, WA, and grown under the same conditions as the other grasses (described above) from July to late September, 2010. *Chusquea* plants were cut back to ~30 cm, and three stems on each plant were marked with string to differentiate new growth prior to initiating the light experiment.

For all grass species, three mature leaves were selected for harvest, and leaf length and width measurements were recorded. Epidermal peels were taken from both ab- and adaxial sides of the middle of each leaf, using clear acrylic nail polish and scotch tape. The peels were mounted on microscope slides and three sections of the slides were randomly selected and photographed under 400x magnification (Fig. 3.2). Using Photoshop C4 Extended Version, cell characters (area, perimeter, maximum cell height and maximum cell width) were measured by tracing cells occurring along pre-determined vertical transects from the photographs.

Following harvest and sampling, all plants were removed from the pots (except for *Chusquea*), soil from the roots was removed, and the plants were placed in plant presses and dried at 70°C for four days. Plants were weighed to determine total dry biomass. All plants were mounted on herbarium sheets and are cataloged as vouchers in

the UW Burke Museum (UWBM) Herbarium collections (Table A2.1, Appendix 2). Slides are deposited in the UWBM Paleobotany Reference Collection.

Measuring cell shape (undulation)–To measure cell undulation, we used an Undulation Index (UI) that measures the difference in area between a cell and a rectangle that encloses the cell entirely, or the convex hull where $UI=1-(A_C/A_{CH})$ (Raghavan et al., 2005). A_C is the measured area of the cell; and A_{CH} is the area of the convex hull, or the maximum cell length x maximum cell width (Fig. 3.3). UI ranges from 0 to 1 with increasing undulation towards 1. In this sense, "more undulated" or complex cells have more lobes that are more deeply incised. Other measures for undulation which involve shape corrections such as the UI of Kürschner (1997), calculated as the circumference of a cell divided by the circumference of a circle with the same area as the cell, and another method used in landscape ecology to determine amount of edge in a patch (perimeter of the patch divided by the perimeter of a square of the same area (Farina, 2006) were found to be inappropriate for calculating undulation in rectangular grass cells. In both of these shape corrections, UI is highly dependent on cell length, whereas the UI method we used is independent of cell length.

Data Analyses–Total means for each leaf were calculated using both abaxial and adaxial side measurements. Means were calculated in this manner considering that phytolith production occurs on both sides of the leaf epidermis (Motomura et al., 2000; Watson and Dallwitz, 1992). Using the leaf means, we conducted one-way ANOVA and post-hoc Tukey's tests to evaluate the significance of

variation in UI, cell area, cell length and cell width among the treatment groups. To look for potential relationships among gross morphology (leaf lamina measurements) and anatomy of individual leaves, leaf area, length and width were compared to mean cell parameters (area, length and width) for each leaf per species through linear regression analysis. Two-way ANOVA analyses were used to determine interactions between cell dimensions and leaf dimensions among the treatments. For all analyses, the statistical software package R was used (R Developmental Core Team, 2008).

RESULTS

Shading reduces plant biomass **–**The total mean biomass for all species tested (*Chusquea* not included in this analysis) was significantly ($p<0.01$) affected by light levels (Fig. 3.4A; Fig. A2.2 (Appendix 2); Table 3.1). Biomass reductions between 90-97% of the control occurred in the 20% light treatment in all species, with shade intolerant *Sporobolus* suffering the highest reduction. Partial shading (60% light) reduced biomass in *Sporobolus*, *Schizachyrium*, and *Stipa* between 68-77% compared to the control with the greatest reduction occurring in *Sporobolus*, whereas the moderately shade tolerant *Poa* was not significantly affected. *Sporobolus* was the only species to demonstrate significantly enhanced biomass (1.31 times) in the enhanced light (120% light) compared to the control.

Shading has variable effects on leaf dimensions**–**Means of the leaf measurements (length, width and area) of the harvested leaves (3 from each plant x 5

plants = 15 leaves for each species within each treatment) were compared among light treatments with one-way ANOVA analyses and post-hoc Tukey's tests.

Leaf Lengths–Leaf lengths were affected differentially according to species (Fig. 3.4B; Table 3.1) and no consistent pattern was found. *Chusquea* showed no change in leaf length among the treatments. *Sporobolus* showed large variation in leaf length in the treatments however, none of the values were significantly different. Leaves of *Poa* and *Schizachyrium* were around 1.5 times longer in the 20% treatment compared to the 120% treatment. None of the species showed significant differences in leaf lengths between the control treatment and the 120% treatment. *Stipa* had by far the longest leaves in the 60% treatment compared to the other treatments.

Leaf Widths–Leaf widths also failed to show a consistent pattern in response to light treatment although the values tend to follow a parabolic pattern where leaves were thinner in the 20% and 120% treatments compared to the 60 and 100% treatments (Fig. 3.4C), though none of the leaves in the 120% treatment were significantly thinner than the control treatment. Leaf widths are significantly reduced in the 20% treatment compared to the control in *Chusquea* (16%), *Sporobolus* (56%), *Schizachyrium* (51%), and *Stipa* (35%) whereas *Poa* shows no difference among any of the light treatments.

Leaf Area–Comparisons of leaf area (leaf width in the center of the leaf x leaf length) and light level also show species specific responses (Fig. 3.4D). *Chusquea* shows no change in leaf area, whereas *Poa* has larger leaves in the shade treatments compared to

the control and 120% treatments, an effect of increased leaf length in the shaded treatments. *Sporobolus* and *Schizachyrium* leaves in 20% treatment are significantly smaller than the control treatments due to the severe reduction in leaf width in the 20% treatment.

Shading effects on epidermal cell morphology–One-way ANOVA tests with post-hoc Tukey's tests were performed to compare cell undulation, area, length and width among treatments for each species. The means and standard error values are found in Table 3.2, and P- and F-values for each test in Table 3.3.

Cell undulation– Undulation values range from 0.42-0.31 for grass long cells, and there is no pattern for differences among the light treatments (Fig. 3.5A, Tables 3.2 and 3.3). *Chusquea*, *Poa*, and *Sporobolus* show no significant differences in UI in any of the treatments. In *Schizachyrium*, long cells in the 120% treatment are significantly less undulated compared to the 60% and the control treatments. The opposite pattern is seen in *Stipa* where undulation in the 20% treatment is significantly lower than the control treatment. Comparisons among species show that *Sporobolus* long cells are the most undulated (0.40-0.42), followed by *Chusquea* (0.37-0.39) while the other species UI values range between 0.31-0.35. UI values of *Poa* are similar to those of the other species despite the fact that *Poa* long cells have smooth cell walls (Fig. 3.2B). The reason for this is that the undulation values of *Poa* represent the curvature of the cells in relation to their convex hull. Thus, UI measured according to our method does not measure only the

sinuosity of the cell wall relative to the overall shape of the cell, but also includes the sinuosity of the cell as a whole relative to other epidermal cells in the lamina.

Short cells have undulation values that range from 0.29-0.36 (Fig. 3.5B), and none of the values are significantly different in any of the light treatments. Bilobate cells of *Schizachyrium* have the highest UI values (0.36) compared to bilobate cells of *Chusquea* (0.33-0.34).

Cell Area–The long cell area of all species except *Chusquea* are 1.15-1.42 times greater in the 20% treatment than in the 120% treatment. In *Schizachyrium* and *Stipa*, cells in the 20% treatment are 1.2 and 1.4 times larger respectively than the control treatment (Fig. 3.5C).

The pattern among short cells is similar to that of long cells in *Poa* and *Stipa*. The crenate short cells of *Poa* consistently decline in area with increasing irradiance whereas the 20% treatment cells are 1.2 times larger than the control and 1.37 times larger than the 120% treatment (Fig. 3.5D). Polylobate short cells of *Stipa* show a similar pattern; however, there is no significant difference in cell area between the control and 120% treatments. Bilobate short cells of *Schizachyrium* show no change in area, whereas those of *Chusquea* are 1.15 times larger in 120% treatment than in the 20% treatment. Saddle short cells of *Sporobolus* did not differ in area across treatments.

Cell Length–With the exception of *Chusquea*, all grass species show a dramatic increase in cell length with reduced irradiance, but they are affected differently (Fig. 3.5E). Cells of *Poa*, *Sporobolus*, *Schizachyrium* and *Stipa* in the 20% treatment are

significantly larger (1.14-1.21 times) than those in the 60% treatment and 1.11-1.56 times larger compared to the controls. The largest differences in cell length are between the 20 and 120% treatments, with 1.23-1.53 times larger cells in the 20% treatment. Only *Sporobolus* and *Schizachyrium* show significantly larger cells (1.15 times) also in the control compared to the 120% treatment.

Whereas the bilobate cells of *Chusquea* and the saddle short cells of *Sporobolus* show no change in length with light treatment, short cells of *Poa*, *Stipa* and *Schizachyrium* show a pattern that parallels that seen in long cells, whereby cells are longest in the shade treatments (Fig. 3.5F). Crenate short cells of *Poa* decrease nearly linearly in length with increased irradiance. Only the 20% and 120% treatments are significantly different, with 1.18 times longer cells in the 20% treatment than the 120% treatment. The polylobate cells of *Stipa* show a similar increase in cell length. Both shade treatments have significantly longer cells than the control and 120% light treatments, which do not differ significantly. Thus, short cells of *Stipa* are 32% longer in the 20% light treatment compared to the 120% treatment, 18% larger compared to the control light treatment and 12% larger than the 60% treatment. Bilobate short cells of *Schizachyrium* are significantly smaller (~20% smaller) in the 120% treatment compared to any of the other treatments.

Cell Width–Long cell width is unaffected by light treatment in *Chusquea*, *Sporobolus* and *Schizachyrium*. In contrast, while *Stipa* and *Poa* differ in opposite ways (Fig. 3.5G). *Stipa* has significantly thinner cells (14%) in the 20% treatment compared to

all other treatments and *Poa* has the widest cells in the control treatment which differed significantly from both the 20 and 120% treatments.

Short cell width in *Chusquea*, *Sporobolus* and *Schizachyrium* is unaffected by light treatment, whereas *Poa* and *Stipa* show a conflicting pattern (Fig. 3.5H). In the 20% treatment cells of *Stipa* are between 10-12% thinner compared to all other treatments, and in *Poa*, cells in the 20% treatment are 15% wider compared to the 120% treatment. In summary, there appears to be no clear trend in cell width among species in the varying light treatments.

Relationship between leaf dimensions and cell dimensions–To test whether variation in leaf size was a controlling factor in cell size and shape, comparisons between leaf parameters (leaf area, length, and width) and cell parameters (cell area, length and width) were made using linear regressions. All cell measurements for both long and short cells from all treatments were compared to their corresponding leaf dimensions. In several cases, leaf dimensions were significantly correlated with R^2 values ranging from 0.001-0.069 (Table 3.4). Therefore it appears that cell dimensions are not a function of the leaf dimensions. However, because these weak correlations exist, we tested whether leaf dimensions and cell dimensions are interacting factors that in part explain changes in cell morphology within the light treatments using two-way ANOVA analyses. For each species, interactions between cell length and leaf length, cell area and leaf area, and cell width and leaf width were tested.

Whereas both mean leaf length and cell length tend to increase with shaded conditions (Figs. 3.4B, 3.5E and 3.5F), cell length was not affected by leaf length in any

species. The same is true for cell width and leaf width among treatments. Cell area and leaf area showed a significant interaction among treatments only in *Poa* where long cell area was related to leaf area (ANOVA $F_{3,52}$= 4.1855, P= 0.01), but note that leaf area only explains 2% of the variation in cell area in this species. These analyses confirm that the variability in cell dimensions is more likely the result of irradiation than leaf size.

DISCUSSION

***Effect of shade on grass biomass*–**Shading had a strong effect on total biomass of these grass species. Even partial shading had profound exponential impacts on grass biomass. In nature, studies concerned with grassland/forest transitions have shown that grass biomass is greatly affected by even limited tree cover (20%-60%) (Jameson, 1967; Scholes and Archer, 1997). This reduction of grass biomass with shading from small increments of tree cover should be reflected in the amount of grass phytoliths being deposited into the soil (and thus preserved as fossils) relative to phytoliths from shrubs and trees, and allow for distinction between phytolith assemblages formed under grasslands and forests, respectively. Indeed, studies from many ecosystems, primarily in the tropics and subtropics, have documented the utility of phytolith studies in reconstructing grassland-forest dynamics also over short distances (Alexandre et al., 1997; Barboni et al., 2007; Bremond et al., 2005; Kerns et al., 2001; Mercader et al., 2011).

Effect of shade on leaf dimensions–While the literature commonly states that sun leaves are smaller than shade leaves, many studies show that reduced light can result in either a reduction or an increase in leaf expansion (e.g. Cookson and Granier, 2006; Uhl and Walther, 2000). The effects of shading on grass leaf dimensions in our study were variable and appear to be species specific. Three species of grasses (*Sporobolus*, *Schizachyrium*, and *Stipa*) demonstrated reduced leaf area in deep shade, one species had increased leaf area (*Poa*), and one species was unaffected (*Chusquea*). Significant increases in leaf length between the deep shade and enhanced light treatments occurred only in two species (*Poa* and *Schizachyrium*). Leaf width was more often affected by reduced light than leaf length with four species (*Chusquea*, *Sporobolus*, *Schizachyrium*, *Stipa*) showing reduced widths between 16-51% in the deep shade compared to the control and enhanced light conditions. Increased leaf length with shade has been noted in garlic (Rahim and Fordham, 1990) and in some grasses such as *Triticum* sp. (Friend and Pomeroy, 1970), *Trichanche californica*, *Setaria macrostachya* and *Muhlenbergia porteri*, but not in other grasses such as *Bouteloua eriopoda* (Tiedemann et al., 1971). Such varying results indicate that each species responds uniquely to shade in terms of plant gross morphology.

Cell Undulation not reliably controlled by irradiance in grasses–Irradiance is well known to affect undulation of anticlinal epidermal cells in eudicots such as ivy, oak and tobacco (Watson, 1942; Kürschner, 1998; Thomas et al, 2003). Our results suggest that grasses do not show this pattern. Instead grass both long and short cells exhibit relative uniformity in undulation across an irradiance gradient. One of the species tested,

Schizachyrium, constitutes a possible exception. Its long cells show decreased undulation values in the enhanced light treatment compared to the control and partial shade treatments. The direction of change conforms to that predicted based on the effects of irradiance on eudicot pavement cell shape. However, the reverse pattern is seen in *Stipa* long cells where undulation values are lower in the deep shade treatment relative to the control. These conflicting results, along with the lack of significant change in all types of short cells tested, indicate that grass cell wall shape is not consistently affected during morphogenesis in the same way as in other angiosperms.

Lobe formation in epidermal cell walls is determined by components of the cell cytoskeleton that require the coordination of microtubules and actin filament activities (Smith and Oppenheimer, 2005). Different gene complexes controlling these processes have been identified in *Arabadopsis* and *Zea* (Smith, 2003). However, it is not well-understood how environmental cues, such as light, regulate cytoskeleton formation during cell morphogenesis and expansion. Grasses might provide an interesting contrast for future studies examining the process and adaptation of epidermal cell undulation to light.

Shade induced cellular plasticity–Though grass cell undulation is not reliably affected by irradiance, other aspects of cell morphology are and may therefore be candidates for further study for applications in fossil phytolith research. Among the variables tested, cell length and cell area hold the most promise.

Cell length–With the exception of *Chusquea*, grass long cells of the four other grass species tested, as well as the crenate and polylobate short cells of *Poa* and *Stipa* were consistently longer in reduced light. This pattern has been described in other taxa such as *Lactuca* (Wargent et al, 2009), garlic (Rahim and Fordham, 1990) and the grasses *Deschampsia antarctica* (Ruhland and Day, 2000), and *Triticum* (Friend and Pomeroy, 1970). Whereas two of these studies associate shorter cells with shorter leaf blades (Rahim and Fordham, 1990; Friend and Pomeroy, 1970), we found only weak correlations between leaf length and cell length. Hence, we suggest that cell length is physiologically determined by irradiance during cell morphogenesis and later plant growth rather than a side effect of leaf elongation.

Why do long cells shorten in higher light environments? One hypothesis for what might influence long cell length relates to the differentiation of certain epidermal cells as trichomes and stomatal guard cells. In grass epidermis, trichomes and stomatal complexes are located between long cells (Fig. 3.2); hence their addition to the epidermal cell file may constrain the length of long cells. Densities of both stomata and trichomes are known to increase with irradiance in grasses. In *Festuca* stomatal densities decrease by 17-24% at low irradiance compared to high irradiance treatments (Allard et al., 1991); the same pattern has been observed in *Andropogon* (Knapp and Gilliam, 1985) and *Allium* (Rahim and Fordham, 1991). Trichome density is known to decrease in shade in *Sebastiania* (Euphorbiaceae; Marques et al., 1999), *Olea* and *Quercus* (Liakoura et al., 1997). Based on these patterns, we hypothesize that higher stomatal and trichome densities in the control and enhanced light treatments relative to the shade treatments resulted in long cells that were more often truncated and therefore shorter. Although we

have not yet quantified stomatal or trichome densities, we are currently testing their relationship further.

Cell Area–A similar relationship is found between irradiance levels and cell area. With the exception of *Chusquea*, all other species show significantly larger long cells in deep shade, as do the crenate and polylobate short cells of *Poa* and *Stipa*. Since the area of rectangular grass cells is mostly affected by changes in cell length, observed changes in cell area across light treatments may be under the same control as cell length. Therefore, we similarly hypothesize that cell area in grasses is negatively correlated with stomatal and trichome densities.

Increased cell area in leaves grown under reduced irradiance has been documented in eudicotyledonous and monocotyledonous species such as ivy (Watson, 1942), tobacco (Thomas et al., 2003), and garlic (Rahim and Fordham, 1990). In these species, increased cell area was associated with increased lamina size. Functionally, it is hypothesized that larger leaves increase light capture and CO_2 assimilation rates in environments with more diffuse irradiation (Horn, 1971, Sack *et al.,* 2006 and references therein). We found increased cell size in *Poa*, *Sporobolus*, *Schizachyrium* and *Stipa*, with decreased irradiance, but we do not find the same relationship with leaf dimensions.

In contrast to pattern predicted from other types of plants, saddle and bilobate shaped epidermal short cells of *Sporobolus* and *Schizachyrium* do not vary in size among light treatments. In addition, the bilobate short cells of *Chusquea* show the opposite pattern compared to all other cell types and species, whereby short cells are significantly larger in the enhanced light treatment. For this reason, bilobate and saddle shaped short

cells do not seem to hold potential as candidates for a potential proxy for light environments in the fossil record, but aspects of the morphology (area and length) of crenate and polylobate short cells do, and should be investigated further.

Cell dimensions do not track leaf dimensions–Our investigation of potential relationships between cell parameters (area, length, and width) and leaf size showed that cell measurements only weakly correlate with leaf measurements in a few cases (Table 3.4). Instead, it appears that most of the observed changes in cell morphology are independent of leaf morphology and, hence, potentially linked to irradiation exposure.

Why is bamboo always the exception?–The bamboo, *Chusquea culeou,* did not exhibit the predicted pattern in cell shape, area or length from low to high light conditions. It is unclear whether the patterns observed are a result of experimental design, or if they are a product of plant biology. The *Chusquea* plants were not cultivated from seed (see Methods); instead we used one-year old plants propagated from tissue culture that we grew under the light treatments for three months before selecting leaves from new growth for analysis. This protocol assumed that recently developed leaves would reflect the new light exposure, based on results from experiments with tobacco that show that leaf formation at the shoot apex is influenced by irradiance exposure of already mature leaves at the time of new leaf development (Thomas *et al.,* 2003). However, if this assumption is not valid, a possible explanation for the pattern seen in *Chusquea* is that the properties of newly developing leaves were influenced by prior light conditions (in the BooShoot Gardens greenhouses).

An alternative, biologically based hypothesis is that forest grasses, or shade tolerant species in general, have less phenotypic plasticity relative to their close relatives that live in more sun exposed habitats (Smith, 1982). Mulkey (1986) suggested that species inhabiting the understory of late-successional habitats may have limited potential for photosynthetic acclimation if natural selection favored species that conserve low-light photosynthetic efficiency. Widmer (1998) found that *Chusquea talamancensis*, a very shade tolerant species in Costa Rica, demonstrated less phenotypic plasticity in growth form under varying canopy closures compared to two other species of bamboo deemed less shade tolerant. In contrast, a more recent study found significant differences in leaf morphology between sun and shade leaves of *Chusquea culeo* by which shade leaves were longer, with thinner lamina, and wider vein spacing (March and Clark, 2011). Unfortunately, their study did not investigate cellular features. A field study that compared epidermis of *Chusquea culeo* from shaded and more open habitats would help discriminate between these hypotheses.

***Developing a Proxy for Ancient Habitat Openness*–**Could the observed, light-related phenotypic plasticity of cell length and potentially area in grass long cells and crenate and polylobate short cells be used to design a proxy for light regime (habitat openness) in the fossil record? The answer, we think, is maybe, but it involves several important caveats.

First, because long cell morphology demonstrates strong interspecific in addition to intraspecific variation, it may not be possible to define discrete limits on cell length or area per light environment. A better approach might be to develop a proxy using measurements from phytolith pools derived from grass communities growing along

natural gradients from closed to open habitats, including open grasslands, savanna, shrubland, woodland, and forested habitats (Dunn et al., 2012). Such an approach should capture any variation relating to the particular makeup of grass communities that might influence cell morphology. For example, whereas many PACMADs or pooids are typically associated with open grasslands or savannas, others are found primarily in shaded habitats (e.g., *Zeugites*, *Poecilostachys*, *Nardus*; Osborne and Freckleton 2009). These species may display lineage specific phenotypic responses in terms of epidermal cell morphology to light environment that would impact cell dimensions of grass communities in which those species were preferentially found. However, note that until we know more about at what taxonomic level these differences in phenotypic plasticity exist (species, genus, subfamily etc.), such a proxy would be limited to ecosystems where the species composition of grass communities could be assumed to be similar to today.

Second, we cannot exclude that long and short cells of grasses show shape and size variation relating to untested environmental parameters. In particular, it has been suggested that features of short cells such as phytolith area (Brown, 1984) and length of the shank of bilobate types may relate to water availability (Lu and Liu, 2003). A third consideration in the development of this proxy is taphonomic bias. For example, the fossil record may be biased towards the preservation of shorter long cell phytoliths, as longer phytoliths have more potential to break during pedogenic and preservational processes. An alternative approach would be to only measure crenate and polylobate short cells because they are shorter and more durable than grass long cells, but this would restrict the utility of the proxy to soil and fossil phytolith assemblages where these types of short cells are present.

Lastly, because our partial shade treatment (60% light) and control treatment (100% light) produced nearly indiscernible cell morphologies, it may be difficult to distinguish partially shaded environments from open environments using cell measurements alone. It is possible that in nature, where irradiance values are much higher than in the greenhouse at the University of Washington, even partial shading is detectable. We are exploring this possibility using an approach that involves all epidermal phytoliths (from both grasses and dicotyledons) in assemblages extracted from modern soils (see Dunn et al., 2012).

In summary, grass epidermal cells do not exhibit irradiance-induced plasticity in undulation as occurs in other angiosperms. However, grass cells demonstrate variable cell lengths and area according to light environment independent of leaf size. We hypothesize that changes in cell length and area may be the result of concomitant changes in trichome and stomatal densities whose response to irradiance cues is well known. The light induced plasticity exhibited by grass epidermal cells has the potential to help describe ancient light environments.

ACKNOWLEDGEMENTS

We thank Doug Ewing and the UW Biology Greenhouse staff, and these undergraduate researchers for their work tracing cells: Darshi Banan, Terry Huang, Ross Fletcher Hill, Tony Jijina, Josh Johnson, and Aidan Loeser. This research was funded in part by National Science Foundation Grants DEB-1110354 to C.A.E. Strömberg and R.E. Dunn (Doctoral Dissertation Improvement Grant) and EAR-0819910 to C.A.E. Strömberg and UW-HHMI and Boeing/OMA to T.-Y. Le.

LITERATURE CITED

Alexandre A, Meunier, J.D., Lévine A.M., Vincens A., Schwartz D. 1997. Phytoliths indicators of grasslands dynamics during the late Holocene in intertropical Africa: *Palaeogeography, Palaeoclimatology, Palaeoecology* **136**: 213–219.

Allard, G., Nelson, C.J., and Pallardy, S.G., 1991, Shade effects on growth of tall Fescue: I. Leaf anatomy and dry matter partitioning: Crop Science, v. 31, p. 163–167.

Anheisser R. 1900. Über die aruncoide Blattspreite. *Flora* **87**: 64.

Areschoug, FWC. 1897. Über die physiologischen Leistungen und die Entwickelung des Grundgewebes des Blattes. E. Malmströms Buchdruckerei.

Barbacka M, van Konunenburg-van Cittert J. 1998. Shade leaves in two Jurassic species of Pteridosperms. *Review of Palaeobotany and Palynology* **103**: 209–221.

Barboni D, Bremond L, Bonnefille R. 2007. Comparative study of modern phytolith assemblages from inter-tropical Africa. *Palaeogreography, Palaeoclimatology, Palaeoecology* **246**: 454–470.

Bond BJ, Farnsworth BT, Coulombe RA, Winner WE. 1999. Foliage physiology and biochemistry in response to light gradient in conifers with varying shade tolerance. *Oecologia* **120**: 183–192.

Bongers F, Popma J. 1988. Is exposure-related variation in leaf characteristics of tropical rain forest species adaptive? In: Werger MJA, van der Aart PJM, During HJ, Verhoeven JTA, eds. *Plant form and vegetation structure*. The Hague, Netherlands. SPB Academic, 191–200.

Boyer JS. 1968. Relationship of water potential to growth of leaves: *Plant Physiology* **43**: 1056-1062.

Boyer JS. 1970. Leaf enlargement and metabolic rates in corn, soybean and sunflower at various leaf water potentials. *Plant Physiology* **46**: 233-235.

Bozarth SR. 1993. Biosilicate assemblages of boreal forests and aspen parklands. In: Pearsall, DM, Piperno DR. *Current Research in Phytolith Analysis: Applications in Archaeology and Paleoecology*. MASCA Research Papers in Science and Archaeology vol. 10. University Museum of Archaeology and Anthropology, University of Pennsylvania, Philadelphia, pp. 95–105.

Bremond L, Alexandre A, Véla E, Guiot J. 2004. Advantages and disadvantages of phytolith analysis for the reconstruction of Mediterranean vegetation: an assessment based on modern phytolith, pollen and botanical data (Luberon, France). *Review of Palaeobotany and Palynology* **129**: 213–228.

Bremond, L., Alexandre, A., Hély, C., Guiot, J., 2005, A phytolith index as a proxy of tree cover density in tropical areas: Calibration with Leaf Area Index along a forest–savanna transect in southeastern Cameroon. *Global and Planetary Change* **45**: 277–293.

Brown, DA. 1984. Prospects and limits of a phytolith key for grasses in the central United States: Journal of Archaeological Science, v. 11, p. 345–368.

Cookson, S.J., and Granier, C., 2006, A Dynamic analysis of the shade-induced plasticity in *Arabidopsis thaliana* rosette leaf development reveals new components of the shade-adaptative response, Annals of Botany, v. 97, p. 443–452.

Dannenhoffer, J.M., Ebert, W. Jr., and Evert, R.F., 1990, Leaf vasculature in barley, *Hordeum vulagre* (Poaceae). *American Journal of Botany* **77**: 636–652.

Dorweiler JE, Doebley J. 1997**.** Developmental analysis of *Teosinte* glume architecture: a key locus in the evolution of maize (Poaceae). *American Journal of Botany* **84**: 1313–1322.

Dunn, RE, Strömberg CAE, Le T, Loeser AC. 2012. Seeing the forest through the trees: reconstructing vegetation structure from the cellular level using phytoliths. GSA Abstracts with Programs **44.**

Gibson DJ. 2009. *Grasses and Grassland Ecology*. New York, USA: Oxford University Press.

Edwards EJ, Smith SA. 2010. Phylogenetic analyses reveal the shady history of C_4 grasses. *Proceedings of the National Academy of Science, USA* **107**: 2532-2537.

Farina, A. 2006 *Principles and methods in landscape ecology: towards a science of the landscape*. Vol. 3. Springer.

Friend DJC, Pomeroy ME. 1970. Changes in cell size and number associated with the effects of light intensity and temperature on the leaf morphology of wheat. *Canadian Journal of Botany* **48**: 85–90.

Givnish TJ. 1988. Adaptation to sun and shade: whole-plant perpective. *Australian Journal of Plant Physiology* **15**: 63–92.

Hanson HC. 1917. Leaf structure as related to environment. *American Journal of Botany* **4**: 533–560.

Hirota M, Holmgren M, Van Nes EH, Scheffer M. 2011. Global resilience of tropical forest and savanna to critical transitions. *Science* 334: 232–235.

Hoffman WA, da Silva R, Machado GC, Bucci SJ, Scholz FG, Goldstein G, Meinzer FC. 2005. Seasonal leaf dynamics across a tree density gradient in a Brazilian savanna. *Oecologia* 145: 307–316.

Horn, HS. 1971. *The adaptive geometry of trees*. Princeton, New Jersey, USA: Princeton University Press.

Hyland, E, Smith SY, Sheldon, ND. 2013. Representational bias in phytoliths from modern soils of central North America: implications for paleovegetation reconstructions. *Palaeogeography, Palaeoclimatology, Palaeoecolgy* 374: 338–348.

Jacobs BF, Kingston JD, Jacobs LL. 1999. The origin of grass-dominated ecosystems: *Annals of the Missouri Botanical Garden* **86**: 590–643.

Jameson, DA. 1967. The relationship of tree overstory and herbaceous understory vegetation. *Journal of Range Management* **20**: 247–249.

Kellogg EA. 2001. Evolutionary history of the grasses. *Plant Physiology* **125**: 1198-1205.

Kerns, BK., Moore, MM, Hart, SC. 2001. Estimating forest grassland dynamics using soil phytolith assemblages and D13C of soil organic matter: *Ecoscience* 8, 478–488.

Knapp, A.K., and Gilliam, F.S., 1985, Response of Andropogon gerardii (Poaceae) to fire-induced high vs. low irradiance environments in tallgrass prairie: leaf structure and photosynthetic pigments: American Journal of Botany, v. 72, p. 1668-1671.

Kürschner WM. 1997. The anatomical diversity of reent and fossil leaves of the durmast oak (*Quercus petraea* Lieblien/*Q. pseudocastanea* Goeppert)-implications for their use as biosensors of palaeoatmospheric CO2 levels: *Review of Palaeobotany and Palynology* **96**: 1–30.

Lehmann CER, Archibald SA, Hoffman WA, Bond WJ. 2011. Deciphering the distribution of the savanna biome. *New Phytologist*. doi: 10.1111/j.1469-8137.2011.03689.x

Lu, H., Liu, K. 2003. Morphological variations of lobate phytoliths from grasses in China and the south-eastern United States: Diversity and Distributions, v. 9, p. 73–87.

Liakoura, V., Stefanou, M., Manetas, Y., Cholevas, C., and Karabournioites, G., 1997, Trichome density and its UV-B protective potential are affected by shading and leaf position on the canopy: Environmental and Experimental Botany, v. 38, p. 223–229.

Lichtenthaler, H.K., 1985, Differences in morphology and chemical composition of leaves grown at different light intensities and qualities. *In* N.R. Baker, W.J. Davies and C.K. Ong (Eds), Control of Leaf Growth, Cambridge Univ. Press, Cambridge, p. 201–221.

March RH, Clark LG. 2011. Sun-shade variation in bamboo (Poaceae: Bambusoideae) leaves. *Telopea* **13**: 93–104.

Marques, A.R., Garcia, Q.S. and Fernandes, G.W., 1999, Effects of sun and shade on leaf structure and sclerophylly of Sebastiania myrtilloides (Euphorbiaceae) from Serra do Cipó, Minas Gerias, Brazil: Boletim Botânico, v. 18, p. 21–27.

Mercader J, Bennett T, Esselmont C, Simpson S, Walde D. 2011. Soil phytoliths from miombo woodlands in Mozambique. *Quaternary Research* **75**: 138–150.

Metcalf CR. 1960. *Anatomy of the Monocotyledons I. Gramineae*. London: UK: Oxford University Press.

Metcalfe CR, Chalk L. 1979. 12/17/13 1:14 PM*Anatomy of the dicotyledons, Vol. I Systematic anatomy of the leaf and stem*. Oxford, UK: Oxford University Press.

Motomura H, Fujii T, Suzuki M. 2000. Distribution of silicified cells in the leaf blades of Pleioblastus chino (Franchet et Savatier) Makino (Bambusoideae). *Annals of Botany* **85**: 751–757.

Mulkey SS. 1986. Photosynthetic acclimation and water-use efficiency of three species of understory herbaceous bamboo (Gramineae) in Panama. *Oecologia* **70**: 514–519.

Nardini A, Gortan E, Salleo S. 2005. Hydraulic efficiency of the leaf venation system in sun- and shade-adapted species. *Functional Plant Biology* **32**: 953–961.

Osborne CP, Freckleton, RP. 2009. Ecological selection pressures for C_4 photosynthesis in the grasses. *Proceedings of the Royal Society B.* doi: 10.1098/rspb.2008.1762.

Piperno DR. 2006. *Phytoliths: a comprehensive guide for archaeologists and paleoecologists*. New York, USA: AltaMira Press.

Raghavan, M., Ma, B., Harbaugh, R., Quantified aneurysm shape and rupture risk: Journal of Neurosurgery **102**: 355–362.

R Development Core Team (2008). R: A language and environment for statistical computing. R Foundation for Statistical Computing, Vienna, Austria. ISBN 3-900051-07-0, URL http://www.R-project.org.

Rahim MA, Fordham R. 1991. Effect of shade on leaf and cell size and number of epidermal cells in garlic (*Allium sativum*). *Annals of Botany* **67**: 167–171.

Ruhland CT, Day TA. 2000. Effects of ultraviolet-B radiation of leaf elongation, production and phenylpropanoid concentrations of *Deschampsia antarctica* and *Colobanthus quitensis* in Antarctica. *Physiologia Plantarum* **109**: 244–251.

Russell SH, Evert RF. 1985 Leaf vasculature in Zea mays L. *Planta* **164**: 448–458.

Sack, L, Cowan PD, Jaikumar N, Holbrook NM. 2003. The 'hydrology' of leaves: co-ordination of structure and function in temperate woody species. *Plant, Cell & Environment* **26**: 1343–1356.

Sack L, Melcher P, Liu WH, Middleton E, Pardee T. 2006. How strong is intracanopy leaf plasticity in temperate deciduous trees? *American Journal of Botany* **93**: 829–839.

Sankaran, M, Ratnam, J, Hanan, N. 2008. Woody cover in African savannas: the role of resources, fire and herbivory. *Global Ecology and Biogeography* **17**: 236–245.

Schramm R. 1912. Über die anatomischen Jugendformen der Blätter einheimischer Holzpflanzen. *Flora* **104**: 225–295.

Schuster W. 1908. Die Blattaderung des dictoylenblattes und ihre Abhängigkeit von äusseren Einflüssen. Berichte der Deutschen Botanischen Gesellschaft. **26**: 194–237.

Scholes RJ, Archer SR. 1997. Tree-grass interactions in savannas. *Annual Review of Ecology and Systematics* **28**: 517–544.

Smith H. 1982. Light quality, photoperception, and plant strategy. *Annual Reviews of Plant Physiology* **33**: 481–518.

Strömberg, C.A.E**.**, 2003. The origin and spread of grass-dominated ecosystems during the Tertiary of North America and how it relates to the evolution of hypsodonty in equids. Ph.D. thesis, Department of Integrative Biology, University of California at Berkeley. 779 pp.

Strömberg CAE. 2004. Using phytolith assemblages to reconstruct the origin and spread of grass-dominated habits in the Great Plains of North America during the late Eocene to early Miocene. *Palaeogeography, Palaeoclimatology, Palaeoecology* **207**: 239–275.

Strömberg CAE. 2005. Decoupled taxonomic radiation and ecological expansion of open-habitat grasses in the Cenozoic of North America. *Proceedings of the National Academy of Sciences of the United States of America* **102**: 11980–11984.

Strömberg CAE. 2006. Evolution of hypsodonty in equids: testing a hypothesis of adaptation. *Paleobiology* **32**: 236–258.

Strömberg CAE. 2007. The spread of grass-dominated habitats in Turkey and surrounding areas during the Cenozoic: Phytolith evidence. *Palaeogeography, Palaeoclimatology, Palaeoecology* **250**: 18–49.

Strömberg CAE. 2011. Evolution of grasses and grassland ecosystems. *Annual Review of Earth and Planetary Sciences* **39**: 517–544.

Strömberg CAE, Dunn RE, Madden RH, Kohn MJ, Carlini A. 2013. Decoupling the spread of grasslands from the evolution of "grazers" in South America. Nature Communications. DOI: 10.1038/ncomms250.

Talbert CM, Holch AE. 1957. A study of the lobing of sun and shade leaves. *Ecology* **38**: 655–658.

Thorn, V.C., 2004, Phytoliths from subantarctic Campbell Island: plant production and soil surface spectra: Review of Palaeobotany & Palynology, v. 132, p 37-59.

Thomas PW, Woodward IF, Quick WP. 2003. Systemic irradiance signaling in tobacco: *New Phytologist* **161**: 193–198.

Tiedemann, A.R., Klemmedson, J.O., and Ogden, P.R., 1971, Response of four perennial southwestern grasses to shade: Journal of Range Management, v. 24, p. 442–447.

Uhl D, Walther H. 2000. Sun leaf or shade leaf?–Known facts in the light of new data with implications for palaeobotany. *Feddes Repertorium* **111**: 165–174.

Veblin TT. 1982. Growth patterns of *Chusquea* bamboos in the understory of Chilean *Nothofagus* forest and their influences in forest dynamics. *Bulletin of the Torrey Botanical Club* **109**: 474–487.

Wargent JJ, Moore JP, Ennos AR, Paul ND. 2009. Ultraviolet radiation as a limiting factor in leaf expansion and development. *Photochemistry and Photobiology* **85**: 279–286.

Watson L, Dallwitz MJ. 1992 onwards. Grass genera of the world: Descriptions, illustrations, identification, and information retrieval; including synonyms, morphology, anatomy, physiology, phytochemistry, cytology, classification, pathogens, world and local distribution, and references. Version: 23rd April 2010.

Watson RW. 1942. The effect of cuticular hardening on the form of epidermal cells. *New Phytologist* **41**: 223–229.

Widmer Y. 1998. Pattern and performance of understory bamboos (Chusquea spp.) under different canopy closures in old-growth oak forests in Costa Rica. *Biotropica* **30**: 400–415.

Wylie, RF. 1939. Relations between tissue organization and vein distribution in dicotyledon leaves. *American Journal of Botany* **26**: 219-225.

Wylie RF. 1949. Differences in foliar organization among leaves from four locations in the crown of an isolated tree (*Acer platanoides*). *Proceedings of the Iowa Academy of Sciences* **38:** 355–361.

Zheng Y, Dong Y, Matsui A, Udatsu T, Fujiwara H. 2003**.** Molecular Genetic Basis of Determining Subspecies of Ancient Rice Using the Shape of Phytoliths: *Journal of Archaeological Science* **30**: 1215–1221

Zucol, A. F., Brea, M., and Bellosi, E. S., 2010, Phytolith studies in Gran Barranca (central Patagonia, Argentina): the middle–late Eocene, *in* Madden, R.H., Carlini, A.A., Vucetich, M.G., and Kay, R.F., *eds.,* The Paleontology of Gran Barranca: Evolution and Environmental Change through the Middle Cenozoic of Patagonia: Cambridge, UK, Cambridge University Press, p. 317–340.

Table 3.1. Means of total biomass and leaf measurements

Species	% Light	Total Dry Biomass[1] (g)	Leaf Length (cm)	Leaf Width (cm)	Leaf Area[2] (cm^2)
CC	20	–	7.56 (1.16)	**0.67 (0.13)**^{*100}	5.22 (1.83)
CC	60	–	7.43 (0.66)	0.72 (0.07)	5.42 (0.64)
CC	100	–	7.32 (0.92)	**0.8 (0.12)**^{*20}	5.97 (1.58)
CC	120	–	7.22 (0.27)	0.76 (0.12)	5.25 (0.99)
PS	20	**0.19 (0.12)**^{**100,*60,120}	**15.18 (4.09)**^{**100,120}	0.17 (0.04)	**2.71 (1.17)**^{*120}
PS	60	**2.05 (0.96)**^{*20}	**14.72 (2.2)**^{**100,120}	0.21 (0.02)	**3.13 (0.68)**^{**100,**120}
PS	100	**2.86 (0.71)**^{**20}	**10.39 (0.56)**^{**20,60}	0.2 (0.04)	**2.07 (0.29)**^{**60}
PS	120	**1.86 (1.41)**^{*20}	**10.11 (2.24)**^{**20,60}	0.17 (0.03)	**1.73 (0.49)**^{**20,**60}
SA	20	**0.15 (0.04)**^{**100,120}	42.36 (10.61)	**0.17 (0.02)**^{**all}	**7.82 (2.44)**^{*100}
SA	60	**1.2 (0.51)**^{**100,120}	32.89 (13.87)	**0.29 (0.09)**^{**20,*100,120}	10.26 (5.91)
SA	100	**5.22 (0.56)**^{**all}	39.75 (11.67)	**0.39 (0.05)**^{**20,*60}	**16.86 (6.41)**^{*20}
SA	120	**6.85 (1.12)**^{**all}	27.74 (9.63)	**0.39 (0.08)**^{**20,*60}	11.91 (6.38)
SS	20	**0.13 (0.04)**^{**100,120}	**21.3 (6.22)**^{**120}	**0.19 (0.02)**^{**all}	**4.21 (1.63)**^{**60,100}
SS	60	**1.02 (0.37)**^{**100,120}	**20.67 (4.54)**^{*120}	**0.33 (0.07)**^{**20}	**7.16 (2.71)**^{**20}
SS	100	**3.63 (0.81)**^{**20,60}	18.95 (4.42)	**0.39 (0.07)**^{**20}	**7.31 (1.36)**^{**20}
SS	120	**3.09 (2.07)**^{**20,*60}	**14.58 (1.84)**^{**20,*60}	**0.33 (0.07)**^{**20}	4.95 (1.34)
SV	20	**0.5 (0.16)**^{**100,120}	**31.52 (6.95)**^{*60}	**0.27 (0.03)**^{**100,120,*60}	**8.99 (2.86)**^{*60}
SV	60	**3.55 (0.67)**^{**100,120}	**45.05 (12.05)**^{*20}	**0.39 (0.12)**^{*20}	**18.61 (7.88)**^{*20}
SV	100	**11.19 (3.16)**^{**20,60}	33.99 (9.61)	**0.44 (0.08)**^{**20}	16.72 (7.71)
SV	120	**12.43 (2.52)**^{**20,60}	35.05 (7.24)	**0.42 (0.09)**^{**20}	15.56 (5.51)

Notes: [1]Total Dry Biomass is mass of whole plants (shoots and roots), washed of soil and dried (n=5 plants per treatment). Standard error in parentheses. Df = 3 for all ANOVA analyses per species. Leaf measurements are means of 3 leaves per plant, 5 plants per treatment/species for a total n=15 leaves per analysis. [2]Leaf Area calculated as (leaf length x leaf width). Significant means are bolded ($\alpha \leq 0.05$). (*) denotes P-values ≤ 0.05; (**) denotes P-values ≤ 0.01. Numbers in superscript refers to treatment/s that the sample varies from significantly (Tukey's Tests). Species abbreviations are: (CC) = *Chusquea culeo*; (PS) = *Poa secunda*; (SA) = *Sporobolus asper*; (SS) = *Schizachyrium scoparius*; (SV) = *Stipa viridula*.

Table 3.2. All Plant Means per Treatment

Species (abbr.)	Cell Type	% Light	n (cells)	Mean UI	Mean Area (μm^2)	Mean Length (μm)	Mean Width (μm)
CC	Long	20	292	0.38 (0.03)	933 (163)	94 (15)	16 (2)
		60	333	0.37 (0.05)	1010 (200)	95 (14)	18 (5)
		100	279	0.39 (0.03)	945 (108)	96 (8)	16 (1)
		120	194	0.38 (0.03)	1024 (213)	95 (10)	17 (3)
PS	Long	20	419	0.34 (0.04)	**4388 (516)**^{**120}	**382 (40)**^{**100,120,*60}	**17 (1)**^{**100}
		60	427	0.32 (0.03)	**4257 (778)**^{**120}	**334 (42)**^{*20,120}	19 (2)
		100	436	0.32 (0.03)	3805 (438)	**295 (38)**^{**20}	**20 (2)**^{**20,**120}
		120	432	0.32 (0.03)	**3404 (825)**^{**20,60}	**287 (54)**^{**20,*60}	**17 (1)**^{**100}
SA	Long	20	308	0.40 (0.03)	**1190 (150)**^{*120}	**138 (12)**^{**60,120,*100}	15 (2)
		60	262	0.42 (0.03)	1122 (94)	**123 (11)**^{**20,*120}	16 (1)
		100	298	0.42 (0.03)	1127 (136)	**124 (12)**^{*20,120}	16 (2)
		120	285	0.40 (0.02)	**1030 (164)**^{*20}	**112 (13)**^{**20,*60,100}	15 (2)
SS	Long	20	619	0.34 (0.03)	**3514 (571)**^{*100,**120}	**188 (22)**^{**all}	27 (4)
		60	623	**0.35 (0.03)**^{*120}	3223 (797)	**161 (23)**^{**20,120}	29 (4)
		100	718	**0.35 (0.02)**^{*120}	**2909 (426)**^{*20}	**149 (11)**^{**20,*120}	28 (3)
		120	654	**0.32 (0.03)**^{*60,100}	**2728 (636)**^{**20}	**130 (19)**$^{**20, 60,*100}$	30 (4)
SV	Long	20	246	**0.31 (0.04)**^{**100}	**1880 (305)**^{**100,120}	**195 (26)**^{**all}	**14 (2)**^{**60,*100,120}
		60	251	0.34 (0.03)	**1757 (389)**^{**100,120}	**160 (24)**^{**all}	**16 (2)**^{**20}
		100	283	**0.35 (0.03)**^{**20}	**1304 (311)**^{**20,60}	**125 (20)**^{**20,60}	**16 (2)**^{*20}
		120	254	0.34 (0.03)	**1326 (423)**^{**20,60}	**127 (28)**^{**20,60}	**16 (2)**^{*20}
CC	Short	20	262	0.34 (0.02)	**85 (8)**^{*120}	14 (1)	9 (1)
		60	308	0.33 (0.02)	92 (13)	14 (1)	10 (1)
		100	273	0.33 (0.03)	97 (16)	14 (2)	10 (1)
		120	292	0.34 (0.02)	**98 (11)**^{*20}	15 (1)	10 (1)
PS	Short	20	653	0.29 (0.02)	**649 (102)**^{**120,*100}	**71(11)**^{**120}	**13 (2)**^{**120}
		60	584	0.30 (0.02)	564 (90)	67 (7)	12 (1)
		100	794	0.30 (0.03)	**538 (85)**^{*20}	62 (8)	12 (1)
		120	735	0.29 (0.03)	**473 (100)**^{**20}	**60 (11)**^{**20}	**11 (1)**^{**20}
SA	Short	20	426	0.30 (0.02)	132 (27)	14.8 (1.4)	12.6 (1.4)
		60	371	0.30 (0.02)	133 (19)	15.1 (1)	12.4 (1.3)
		100	442	0.29 (0.02)	147 (22)	15.6 (1.3)	13.1 (1.4)
		120	396	0.29 (0.01)	144 (19)	15.5 (0.8)	12.9 (1.2)
SS	Short	20	560	0.36 (0.03)	212 (37)	**30 (4)**^{**120}	11 (1)
		60	720	0.36 (0.02)	201 (30)	**29 (4)**^{*120}	11 (1)
		100	684	0.36 (0.02)	210 (39)	**29 (3)**^{*120}	11 (1)
		120	721	0.36 (0.03)	190 (44)	**25 (4)**^{**20,*60,100}	12 (1)
SV	Short	20	336	0.30 (0.02)	**261 (36)**^{*100}	**37 (3)**^{**120,100,*60}	**10 (1)**^{**60,120,*100}
		60	337	0.31 (0.02)	**261 (38)**^{*100}	**33 (4)**^{*20,100,**120}	**12 (1)**^{**20}
		100	462	0.32 (0.03)	**219 (33)**^{*20,60}	**28 (4)**^{**20,*60}	**11 (1)**^{*20}
		120	494	0.30 (0.03)	225 (53)	**28 (5)**$^{**20.60}$	**12 (1)**^{**20}

Notes: Bold font indicates means that are significant ($\alpha = 0.05$) as determined from one-way ANOVA tests with post-hoc Tukeys tests. (*) denotes p-values ≤ 0.05; (**) denotes p-values ≤ 0.01. Numbers in superscript refers to treatment/s that the sample varies from significantly (Tukey's Tests). All *P*-values can be found in Table S1 in the supplementary data file. Species abbreviations are: CC = *Chusquea culeo*; PS = *Poa secunda*; SA = *Sporobolus asper*; SS = *Schizachyrium scoparius*; SV = *Stipa viridula*.

Table 3.3. *P*- and F-values for one-way ANOVA tests.

Species	**CC**		**PS**		**SA**		**SS**		**SV**	
Variable	*P*	F	*P*	F	*P*	F	*P*	F	*P*	F
Long Cell UI										
ANOVA	0.6098	0.612	0.4389	0.916	0.0901	2.271	**0.0175**	3.665	0.0060	4.592
Tukey's										
120-20	1.0000		0.5429		0.9997		0.2640		0.0714	
100-20	0.8403		0.4742		0.2141		0.8413		**0.0039**	
60-20	0.9572		0.6035		0.2788		0.6341		0.0714	
120-60	0.9584		0.9967		0.3232		**0.0185**		0.9999	
120-100	0.8379		0.9994		0.2518		**0.0472**		0.6932	
100-60	0.5446		0.9966		0.9987		0.9831		0.7026	
Long Ccll Length										
ANOVA	0.9546	0.108	**3.7E-07**	14.651	**2.4E-06**	12.435	**5.2E-10**	23.6300	**1.5E-10**	25.603
Tukey's										
120-20	0.9869		**1.3E-06**		**6.0E-07**		**0**		**0**	
100-20	0.9411		**6.9E-06**		**0.0131**		**7.0E-06**		**0**	
60-20	0.9888		**0.0197**		**0.0059**		**0.0017**		**0.0024**	
120-60	0.9999		**0.0279**		**0.0500**		**0.0003**		**0.0034**	
120-100	0.9954		0.9705		**0.0246**		**0.0354**		0.9968	
100-60	0.9944		0.0819		0.9922		0.3865		**0.0018**	
Long Cell Width										
ANOVA	0.1844	1.667	**0.0014**	5.921	0.1350	1.931	0.2192	1.520	**0.0023**	5.481
Tukey's										
120-20	0.6517		0.9974		0.6086		0.2401		**0.0227**	
100-20	0.9999		**0.0070**		0.2148		0.8798		**0.0142**	
60-20	0.2491		0.1650		0.1418		0.3576		**0.0029**	
120-60	0.8911		0.1117		0.7806		0.9948		0.8916	
120-100	0.6794		**0.0040**		0.8853		0.6559		0.9981	
100-60	0.2690		0.5808		0.9963		0.7985		0.9488	
Long Cell Area										
ANOVA	0.3941	1.012	**0.0005**	6.930	**0.0242**	3.388	**0.0055**	4.673	**2.2E-05**	10.014
Tukey's										
120-20	0.4965		**0.0008**		**0.0132**		**0.0055**		**0.0005**	
100-20	0.9979		0.0860		0.6006		**0.0483**		**0.0003**	
60-20	0.6301		0.9490		0.5422		0.5796		0.7862	
120-60	0.9964		**0.0043**		0.2741		0.1404		**0.0098**	
120-100	0.6081		0.3513		0.2335		0.8539		0.9984	
100-60	0.7388		0.2505		0.9997		0.5152		**0.0061**	
Short Cell UI										
ANOVA	0.4438	0.907	0.3931	1.014	0.2507	1.405	0.6293	0.582	0.2149	1.537
Tukey's										
120-20	0.8898		0.9963		0.6427		0.7864		0.9988	
100-20	0.9052		0.7952		0.4447		0.5890		0.2942	
60-20	0.9279		0.4049		0.9993		0.9304		0.9125	
120-60	0.5176		0.5349		0.5366		0.9874		0.8528	
120-100	0.4759		0.8960		0.9878		0.9874		0.2296	
100-60	0.9999		0.9152		0.3437		0.9113		0.6778	

Short Cell Length										
ANOVA	0.133	1.9422	**0.0075**	4.406	0.1918	1.633	**0.0016**	5.808	**5.2E-08**	17.106
Tukey's										
120-20	0.1849		**0.0083**		0.3723		**0.0020**		**3.0E-7**	
100-20	0.7185		0.0571		0.2081		0.8711		**2.5E-6**	
60-20	0.9999		0.6580		0.9001		0.9407		**0.0459**	
120-60	0.1817		0.1437		0.7623		**0.0111**		**0.0033**	
120-100	0.7343		0.8833		0.9840		**0.0189**		0.9338	
100-60	0.7350		0.4811		0.5400		0.9974		**0.0183**	
Short Cell Width										
ANOVA	0.0920	2.258	**0.0181**	3.639	0.2389	1.447	0.2445	1.427	0.0027	5.331
Tukey's										
120-20	0.0962		**0.0103**		0.7418		0.4408		**0.0046**	
100-20	0.1530		0.6579		0.5302		0.9969		**0.0310**	
60-20	0.2700		0.3354		0.9774		0.9660		**0.0093**	
120-60	0.9452		0.4144		0.4676		0.2105		0.9949	
120-100	0.9956		0.1679		0.9851		0.5669		0.9022	
100-60	0.9883		0.9484		0.2763		0.9069		0.9706	
Short Cell Area										
ANOVA	**0.0220**	3.479	**6.3E-05**	8.929	0.1828	1.674	0.5033	0.792	0.0065	4.535
Tukey's										
120-20	**0.0253**		**2.0E-05**		0.4961		0.5272		0.0930	
100-20	0.0553		**0.0110**		0.2885		0.9989		**0.0376**	
60-20	0.4769		0.0734		0.9991		0.8522		1.0000	
120-60	0.4258		0.0534		0.5512		0.9436		0.0841	
120-100	0.9879		0.2478		0.9806		0.6187		0.9805	
100-60	0.6254		0.8807		0.3259		0.9123		**0.0336**	

Notes: For all one-way ANOVA tests, df = 3,56. Bold font indicates significant p-values ($P<0.05$).

Table 3.4. Significance (P-values) and R^2 values for linear regressions of leaf and cell parameter comparisons.

Species	Cell Type	P & R^2 values	Cell Area & Leaf Area	Cell Length & Leaf length	Cell Width & Leaf Width
CC	Long	P	0.0020	0.0478	0.4430
		R^2	0.007	0.002	-
PS	Long	P	<0.0001	<0.0001	0.0080
		R^2	0.0230	0.041	0.004
SA	Long	P	0.2980	<0.0001	0.0060
		R^2	-	0.0140	0.060
SS	Long	P	0.0317	<0.0001	0.0450
		R^2	0.001	0.042	0.001
SV	Long	P	0.0060	0.7190	<0.0001
		R^2	0.006	-	0.069
CC	Short	P	0.3810	0.2430	<0.0001
		R^2	-	-	0.012
PS	Short	P	<0.0001	0.1820	<0.0001
		R^2	0.008	-	0.007
SA	Short	P	<0.0001	0.0230	<0.0001
		R^2	0.063	0.003	0.043
SS	Short	P	0.0220	<0.0001	0.3820
		R^2	0.002	0.015	-
SV	Short	P	<0.0001	0.3460	<0.0001
		R^2	0.034	-	0.008

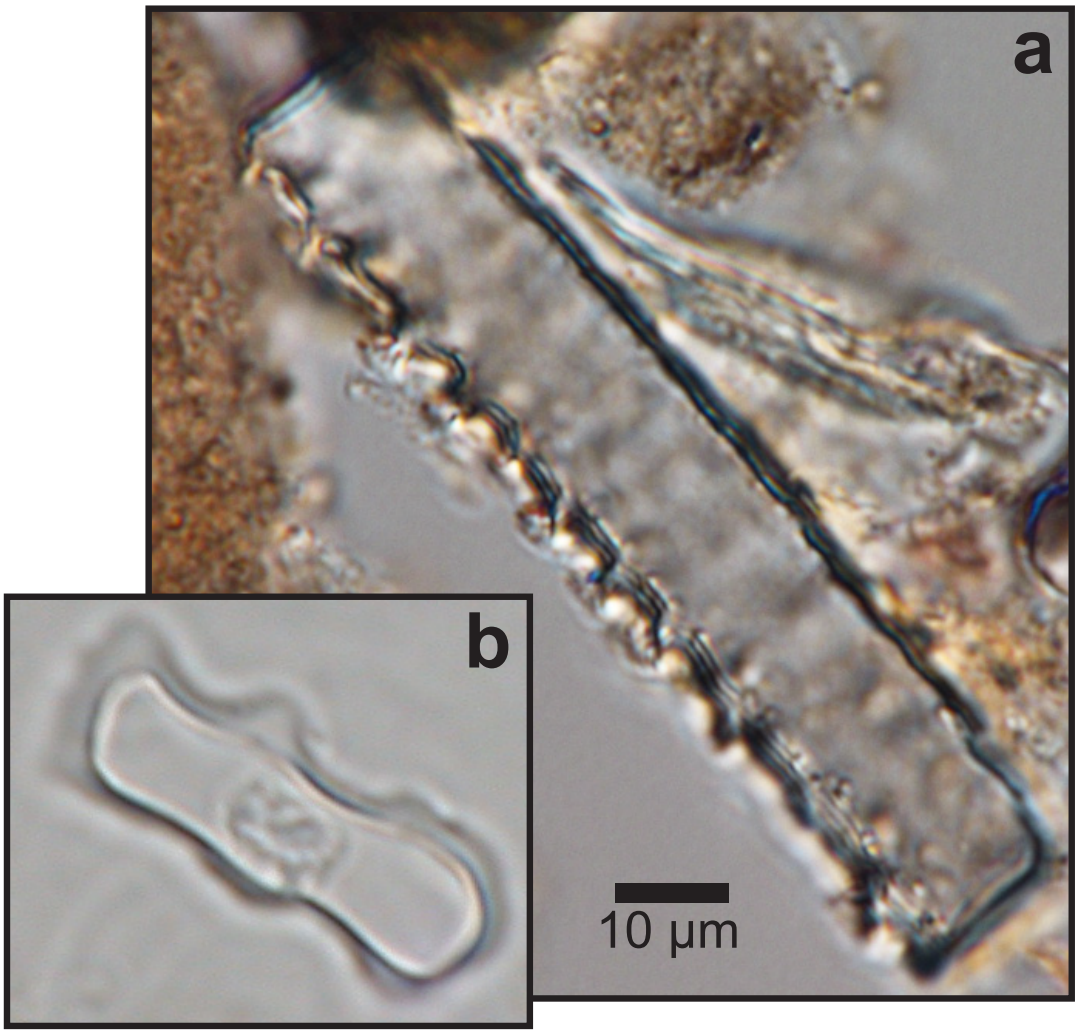

Fig 3.1. Examples of fossil phytoliths extracted from the Sarmiento Formation (42 Ma), Gran Barranca, Argentina: a) long cell phytolith; b) polylobate GSSC.

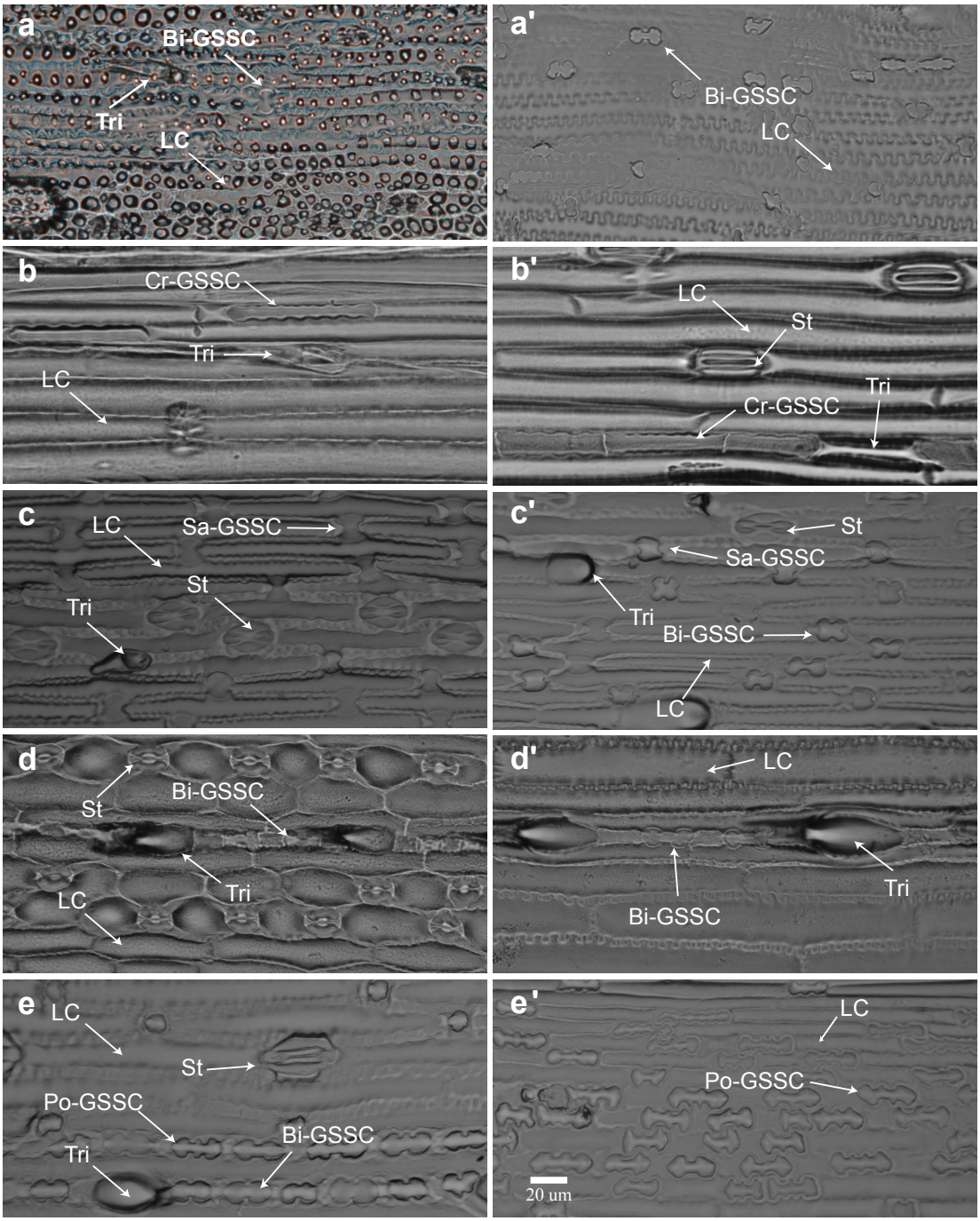

Fig. 3.2. Photographs of epidermal peels for the five species of grass grown. Left side of figure (A-E) are abaxial surfaces. Right side are adaxial surfaces (A'-E'). (A,A'): Chusquea culeo; (B,B'): Poa secunda; (C,C'): Sporobolus asper; (D,D'): Schizachyrium scoparius; (E,E'): Stipa viridula. GSSC = Grass Silica Short Cell; Bi = Bilobate; Sa = Saddle; Po = Polylobate; Cr = Crenate; Tri = Trichome; LC = Long Cell; St= Stomata.

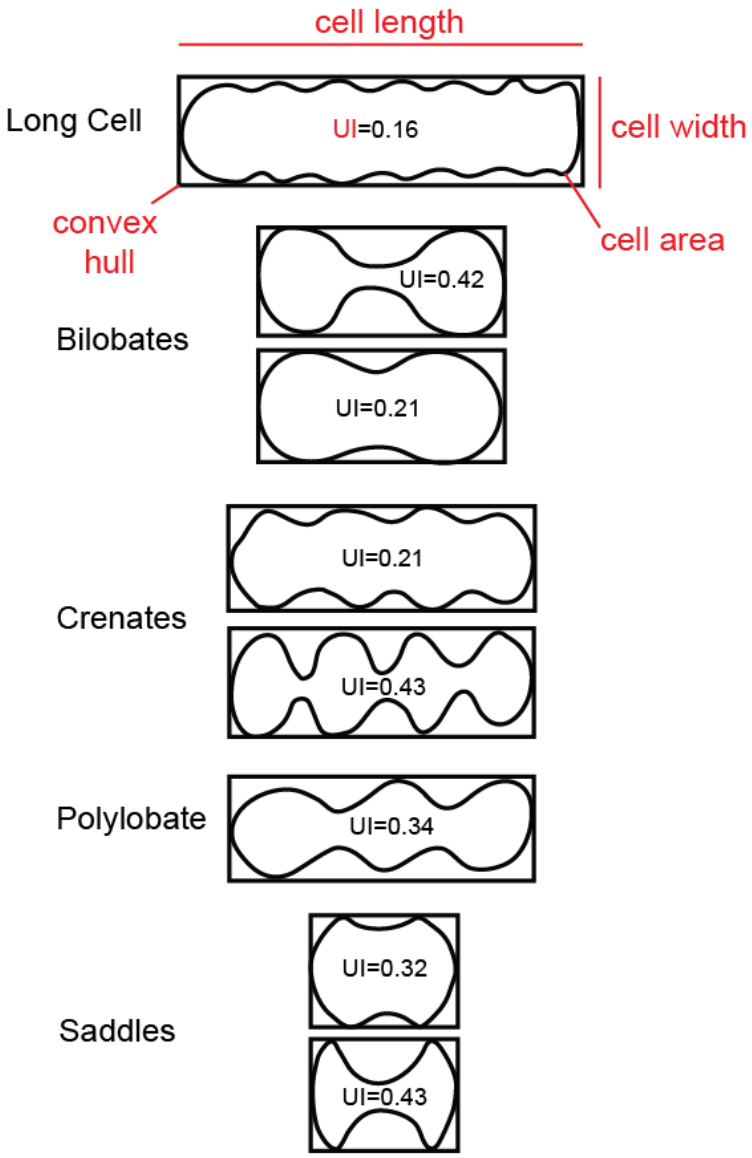

Fig. 3.3. Demonstration of cell measurements and cell types. Length is the long axis of the cell, width the short axis, and area is the area contained within the cell. The convex hull is the rectangular shape that encompasses all parts of the cell outlines. UI (Undulation Index) values are indicated within each of the hypothetical cells to show how UI values differ among cell shapes. Cell considered more undulated have higher UI values.

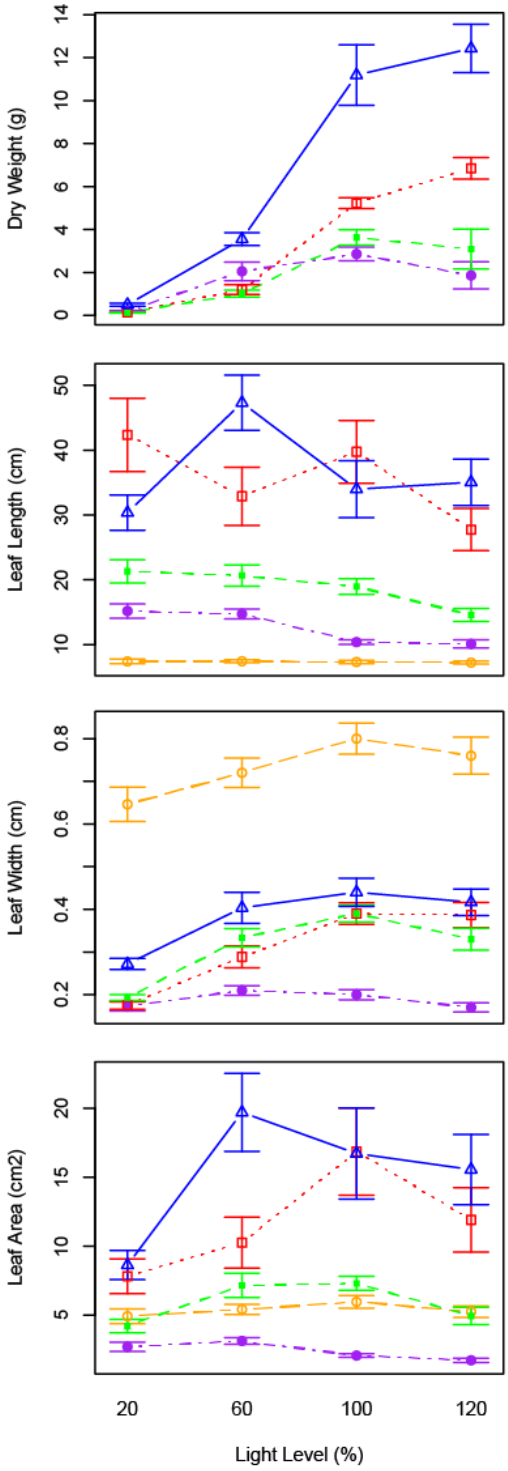

Fig. 3.4. Relationship between mean plant biomass and leaf measurements with irradiance (% light), with 95% confidence intervals: (A) total dry biomass of grass plants; (B) leaf length; (C) leaf width; and (D) leaf area. See Table 3.1 for values. Yellow open circles = *Chusquea culeo* (CC); purple closed circles = *Poa secunda* (PS); red open squares = *Sporobolus asper* (SA); green closed squares = *Schizachyrium scoparium* (SS); and blue triangles = *Stipa viridula* (SV).

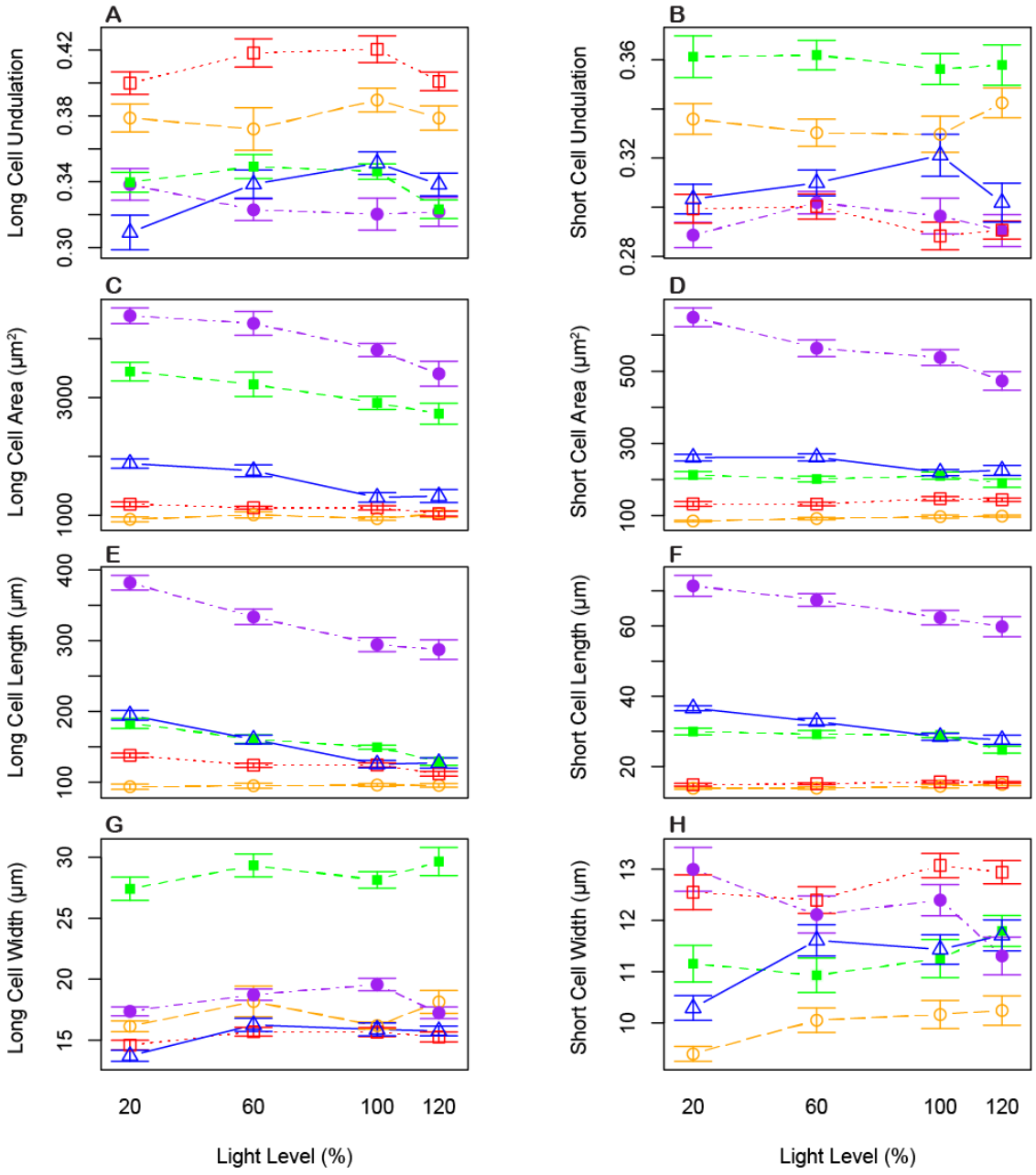

Fig. 3.5. Relationship between mean cell measurements and irradiance (% light) with 95% confidence intervals: (A) long cell UI, (B) short cell UI, (C) long cell area, (D) short cell area, (E) long cell length, (F) short cell length, (G) long cell width, (H) short cell width. See Table 3.2 for values. Yellow open circles = *Chusquea culeo* (CC); purple closed circles = *Poa secunda* (PS); red open squares = *Sporobolus asper* (SA); green closed squares = *Schizachyrium scoparium* (SS); and blue triangles = *Stipa viridula* (SV).

CHAPTER IV: Major habitat change in Patagonia pre-dates Eocene-Oligocene Transition: A record of Leaf Area Index based on a new proxy from phytoliths

ABSTRACT

Difficulty quantifying habitat change in the fossil record has hampered our understanding of the effect of climate change on vegetation structure in deep time. We present a new method for reconstructing Leaf Area Index (LAI) using the phytolith morphology of pavement cells from leaf epidermis. Using the new proxy, we reconstructed LAI from phytolith assemblages from Patagonia, Argentina between 50 and 11 Ma in the Cenozoic. Significant opening-up of habitats pre-dated the Eocene-Oligocene transition by 4 million years, indicating a possible link between habitat structure, cooling temperatures, and the opening of the Drake Passage in the middle Eocene. Habitats became closed again during the Middle Miocene Climatic Optimum (~15 Ma).

INTRODUCTION

Vegetation structure is a key component of the terrestrial biosphere that directly relates to primary productivity, hydrological cycling, carbon reservoirs, fluxes in energy and atmospheric gases, fire regime, soil properties, erosion and composition of mammalian faunas (*1*, *2*). Much effort has gone into predicting how vegetation will change with future climate, but comparatively little work has been done to understand how climate change effected vegetation structure in the past. This gap exists largely because there is no reliable way to quantify habitat structure in the fossil record.

Here we present a novel, phytolith (plant silica) based proxy for estimating Leaf Area Index [LAI, the one-sided leaf area per unit area of ground], a key parameter for quantifying vegetation structure in ecological studies (*1*). Our method uses morphological variation in leaf epidermal cells (and the phytoliths derived from them) of non-grass plants (dicots, non-herbaceous monocots, and ferns). To demonstrate the utility of this previously untapped paleobotanical archive, we apply the proxy towards constructing a record of LAI for the middle Cenozoic of Patagonia, We then compare LAI change to records of climate and mammalian evolution to address two outstanding questions in terrestrial paleoecology: 1) How did the structure of vegetation change in response to major Cenozoic (50-11 Ma) climatic fluctuations; and 2) how do changes in habitat type influence the evolution of hypsodonty, or high crowned, grazer-like tooth morphologies in mammals?

LAI proxy development–Cell patterning in leaf epidermis is determined by environmental conditions, principally light exposure (*3*). We focused on size and shape of pavement cells whose phytoliths are regularly preserved in modern and fossil soils (Fig. 4.1). In several eudicotyledonous taxa, these cell types are known to have larger area and more undulated outline when grown in shade (*3–5*). Based on this relationship, we hypothesized that epidermal cells and their phytoliths will on average be larger and more undulated in closed forest environments than open habitats, and that the relationship will be linear across a canopy density gradient. Because these types of phytoliths are taxonomically non-diagnostic, we cannot control for phylogenetic variation in cell morphology. Instead, we tested our hypotheses using pavement cell phytoliths in biosilica

assemblages extracted from modern surface soils collected across an LAI gradient in undisturbed areas of Costa Rica. Our sampling protocol for modern soils was designed to mimic our fossil phytolith sampling procedure (Appendix 3). Standardizing phytolith undulation through the Undulation Index (UI) (*4*), we compared mean phytolith UI (PUI) and mean phytolith area at each site to its measured LAI value and constructed a model to predict rLAI (reconstructed LAI) from these variables.

In the modern calibration dataset of 45 sample sites in Costa Rica (Table A3.1, Appendix 3), LAI is significantly correlated with site mean PUI (LAI = 13.92*μPUI - 17.31; R^2=0.59, SE=0.74, p<0.0001, Fig. 4.2a) and site mean phytolith area (eLAI=0.002762*μArea + 0.530964; R^2=0.44, SE=0.856, p<0.0001, Fig. 4.2b). A multiple regression analysis including both PUI and phytolith area improves the correlation with LAI (rLAI=0.001224*μArea + 10.411777*μPUI - 13.162070, R^2=0.63, SE=0.65, p<0.0001). On average, epidermal phytolith UI and area vary predictably with LAI where increasingly larger and more undulated soil phytoliths are found under denser and more complex canopies. Our model appears to be a robust way to reconstruct LAI from fossil phytolith assemblages.

Middle Cenozoic habitat change—In modern environments, LAI changes with atmospheric temperature, precipitation, and moisture seasonality (*6–8*). Middle Cenozoic (Eocene-Miocene) marine and terrestrial records document dramatic changes in temperature and precipitation over the last 50 million years, variation that appears to be intimately tied to the tectonic and thermal isolation of Antarctica (Fig. 4.3)(*9*). The narrow landmass of Patagonia is particularly sensitive to climatic conditions of the

surrounding Southern Ocean and in Antarctica. Its sedimentary record reflects Cenozoic climatic shifts as alternating sequences of fluvial (wet climate) and eolian (dry climate) deposition (*10*).

Anticlinal epidermal phytoliths along with other diverse forms are abundantly preserved in well-dated Cenozoic volcaniclastic paleosol sequences in Patagonia (Fig. 4.1) (*11–14*). Using our statistical model, we estimate rLAI values from 44 stratigraphic levels between 50 and 11 Ma (Fig. 4.3, Table A3.2 in Appendix 3).

Consistent with expectations, we find that rLAI values gradually declined from ~4 to ~0.6 between 49 and 32.3 Ma indicating that woody-plant and palm-dominated habitats became progressively more open during this long cooling interval. Habitats were maximally open (rLAI of <1) at 38 Ma and ~35–33 Ma. In contrast, we find no change in rLAI across the Eocene-Oligocene Transition (EOT-33.9 Ma) and into Oi-1. We interpret these changes in rLAI as a decline in canopy density from broad-leaved forest to more open habitats resembling extant scrub or dry sclerophyllous forests. We further suggest that the low rLAI events at 38 and 35-33 Ma indicate still more open environments dominated by palms and woody vegetation of low stature, possibly palm shrubland with low abundances of grass (*12*) (Table 4.1, Fig. 4.3D). The rare presence of mesic plants such as Zingiberales (gingers) between 41–37.1 Ma indicates relatively warm temperatures and sufficient rainfall during the growing season, yet the habitats were relatively open.

From the middle Oligocene to the early Miocene (30.77-18.9 Ma), rLAI values fluctuated between <1 and 2.4 indicating shifts between sparse vegetation and open forests. Beginning around 16 Ma, there appears to be a re-greening of Patagonia with

rLAI values peaking to 3.5 at 14.6 Ma. Periods of higher LAI, pointing to more closed habitats, coincide with known occurrences of primate fossils in Patagonia (*15*). By ca. 11.78 Ma, rLAI values trend downwards again.

The declining LAI values through the middle-late Eocene coincides with increased abundances of *Nothofagus* pollen in Patagonia (*16*). Thus, increased openness may have been linked to the replacement of thermophilic broad-leaved vegetation with more temperate deciduous elements. Middle Cenozoic macrofloras from Patagonia are not analogous to modern floras as they contain both tropical (e.g., Palmae, Anacardiaceae) and sub-Antarctic (e.g., *Nothofagus*, Podocarpaceae) components, including mesic and xeric elements of each. The sparse canopies of these "mixed paleofloras" (*17*) may, in part relate to decreased rainfall associated with Antarctic glaciation. Evidence for drying in Patagonia include macrofloral-based estimates of annual rainfall after ca. 40 Ma (*18*) and the appearance of arid-adapted pollen types by ca. 26 Ma (*16*). Additionally, paleosol-based estimates of precipitation show generally low, but fluctuating values throughout the interval (Fig. 4.3)(*19*). However, the high abundances of palms and rare gingers preclude extreme aridity typically associated with vegetation types with LAI <1. Rather, frequent input of volcanic tephra and other disturbances (increased herbivore pressure, fire) may have contributed to opening up Eocene-Miocene Patagonian landscapes.

The rLAI record tracks paleotemperature proxy data from deep water and sea surface foraminiferal $\delta^{18}O$ values (*20*, *21*), and local temperatures based on $\delta^{18}O$ values from tooth enamel (*22*). The gradual decline in rLAI during the Eocene is consistent with middle Eocene cooling in the marine record (Fig. 4.3). However, major habitat change

seems to have occurred as early as 38 Ma with pronounced openness predating the EOT (33.9 Ma) by 4 million years. These changes may have been a response to cooling and drying climates associated with opening of the Drake Passage and initiation of the Antarctic Circumpolar Current (*23*, *24*). We detect no major change in rLAI across the EOT and during the Oi-1. Habitats were already open (rLAI<1) by 35 Ma, and contained less than 2% grass cover. The rLAI record is therefore consistent with enamel $\delta^{18}O$ values that show no temperature change (*22*) and phytolith abundance data showing no vegetation alteration (*12*) across the EOT. However, eolian sedimentation rates dramatically increased from 30 mm/year to 170 mm/year beginning ~33.58 Ma (*11*) consistent with the intensification of zonal winds (*25*).

Previous work has indicated that low atmospheric pCO_2 promotes habitat openness by retarding post-fire tree seedling growth (*26*) and, conversely, that high pCO_2 boosts net primary productivity and LAI (*27*). In our study, whereas the gradual pCO_2 drop from 42 to 38 Ma does correspond to declining rLAI, the highest rLAI value (rLAI=3.5) in the middle Miocene (14.6 Ma) occurs during a time of decreasing pCO_2 (*28*). Therefore, at the current sample resolution, we cannot determine whether pCO_2 played a role in shaping vegetation structure through time, but with increased sampling, a better understanding of the interaction between atmospheric pCO_2 and vegetation structure may be possible.

Precocious hypsodonty–Recently, pollen and phytolith studies have rejected the classic assumption that early evolution of high crowned teeth (hypsodonty) in South America signaled the advent of open, grassland habitats (*12*, *29*). Instead, we argue that this

evolutionary trend relates to climatic cooling and drying associated with opening of the Drake Passage, which created more exposed and xeric habitats and which fundamentally changed the physical and chemical weathering properties of Patagonian pyroclastics. Intervals of coincident low LAI, decreased rainfall, and high eolian mineral particle flux correspond to the initiation of hypsodonty in several lineages of herbivores at 38 Ma and also in subsequent pulses during the Oligocene and early Miocene. Volcanism provided thick accumulations of highly vesicular, glass-rich, pyroclastic superabrasives susceptible to erosion and mobilization into animal diets. The sensitivity of Patagonian sediments to slight changes in temperature, rain and wind are reflected in coincident variation in leaf area index and pulses in mammalian tooth evolution.

ACKNOWLEDGEMENTS

This research was funded in part by National Science Foundation Grants DEB-1110354 to C.A.E. Strömberg and R.E. Dunn (Doctoral Dissertation Improvement Grant) and EAR-0819910 to C.A.E. Strömberg, EAR-0819842 to Richard Madden and EAR-0819837 to Matthew Kohn; Proyecto de Investigación en Ciencias y Técnicas 1860 of the Fondo Nacional de Ciencia y Tecnología (FONCyT), and funds from the Geological Society of America. We thank Guiomar Vucetich, Martín Ciancio, and Melanie Conner for field assistance during this project, Aiden Loeser for lab assistance and Pan American Energy for field support.

LITERATURE CITED

1. G. P. Asner, J. M. O. Scurlock, J. A. Hicke, Global synthesis of leaf area index observations: implications for ecological and remote sensing studies, *Global Ecology and Biogeography* **12**, 191–205 (2003).

2. R. F. Kay, R. H. Madden, C. Van Schaik, D. Higdon, Primate species richness is determined by plant productivity: implications for conservation, *Proceedings of the National Academy of Sciences of the United States of America* **94**, 13023–7 (1997).

3. R. W. Watson, the Effect of Cuticular Hardening on the Form of Epidermal Cells, *New Phytologist* **41**, 223–229 (1942).

4. W. M. Kurschner, The anatomical diversity of recent and fossil leaves of the durmast oak (*Quercus petraea* Lieblein/*Q. pseudocastanea* Goeppert) - implications for their use as biosensors of palaeoatmospheric CO2 levels, *Review of Palaeobotany and Palynology* **96**, 1–30 (1997).

5. P. W. Thomas, F. I. Woodward, W. P. Quick, Systemic irradiance signalling in tobacco, *New Phytologist* **161**, 193 –198 (2003).

6. R. Waring, Estimating forest growth and efficiency in relation to canopy leaf area, *Advances in Ecological Research* **13**, 327–354 (1983).

7. A. Iio, K. Hikosaka, N. P. R. Anten, Y. Nakagawa, A. Ito, Global dependence of field-observed leaf area index in woody species on climate: a systematic review, *Global Ecology and Biogeography* , DOI: 10.1111/geb.12133 (2013).

8. T. Luo, Y. Pan, H. Ouyang, P. Shi, Leaf area index and net primary productivity along subtropical to alpine gradients in the Tibetan Plateau, *Global Ecology and Biogeography* **13**, 345–358 (2004).

9. W. Sijp, M. England, Effect of the Drake Passage throughflow on global climate, *Journal of Physical Oceanography*, 1254–1266 (2004).

10. E. S. Bellosi, Loessic and fluvial sedimentation in Sarmiento Formation pyroclastics, middle Cenozoic of central Patagonia in *The paleontology of Gran Barranca: Evolution and environmental change through the middle Cenozoic of Patagonia*, R. H. Madden, A. A. Carlini, M. G. Vucetich, R. Kay, Eds. (Cambridge Univ Press, 2010), pp. 278–292.

11. R. E. Dunn *et al.*, A new chronology for middle Eocene-early Miocene South American Land Mammal Ages, *Geological Society of America Bulletin* **125**, 539–555 (2013).

12. C. A. E. Strömberg, R. E. Dunn, R. H. Madden, M. J. Kohn, A. A. Carlini, Decoupling the spread of grasslands from the evolution of grazer-type herbivores in South America, *Nature communications* **4**, 1478 (2013).

13. E. S. Bellosi, Physical stratigraphy of the Sarmiento formation (middle Eocene-lower Miocene) at Gran Barranca, central Patagonia, *The paleontology of Gran Barranca: evolution and environmental change through the middle Cenozoic of Patagonia. Cambridge University Press, New York* (2010).

14. A. F. Zucol, M. Brea, E. Bellosi, Phytolith studies in Gran Barranca (central Patagonia, Argentina): the middle-late Eocene, *The Paleontology of Gran Barranca: Evolution and Environmental Change through the Middle Cenozoic of Patagonia*, 317–340 (2010).

15. R. F. Kay, A new primate from the early Miocene of Gran Barranca, Chubut Province, Argentina: paleoecological implications, *The Paleontology of Gran Barranca: Evolution and Environmental Change Through the Middle Cenozoic of Patagonia*, 220 (2010).

16. V. Barreda, L. Palazzesi, Patagonian vegetation turnovers during the Paleogene-Early Neogene: Origin of arid-adapted floras, *The Botanical Review* **73**, 31–50 (2007).

17. E. Romero, Fossil Evidence Regarding the Evolution of *Nothofagus* Blume, *Annals of the Missouri Botanical Garden* **73**, 276–283 (1986).

18. L. F. Hinojosa, C. Villagrán, Did South American Mixed Paleofloras evolve under thermal equability or in the absence of an effective Andean barrier during the Cenozoic?, *Palaeogeography, Palaeoclimatology, Palaeoecology* **217**, 1–23 (2005).

19. E. S. Bellosi, M. G. Gonzalez, Paleosols of the middle Cenozoic Sarmiento Formation, central Patagonia, *The Paleontology of Gran Barranca: Evolution and Environmental Change through the Middle Cenozoic of Patagonia*, 293 (2010).

20. J. Zachos, M. Pagani, L. Sloan, E. Thomas, K. Billups, Trends, rhythms, and aberrations in global climate 65 Ma to present, *Science* **292**, 686–93 (2001).

21. S. M. Bohaty, J. C. Zachos, Significant Southern Ocean warming event in the late middle Eocene, *Geology* **31**, 1017–1020 (2003).

22. M. J. Kohn *et al.*, Climate stability across the Eocene-Oligocene transition, southern Argentina, *Geology* **32**, 621 (2004).

23. R. Livermore, C.-D. Hillenbrand, M. Meredith, G. Eagles, Drake Passage and Cenozoic climate: An open and shut case?, *Geochemistry Geophysics Geosystems* **8** (2007), doi:10.1029/2005GC001224.

24. H. D. Scher, E. E. Martin, Timing and climatic consequences of the opening of Drake Passage, *Science* **312**, 428–30 (2006).

25. R. H. Compagnucci, Atmospheric circulation over Patagonia from the Jurassic to present: a review through proxy data and climatic modelling scenarios, *Biological Journal of the Linnean Society* **103**, 229–249 (2011).

26. W. J. Bond, G. F. Midgley, F. I. Woodward, The importance of low atmospheric CO_2 and fire in promoting the spread of grasslands and savannas, *Global Change Biology* **9**, 973–982 (2003).

27. R. J. Norby *et al.*, Forest response to elevated CO_2 is conserved across a broad range of productivity, *Proceedings of the National Academy of Sciences of the United States of America* **102**, 18052–6 (2005).

28. D. J. Beerling, D. L. Royer, Convergent Cenozoic CO_2 history, *Nature Geoscience* **4**, 418–420 (2011).

29. L. Palazzesi, V. Barreda, Fossil pollen records reveal a late rise of open-habitat ecosystems in Patagonia, *Nature Communications* **3**, 1294 (2012).

30. S. Ganguly *et al.*, Generating vegetation leaf area index Earth system data record from multiple sensors. Part 2: Implementation, analysis and validation, *Remote Sensing of Environment* **112**, 4318–4332 (2008).

31. E. Gutiérrez, V. Vallejo, R. J, J. Fons, The Subantarctic *Nothofagus* forests of Tierra del Fuego: Distribution, structure and production, *Oecologica aquatica* **10**, 351–366 (1991).

32. W. Woodgate, An intercomparison of passive terrestrial remote sensing technologies to derive LAI and canopy cover metrics, *International Archives of the Photogrammetry, Remote Sensing and Spatial Information Sciences,* **XXXIX-B8**, 457–462 (2012).

33. G. P. Asner, C. E. Borghi, R. a. Ojeda, Desertification in Central Argentina: Changes in Ecosystem Carbon and Nitrogen From Imaging Spectroscopy, *Ecological Applications* **13**, 629–648 (2003).

34. M. Barradas, F. Novo, The Vertical Structure of Mediterranean Scrub in Doñana National Park (SW Spain), *Folia Geobotanica et Phytotaxonomica* **22**, 415–433 (1987).

35. V. Barraza, F. Grings, P. Ferrazzoli, M. Salvia, Monitoring Vegetation Moisture Using Passive Microwave and Optical Indices in the Dry Chaco, *IEEE Journal of Selected Topics in Applied Earth Observations and Remote Sensing*, 1–10 (2013).

36. Z. Zhu *et al.*, Global Data Sets of Vegetation Leaf Area Index (LAI)3g and Fraction of Photosynthetically Active Radiation (FPAR)3g Derived from Global Inventory

Modeling and Mapping Studies (GIMMS) Normalized Difference Vegetation Index (NDVI3g) for the Period 1981 to 2, *Remote Sensing* **5**, 927–948 (2013).

Table 4.1. LAI values from literature

Biome Type	Mean LAI	Min.	Max.	Reference
Wetlands	6.30	2.5	8.4	1
Tropical Evergreen Broad	4.80	1.5	8	1
Temp Evergreen Broadleaf	4.33	0.8	11.6	30; 1
Tropical Decid Broadleaf	3.90	0.6	8.9	1
Temp. Decid Broadleaf	3.56	0.6	5.08	30; 1
Nothofagus Evergreen	3.50	2.5	4.5	31
Nothofagus Decid	2.55	2.3	2.8	31
Sclerophyllous forest Aust.	2.40	-	-	32
Grasslands	1.75	0.08	5	30; 1
Monte	1.70	0.5	2.9	33
Mediterranean scub	1.50	1	4	34
Chaco	1.5	1	3	35
Savanna	1.49	0.78	1.72	30; 36
Sclerophyllous forest Aust.	0.95	-	-	32
Shrublands	0.77	0.1	4.5	30; 1
Desert	0.55	0.9	0.2	1

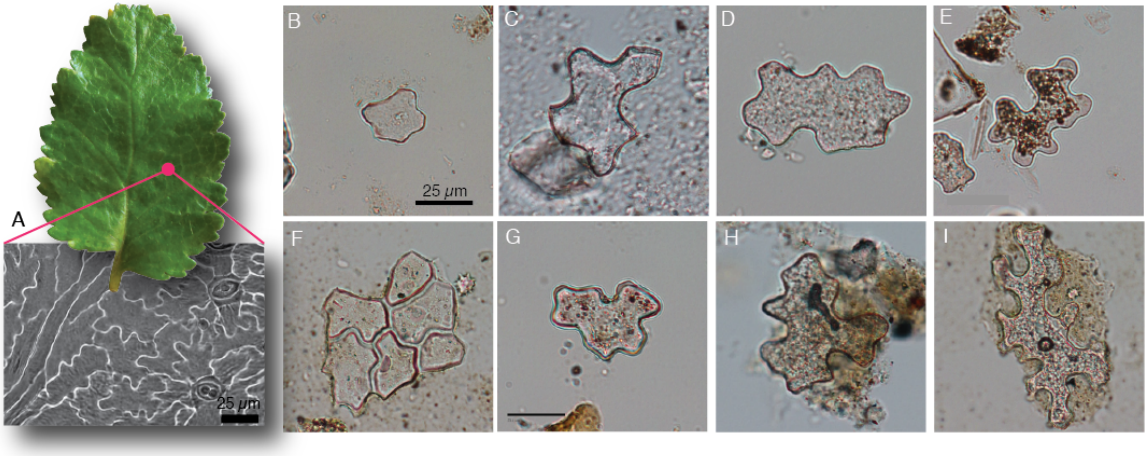

Figure 4.1. Leaf epidermis and examples of soil and fossil epidermal phytoliths. (A) *Nothofagus* leaf and epidermis; (B-E) fossil phytoliths; (F-I) soil phytoliths.

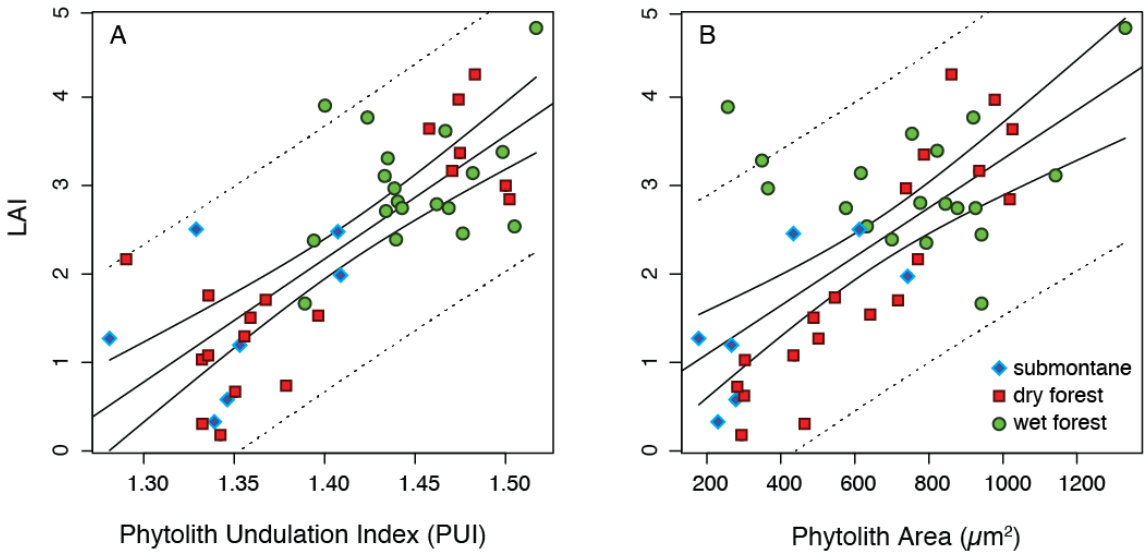

Figure 4.2. Modern soil phytolith variation relationship and LAI with 95% confidence intervals (solid lines) and 95% prediction intevals (dashed lines). (A) Mean Phytolith Undulation Index (PUI) related to LAI; (B) Mean phytolith area and LAI.

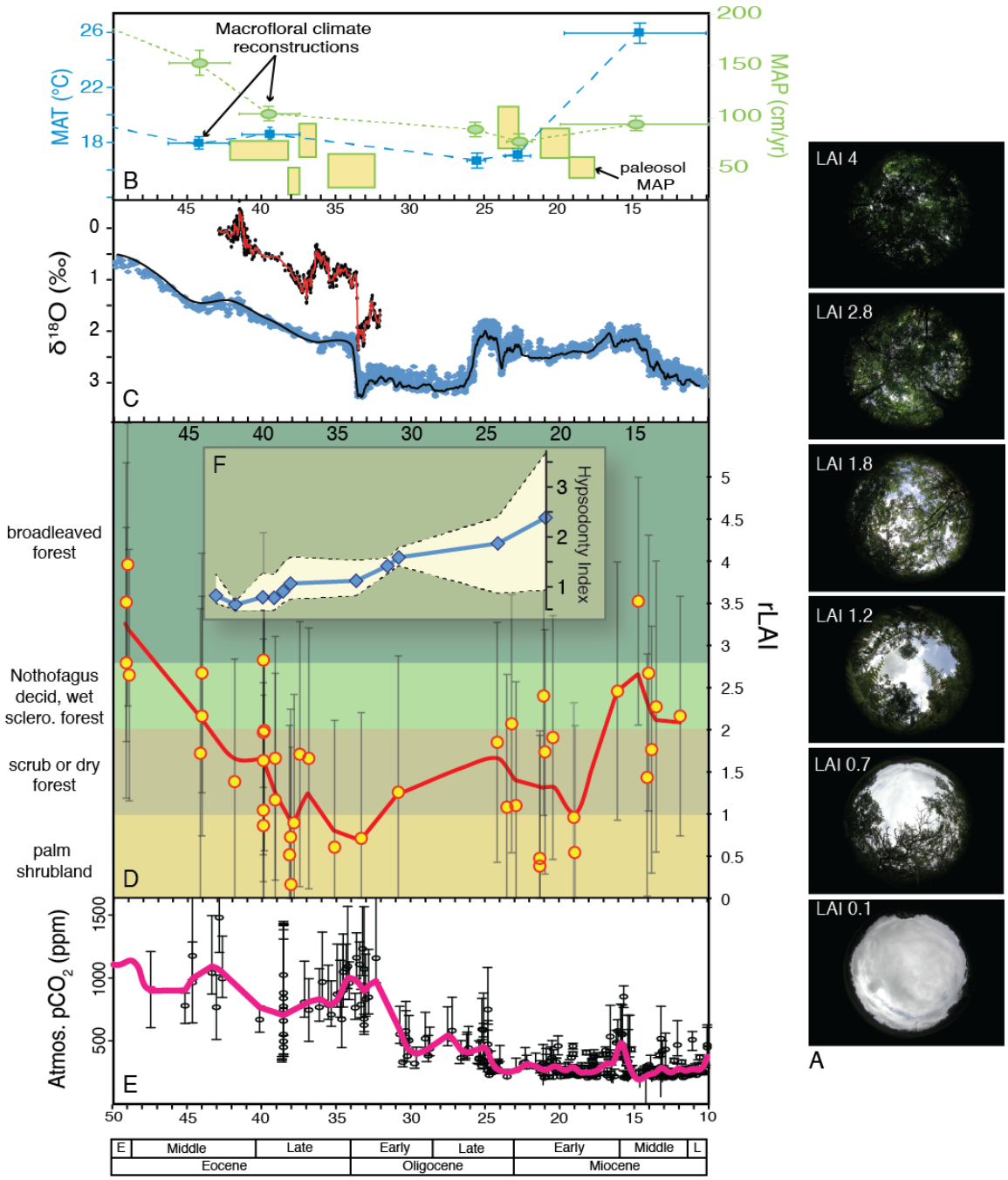

Figure 4.3. Middle Cenozoic rLAI and comparisons to climate records. A) Hemispherical photographs from Costa Rica illustrating LAI measurements. (B) MAT and MAP records from macrofloras (18), MAP records from paleosols (19). (C) Foraminal δ18O records for sea surface (red) (21) and deep sea temperature (blue) (20). (D) rLAI with 95% prediction intervals. (E) Global pCO2 record (28).

Chapter V. Concluding Remarks

DISSERTATION SUMMARY

The main thrusts of this dissertation research were to understand the timing and nature of habitat change during the middle Cenozoic of Patagonia, and how such change affected aspects of mammalian evolution. To answer these questions, I constructed a new chronology for strata from which fossil phytolith samples were collected and I explored new ways to quantify vegetation structure from them. The final result is an important new method that can be used to track changes in Leaf Area Index through time. With this new tool, I was able to construct a unique record of habitat change from Patagonian strata and to link this archive to records of climate and mammalian evolution.

To establish the temporal framework for the vegetation reconstructions, I present a more refined and precise age model for stratigraphic levels at Gran Barranca, building on previous age models based on Ar/Ar dating and magnetostratigraphy (Ré et al., 2010a; Ré et al., 2010b). For this, I dated a total of nine volcanic tuffs using ID-TIMS U/Pb isotopic techniques on single zircon crystals, providing ages for 3 newly identified tuffs and new and more precise ages for six previously dated tuffs. Ages for samples range from 39.861 – 19.041 Ma and have error ranges of <1% in some cases. These dates are important because in combination with the existing magnetostratigraphy, they allowed us to develop a more stable and precise age model for the Sarmiento Formation at Gran Barranca, one of the best for any terrestrial section in the Southern Hemisphere. Additionally, the new chronology helps refine the timing and duration of major hiatuses in deposition in Patagonia. Our new U/Pb date for the La Cancha tuff of 33.581 ± 0.015

Ma confirms that the Vera Member of the Sarmiento Formation records the Eocene-Oligocene Transition and Oi-1 Glaciation events. This is the only terrestrial section in all of the Southern Hemisphere that preserves this interval of time. The Gran Barranca age model also provides the temporal framework for six middle Cenozoic South American Land Mammal Ages (SALMAs) that can be applied more broadly across the continent to date other fossil-bearing sequences based on biochronology. Most importantly, the new age model allows for precise age determination of the more numerous fossil phytolith levels from which the habitat reconstructions were made. This precision is critical when linking climate events in the marine foraminiferal isotope record to the terrestrial record of plants and mammals at Gran Barranca.

The major challenge for reconstructing changes in habitat or vegetation structure in the fossil record was to find a way to detect it and quantify it from microscopic plant remains or phytoliths. In other words, how can a forest canopy be reconstructed from plant cells? My approach was two fold: 1) a grass phytolith approach, and 2) a non-grass phytolith approach.

In Chapter 2, I address the question of whether grass cell morphology changes with light environment in a predictable way. I hypothesized that grass epidermal cell morphology should respond to a gradient of light exposure, or irradiance, as documented for eudicotyledonous plant taxa, whereby cells would be larger and more undulated in shade treatments than in ambient (control) and enhanced light in a controlled growth experiment. We found interspecific variation for the parameters measured. Long cells of four grass species (except shade tolerant bamboo), had significantly longer cells with larger surface areas in the darkest shade treatment (20% light) compared to the control or

enhanced light treatments. The same is true for crenate and polylobate short cells. Unlike the documented pattern of increased cell undulation in shade leaves of some eudicotyledonous species, the grass species grown in our study show no difference in undulation patterns across light treatments.

We conclude that grass cell undulation is not a feature that can be used to track light environment, but that other morphological features such as cell length and surface area have potential, though the pattern is inconsistent among species. Nonetheless, these features of grass cell morphology should be examined further using a field-based approach such as that outlined in Chapter 4.

In contrast, morphology of non-grass epidermal phytoliths derived from soils is to be a much better solution for tracking canopy cover and light environment. Chapter 4 highlights a new method for quantifying vegetation structure by predicting LAI (Leaf Area Index) from morphological characteristics of these phytoliths.

By studying the morphological variation of anticlinal epidermal phytoliths extracted from modern surface soils collected across an LAI gradient in the vegetation of Costa Rica, we found excellent correspondence between both mean phytolith undulation and mean phytolith area with LAI. Consistent with prediction, epidermal phytolith pools extracted from soils were on average more undulated and larger under denser, more complex canopies (higher LAI values). Cell size and undulation are reduced in more open habitats with lower LAI. Incorporating both mean phytolith undulation and mean phytolith area in a multiple linear regression strengthened the robustness of the model (R^2=0.63, $p > 0.0001$); hence, we propose using this as an appropriate method for reconstructing LAI in the fossil record.

Using the newly developed model, I reconstructed LAI (rLAI) values for Patagonian habitats ranging in age from 50-11 Ma to examine the relationship of LAI to two environmental variables known to relate to canopy openness, temperature and precipitation. Specifically, I addressed two questions: 1) how did habitat structure change throughout the Middle Cenozoic, a time of dramatic climate change relating to the opening of the Drake Passage and thermal isolation of Antarctica?; and 2) how did habitat structure relate to the evolution of hypsodonty in South American herbivores?

Reconstructed trends in LAI through the middle Cenozoic of Patagonia appear to track changes in global, as well as in regional temperature and precipitation. Given the strong relationship between MAP and tree cover observed in modern ecosystems (e.g., (Staver et al., 2011), these correlated patterns suggest that precipitation and temperature played a major role in determining vegetation structure in Patagonia. Several aspects of the reconstructed record of openness are of particular interest. First, it demonstrates a gradual transition from closed, likely broadleaved forests (Barreda and Palazzesi, 2007) in the late early Eocene (~49 Ma) to much more open forests and potentially palm shrubland habitats by the late Eocene until the Middle Miocene (~16 Ma) when Patagonia experienced a brief re-greening. The new rLAI archive tracks oxygen isotope records of sea surface and deep-sea temperatures (Bohaty and Zachos, 2003; Zachos et al., 2001), again indicating that vegetation structure at this latitude was highly influenced by changes in temperature and precipitation. However, in contrast to the marine record, which shows a pronounced cooling event at the Eocene-Oligocene Transition (EOT ~33.9 Ma), the rLAI record suggests that major habitat changes on land occurred as early as 38 Ma with a pronounced interval of openness. This event predates the EOT by 4

million years and implies that climate change in Patagonia instead coincided with shallow openings of the Drake Passage and initiation of the development of the Antarctic Circumpolar Current at this time (Livermore et al., 2007).

In addition, the rLAI values demonstrate that habitats were more open than previously interpreted using traditional phytolith analysis (Strömberg et al., 2013). Rather, the non-analogous "mixed paleofloras" of Patagonia fluctuated between open forest and palm shrubland multiple times through the middle Cenozoic. Forests may have been open because of limited rainfall, but the presence of water-loving taxa such as palms and gingers suggest that aridity was not extreme. Alternatively, vegetation may have been more open due to disturbances such as frequent ash inundation, fire and herbivore pressure, but there is limited evidence for this. The lowest rLAI intervals correspond to time periods where eolian sedimentation dominates, suggesting times of decreased precipitation while periods of intermediate rLAI values are associated with fluvial sequences indicative of wetter climates.

For herbivorous mammals, the intervals of low rLAI and eolian sedimentation are coincident with accelerated increases in the evolution of molar crown height, the first at ~38 Ma and followed by two additional pulses. We suggest that a combination of decreased precipitation and sparse vegetation cover changed the nature of sedimentation and pedogenesis whereby unweathered, glass-rich pyroclastic parent materials were susceptible to erosion and mobilization into animal diets. Alternating sequences of fluvial and eolian deposits and fluctuating rLAI values in Patagonia likely reflect changes in ocean circulation and climate instability associated with the protracted opening of the Drake Passage (Livermore et al., 2007). Patagonia is a narrow landmass bordered by the

Southern Ocean, and terrestrial climates there are closely coupled with oceanic conditions. In this sense, it could be viewed that the Sarmiento Formation, the sediments themselves and the biotas preserved within, preserve expressions and consequences of this complex and major tectonic event.

FUTURE DIRECTIONS

The rLAI model presented here is a work it progress, and it needs rigorous testing of its robustness. This research should include sampling soil phytolith assemblages from other ecosystems with differing plant communties, varying soil types, at higher latitudes, and different climatic regimes. Additionally, a phylogenetic comparison of epidermal cell undulation should be undertaken to test whether a phylogeny influences patterns of cell undulation.

While this dissertation research presents one case study as example of the utility of reconstructing LAI from the fossil record, this method has great potential to address many outstanding questions in paleoecology including: 1) How did vegetation structure change during rapid warming events such as the Paleocene-Eocene Thermal Maximum?; 2) Did angiosperms evolve in deep shade or in open environments?; 3) When did multistoried neotropical rainforests evolve and how were they affected during glacial times?; 4) In what type of environments did early hominids evolve?; and 6) What factors lead to the expansion of C4 grasses during the late Miocene?

LAI is a key metric used to describe and quantify vegetation structure in modern ecological studies and in climate modeling. The rLAI estimates add empirical data about

vegetation in the fossil record that can now be included in paleoclimate models involving vegetation feedbacks and climate dynamics.

While the proxy method is geared towards phytolith records, a similar calibration study should be performed on dispersed, organically preserved cuticles in modern soil assemblages. By developing this other training data set, the utility of the rLAI method could be broadened to include all types of fossil plant deposits from any inteval of time so long as epidermal features of leaves are preserved.

LITERATURE CITED:

Barreda, V., and Palazzesi, L., 2007, Patagonian vegetation turnovers during the Paleogene-Early Neogene: Origin of arid-adapted floras: The Botanical Review, v. 73, no. 1, p. 31–50.

Bohaty, S.M., and Zachos, J.C., 2003, Significant Southern Ocean warming event in the late middle Eocene: Geology, v. 31, no. 11, p. 1017–1020.

Livermore, R., Hillenbrand, C.-D., Meredith, M., and Eagles, G., 2007, Drake Passage and Cenozoic climate: An open and shut case?: Geochemistry Geophysics Geosystems, v. 8, no. 1, doi: 10.1029/2005GC001224.

Ré, G.H., Bellosi, E.S., Heizler, M., Vilas, J.F., Madden, R.H., Carlini, A.A., Kay, R.F., Vucetich, M.G., and others, 2010a, A geochronology for the Sarmiento Formation at Gran Barranca: Cambridge, UK: Cambridge University Press.

Ré, G.H., Geuna, S.E., and Vilas, J.F., 2010b, Paleomagnetism and magnetostratigraphy of Sarmiento Formation (Eocene-Miocene) at Gran Barranca, Chubut, Argentina: The Paleontology of Gran Barranca: Evolution and Environmental Change through the Middle Cenozoic of Patagonia, p. 32–45.

Staver, a C., Archibald, S., and Levin, S. a, 2011, The global extent and determinants of savanna and forest as alternative biome states: Science, v. 334, no. 6053, p. 230–232..

Strömberg, C.A.E., Dunn, R.E., Madden, R.H., Kohn, M.J., and Carlini, A.A., 2013, Decoupling the spread of grasslands from the evolution of grazer-type herbivores in South America.: Nature communications, v. 4, p. 1478, doi: 10.1038/ncomms2508.

Zachos, J., Pagani, M., Sloan, L., Thomas, E., and Billups, K., 2001, Trends, rhythms, and aberrations in global climate 65 Ma to present.: Science,v. 292, no. 5517, p. 686–93.

Appendix 1. Supplementary Data For Chapter II.

U/PB Analytical Methods

Zircon crystals were separated from the rock samples using standard techniques. Acicular prismatic zircons with sharply facetted terminations and common axial melt inclusions, which we interpret as volcanic in origin, were hand-picked under ethanol. These crystals were subjected to a modified version of the chemical abrasion method of Mattinson (2005), reflecting a preference to prepare and analyze carefully selected single crystals. Following chemical abrasion, individual residual zircon grains were spiked with the EARTHTIME ^{205}Pb-^{233}U-^{235}U (ET535) tracer and totally dissolved in preparation for the separation and mass spectrometric analysis of Pb and U. Detailed annealing and chemical abrasion, dissolution, ion exchange separation of Pb and U, and mass spectrometric procedures follow those described by Davydov et al. (2010), with the exception of our means of estimating instrumental mass fractionation of the Pb isotopes. Pb fractionation in ET535 spiked analyses is now estimated on the basis of a large database of contemporaneous zircon analyses using the EARTHTIME ^{202}Pb-^{205}Pb-^{233}U-^{235}U (ET2535) tracer.

U-Pb dates and uncertainties (2σ) were calculated using the algorithms of Schmitz and Schoene (2007), assuming ^{235}U/^{205}Pb = 100.206 and ^{233}U/^{235}U = 0.99464 for the ET535 spike tracer solution (Condon, 2005), and the U decay constants of Jaffey et al. (1971). Reported errors on individual analyses are based upon non-systematic analytical uncertainties, including counting statistics, fractionation correction, tracer, blank and initial Pb subtraction. ^{206}Pb/^{238}U ratios

and dates were corrected for initial ^{230}Th disequilibrium assuming a melt Th/U = 3. All common Pb in analyses is attributable to laboratory blank and was subtracted based on the measured laboratory Pb isotopic composition and associated uncertainty. U blanks were <0.1 pg, and negligible compared to sample amounts. Over the course of the experiment, analyses of the 500 Ma EARTHTIME standard solution yielded a weighted mean $^{206}Pb/^{238}U$ age of 499.85 ± 0.06 (n = 14, MSWD = 0.84), and a weighted mean $^{207}Pb/^{206}Pb$ age of 499.73 ± 0.42 (n = 14, MSWD = 1.4).

Non-systematic errors on the sample weighted mean ages are reported in the text and Table 1 as internal 2σ for those samples with probability of fit of >0.05 on the weighted mean date. For the few samples with probability of fit <0.05, errors are at the 95% confidence interval, which is the internal 2σ error expanded by the square root of the MSWD and the Student's t multiplier of n-1 degrees of freedom (Ludwig, 2003). The U-Pb error estimates apply to age comparisons with other laboratories that use EARTHTIME standards. When comparing our dates with those derived from other decay schemes (e.g., $^{40}Ar/^{39}Ar$), systematic uncertainties in tracer calibration (0.05%) and in the ^{238}U decay constant (0.106%) are added to the internal error quadratically. These total errors range from ± 0.035 to ± 0.06 Ma and are noted in parentheses in Table 1.

Stratigraphic Occurrences of Mammalian Faunas

The following text describes the highest and lowest Gran Barranca Vertebrate (GBV) fossil levels for each fauna or SALMA at Gran Barranca with notes about the

stratigraphy, distribution and taxonomic composition of their assemblages. Specific locations and GPS coordinates can be provided upon request.

"Pinturan"

Highest = GBV-54 on Profile A-1 at Colhue-Huapi West

Lowest = GBV-55 on Profile A-1 at Colhue-Huapi West

Fossil mammal remains are distributed through the highest 3.5 m thick portion of the exposed Colhue-Huapi Member. These are the highest fossil mammal levels in the Sarmiento Formation at Gran Barranca. Kramarz et al (2010) describe the assemblage and refer all taxa to the Upper Fossil Zone without distinguishing levels within it. The Upper Fossil Zone occurs within the highest local normal polarity interval of the Sarmiento Formation at Gran Barranca. The assemblage is distinguished from the Colhuehuapian by the presence of *Acaremys* (Acaremyidae) and *Luantus propheticus* (Eocardiidae).

Colhuehuapian

Highest = GBV-15 or Level H at Colhue-Huapi West

Lowest = GBV-44 or Level 15 at Colhue-Huapi West

The Lower Fossil Zone in the Colhue-Huapi Member yields the type Colhuehuapian fauna and occurs in 15 distinct fossil-bearing levels that extend from 2 to 30 meters above the base of the Colhue-Huapi Member. Two additional levels more tentatively referred to the Colhuehuapian occur approximately 35-40 meters above the base of the member. The Colhuehuapian faunal assemblage includes *Colpodon distinctus*

(Leontiniidae), *Cochilius volvens* (Interatheriidae), *Proadinotherium muensteri* (Toxodontidae), and *Protacaremys avunculus* (Echimyidae).

Deseadan

Highest = GBV-35 or Simpson #119 at Profile J and GBV-1 on Profile H.

Lowest = GBV-34 in Profile A.

Fossil mammals of the Deseadan SALMA at Gran Barranca occur in at least three localities in association with the basalts in the Upper Puesto Almendra Member. All three occur in sandstones or conglomerates that contain basalt detritus; the presence of eroded and rounded basalt pebbles in these lenses imply the fossil mammals post-date the age of the basalts, but the age range of the basalts indicates a substantial interval of time elapsed between eruption events. Field relations suggest two distinct "levels" may be distinguished, but substantiating this is made difficult by the discontinuous nature of these particular fossil-bearing sediments, and the complex unconformities associated with the basalts. The most abundant fossil material from these localities is isolated teeth of *Scarrittia* (Leontiniidae), *Parastrapotherium crassum* (Astrapotheriidae), and rare *Pyrotherium*.

"Canteran"

The rich quarries of La Cantera (GBV-19) occur at a level about 10 meters above the Lower Channel Series, which form the base of the UPA. The "Canteran" represents a distinctive fauna with a unique taxonomic assemblage intermediate between the Tinguiririan and Deseadan that includes *Epiklohnia verticalis* (Argyrolagidae),

Patagonhippus (Notohippidae), *Pilchenia intermedia* (Palaeothentidae), and *Sadypus tortuosus* (Eutatini, Dasypodidae).

Tinguirirican

Highest = GBV-28 and GBV-50 at Profile M, and GBV-4 La Cancha at Profile K

Lowest = GBV-49 or Simpson's #147 at Profile M (=Cifelli 17)

The Tinguiririca SALMA at Gran Barranca occurs primarily in a single stratigraphic interval termed the La Cancha Bed that extends between profiles K and M. However, fossil mammals are distributed through a ~3 m interval above the La Cancha Bed at Profile M, and these are assigned to the Tinguiririca SALMA. The taxonomic assemblage at GBV-4 La Cancha includes *Anisotemnus distentus* (Isotemnidae), *Klohnia major* (Argyrolagidae), *Eomorphippus* (Notohippidae), *Pilchenia antiqua* (Palaeothentidae), and *Sadypus minutus* (Eutatini, Dasypodidae). This assemblage is distinct from La Cantera (GBV-19) and El Rosado (GBV-3). The assignment of this assemblage to the Tinguiririca, best known by the type fauna from the Tinguiririca valley in Chile, is made by the shared presence of *Santiagorothia* (Interatheriidae), *Klohnia* (Argyrolagidae) and *Parutaetus chilensis* (Eutatini, Dasypodidae).

Mustersan

Highest = Coley's Quarry, Simpson's #64 (Profile A-3) and #101 at Profile G.

Lowest = GBV-3 El Rosado and GBV-32 or Simpson's #116 and 117 at Profile J. The El Rosado bed at Profile J is a massive tuff weathering pink and yielding 21

mammal taxa, including *Astraponotus* (Astrapotheriidae), 5 cingulate xenarthrans and as many as 11 notoungulates. Coley's Quarry in the basal conglomerate somewhere between Profile G and Profile A-3 has not been relocated, but included material of *Astraponotus* (Astrapotheriidae) the index taxon for the Mustersan. The fossil-bearing basal conglomerate at profiles G and A-3 also occurs at Profile I and corresponds to Simpson's Bed X. When followed eastward, this level becomes the tabular Rosado Bed within the massive pink tuff at Profile J.

El Nuevo

The distinctive fauna from GBV-60 El Nuevo occurs in the Rosado Member at Profile M, 15 to 18 meters above the base of Simpson's Y Tuff. Twenty-two mammalian taxa are known from El Nuevo, including 7 cingulate xenarthrans and 11 notoungulates. The El Nuevo fauna was collected by Simpson in 1930 and based on four taxa collected there Cifelli (1985) assigned the assemblage from his Level 15 to the Barrancan Subage of the Casamayoran, although noted the presence of *Periphragnis*, a Mustersan isotemnid. The taxonomic composition of the assemblage is intermediate between more typical Barrancan levels and the Mustersan at GBV-3 El Rosado. With the Barrancan it shares *Ultrapithecus rutilans* (Oldfieldthomasiidae), *Eohyrax isotemnoides* (Archaeohyracidae), and *Notopithecus adapinus* (Interatheriidae), and with the Mustersan it shares the euphractin dasypodids *Pareutatus chicoensis*, *Anteutatus leni*, and *Mazzoniphractus ingens*.

Barrancan

Highest = Simpson's #241 (=Cifelli 14) at Profile M

Lowest = Simpson's #254 and 256 at Profile N-1 (=Cifelli 18)

Simpson's level with #241 (the isotemnid *Isotemnus primitivus*) occurs at the top of a fine yellow-green clay about 7 meters above Simpson's Y at Profile M, approximately equivalent to stake 2003-9 (site MI09(OB)). Simpson's level with #254 and 256 occurs approximately 4 meters above the base of the Gran Barranca Member at Profile N-1, in the lowest local reversed polarity interval, and 3 meters below the level of the VRS Tuff (GB01-09). Barrancan SALMA fossil mammal taxa include *Albertogaudrya* (Astrapotheriidae), *Trigonostylops wortmani* (Trigonostylopidae), *Homalostylops* and *Notostylops* (Notostylopidae), *Thomashuxleya* (Isotemnidae, Notoungulata), and *Notopithecus adapinus* (Interatheriidae, Notoungulata).

Table A1.1. U-Pb Isotopic Data

								Radiogenic Isotope Ratios								Radiogenic Isotope Dates					
Grain (a)	Th U (b)	^{206}Pb* x10^{-13} mol (c)	mol % ^{206}Pb* (c)	Pb* Pbc (c)	Pbc (pg) (c)	^{206}Pb ^{204}Pb (d)	^{208}Pb ^{206}Pb (e)	^{207}Pb ^{206}Pb (e)	% err (f)	^{207}Pb ^{235}U (e)	% err (f)	^{206}Pb ^{238}U (e)	% err (f)	corr. coef.	^{207}Pb ^{206}Pb (g)	± (f)	^{207}Pb ^{235}U (g)	± (f)	^{206}Pb ^{238}U (g)	± (f)
La Flecha																					
xxx-xxx (La Flecha Tuff)																					
z6	1.672	0.07021	93.5%	5.8	0.40	288	0.543	0.050835	2.070	0.199880	2.207	0.028517	0.253	0.579	233.3	47.8	185.02	3.73	181.26	0.45
z8	1.391	0.18949	97.6%	15.6	0.38	790	0.445	0.049959	0.653	0.196430	0.736	0.028516	0.216	0.513	193.1	15.2	182.10	1.23	181.25	0.39
z3	0.675	0.09337	95.1%	6.2	0.39	380	0.219	0.047141	1.553	0.038854	1.658	0.005978	0.163	0.668	56.4	37.0	38.70	0.63	38.42	0.06
z1	0.702	0.04693	90.6%	3.1	0.40	197	0.230	0.047075	3.586	0.024341	3.779	0.003750	0.228	0.854	53.0	85.4	24.42	0.91	**24.13**	**0.05**
z4	0.666	0.03505	89.3%	2.6	0.35	173	0.218	0.047344	4.566	0.024490	4.748	0.003752	0.243	0.762	66.6	108.5	24.57	1.15	**24.14**	**0.06**
z2	0.710	0.05099	92.5%	4.0	0.34	249	0.234	0.047699	2.490	0.024669	2.632	0.003751	0.168	0.856	84.4	59.0	24.74	0.64	**24.13**	**0.04**
z7	1.093	0.09585	95.2%	7.1	0.40	389	0.362	0.047930	1.577	0.024766	1.679	0.003747	0.131	0.791	95.8	37.3	24.84	0.41	**24.11**	**0.03**
z5	0.715	0.04520	80.7%	1.4	0.89	97	0.244	0.049307	7.040	0.025460	7.401	0.003745	0.412	0.883	162.5	164.4	25.53	1.87	**24.10**	**0.10**
Gran Barranca																					
SGB09-282 (01-24.5 Tuff)																					
z11	1.180	0.05443	89.6%	3.1	0.52	179	0.395	0.048315	3.301	0.019898	3.499	0.002987	0.214	0.930	114.7	77.8	20.01	0.69	19.23	0.04
z2	0.655	0.06571	90.9%	3.2	0.54	205	0.218	0.047933	2.875	0.019689	3.044	0.002979	0.187	0.909	96.0	67.9	19.80	0.60	19.18	0.04
z12	0.642	0.02696	86.2%	2.0	0.35	135	0.220	0.049374	5.379	0.020167	5.616	0.002962	0.295	0.812	165.6	125.5	20.27	1.13	**19.07**	**0.06**
z4	0.692	0.04522	85.5%	1.9	0.63	128	0.231	0.048019	5.116	0.019605	5.382	0.002961	0.296	0.903	100.2	120.8	19.71	1.05	**19.06**	**0.06**
z10	0.734	0.03025	85.8%	2.0	0.41	131	0.248	0.048737	6.059	0.019891	6.282	0.002960	0.300	0.753	135.2	142.1	20.00	1.24	**19.05**	**0.06**
z1	0.791	0.01283	55.6%	0.4	0.84	42	0.253	0.046065	37.865	0.018779	38.649	0.002957	1.315	0.607	1.0	910.8	18.89	7.23	**19.03**	**0.25**
z9	0.709	0.03166	89.2%	2.7	0.32	172	0.235	0.047777	5.148	0.019444	5.325	0.002952	0.254	0.708	88.3	121.8	19.55	1.03	**19.00**	**0.05**
SGB09-275 (Big Mammal Tuff)																					
z14	1.536	0.63905	98.9%	34.1	0.59	1664	0.482	0.050339	0.386	0.262420	0.454	0.037808	0.164	0.566	210	8.9	236.62	0.96	239.23	0.39
z13	0.525	0.13233	96.0%	7.3	0.46	460	0.172	0.047738	1.378	0.039635	1.468	0.006022	0.135	0.692	86.3	32.7	39.47	0.57	38.70	0.05
z12	0.707	0.08906	94.2%	5.2	0.45	319	0.235	0.047901	2.631	0.023677	2.768	0.003585	0.197	0.711	94.4	62.2	23.76	0.65	23.07	0.05
z2	0.638	0.05663	77.1%	1.1	1.38	81	0.215	0.048570	10.135	0.023257	10.551	0.003473	0.572	0.738	127	238	23.34	2.43	22.35	0.13
z11	0.582	0.05590	89.5%	2.7	0.54	178	0.193	0.047921	3.693	0.022405	3.883	0.003391	0.219	0.877	95.4	87.3	22.50	0.86	21.82	0.05
z5	0.864	0.04393	86.7%	2.2	0.56	139	0.290	0.048412	5.740	0.021742	5.983	0.003257	0.317	0.777	119	135	21.84	1.29	**20.96**	**0.07**
z16	0.555	0.06582	93.3%	4.3	0.39	277	0.180	0.046731	2.156	0.020940	2.281	0.003250	0.145	0.873	35.5	51.5	21.04	0.48	**20.92**	**0.03**
z15	0.971	0.04949	89.2%	2.9	0.49	172	0.329	0.048930	4.076	0.021912	4.276	0.003248	0.246	0.824	144	95.5	22.01	0.93	**20.90**	**0.05**
z10	0.971	0.20067	96.7%	9.9	0.57	560	0.315	0.046715	1.031	0.020893	1.102	0.003244	0.095	0.764	34.7	24.7	21.00	0.23	**20.88**	**0.02**
z1	1.155	0.10154	92.0%	4.1	0.73	232	0.378	0.047258	2.576	0.021130	2.730	0.003243	0.175	0.888	62.3	61.3	21.23	0.57	**20.87**	**0.04**
RGB09-007 (Carbon Tuff)																					
z17	0.678	0.28067	97.7%	13.7	0.54	820	0.217	0.046623	0.751	0.036939	0.812	0.005746	0.115	0.577	30.0	18.0	36.83	0.29	36.94	0.04

z18	0.904	0.15685	96.7%	10.0	0.43	571	0.293	0.047083	1.007	0.031145	1.078	0.004798	0.098	0.752	53.4	24.0	31.14	0.33	30.85	0.03
z15	0.968	0.05776	92.1%	4.0	0.41	236	0.317	0.047539	3.043	0.030737	3.211	0.004689	0.252	0.688	76.4	72.2	30.74	0.97	30.16	0.08
z14	0.810	0.12402	96.4%	8.8	0.38	516	0.262	0.046931	1.240	0.028691	1.324	0.004434	0.098	0.869	45.7	29.6	28.72	0.37	28.52	0.03
z4	0.676	0.09057	85.2%	1.8	1.30	125	0.226	0.048485	5.529	0.027482	5.816	0.004111	0.400	0.734	123	130	27.53	1.58	26.45	0.11
z12	1.217	0.15649	96.8%	10.8	0.43	574	0.393	0.046689	1.045	0.023621	1.118	0.003669	0.098	0.758	33.3	25.0	23.71	0.26	23.61	0.02
z5	1.162	0.04793	70.6%	0.8	1.64	63	0.346	0.04293	6.650	0.02147	8.224	0.003627	0.805	0.725	-171	439	21.57	3.89	23.34	0.19
z11	0.947	0.13534	96.4%	9.0	0.42	510	0.308	0.047022	1.087	0.023308	1.162	0.003595	0.097	0.794	50.4	25.9	23.40	0.27	23.13	0.02
SGB09-093 (Cantera Tuff)																				
z12	0.676	0.19381	98.1%	16.7	0.30	993	0.221	0.048328	0.587	0.064232	0.656	0.009640	0.164	0.524	115.3	13.8	63.21	0.40	61.84	0.10
z2	0.911	0.03275	84.4%	1.9	0.50	119	0.315	0.050403	6.541	0.043067	6.932	0.006197	1.340	0.380	213.6	151.4	42.81	2.91	39.83	0.53
z15	0.594	0.09433	95.0%	5.9	0.41	369	0.196	0.047996	1.808	0.038746	1.916	0.005855	0.141	0.781	99.1	42.7	38.60	0.73	37.63	0.05
z14	0.883	0.06480	90.6%	3.2	0.56	197	0.285	0.046986	3.047	0.037015	3.223	0.005714	0.204	0.872	48.5	72.7	36.91	1.17	36.73	0.07
z13	0.588	0.10196	90.8%	3.1	0.85	202	0.190	0.046961	3.110	0.035920	3.289	0.005548	0.205	0.880	47.2	74.2	35.83	1.16	35.66	0.07
z11	0.515	0.25407	98.4%	18.7	0.34	1161	0.166	0.046905	0.515	0.035810	0.563	0.005537	0.078	0.661	44.4	12.3	35.72	0.20	35.60	0.03
z4	0.543	0.12915	93.7%	4.5	0.72	293	0.171	0.045640	2.190	0.030537	2.328	0.004853	0.263	0.563	-21.3	52.9	30.54	0.70	31.21	0.08
z5	0.745	0.12744	85.7%	1.9	1.74	130	0.240	0.046730	4.968	0.030728	5.265	0.004769	0.503	0.621	35.5	118.8	30.73	1.59	30.67	0.15
SGB09-099 (Cantera Tuff)																				
z5	0.617	0.20344	97.7%	13.4	0.39	813	0.200	0.047353	0.730	0.041447	0.795	0.006348	0.145	0.523	67.1	17.4	41.24	0.32	40.79	0.06
z8	0.434	0.94104	99.4%	51.9	0.44	3263	0.140	0.046940	0.200	0.040673	0.241	0.006284	0.070	0.682	46.2	4.8	40.48	0.10	40.39	0.03
z4	0.814	0.45482	99.0%	33.3	0.37	1902	0.263	0.047038	0.299	0.040667	0.341	0.006270	0.072	0.648	51.2	7.1	40.47	0.14	40.30	0.03
z2	1.083	0.41919	99.0%	33.1	0.36	1776	0.349	0.046960	0.317	0.039836	0.358	0.006152	0.068	0.651	47.2	7.6	39.66	0.14	39.54	0.03
z1	0.589	0.48991	98.9%	27.4	0.46	1656	0.191	0.047038	0.343	0.036049	0.384	0.005558	0.070	0.649	51.2	8.2	35.96	0.14	35.73	0.03
z6	0.819	0.09342	95.6%	7.1	0.36	419	0.268	0.047523	1.548	0.032935	1.644	0.005026	0.123	0.799	75.6	36.7	32.90	0.53	32.32	0.04
z3	0.813	0.23993	97.2%	11.6	0.56	673	0.264	0.047084	0.848	0.031536	0.909	0.004858	0.091	0.699	53.5	20.2	31.53	0.28	31.24	0.03
z7	0.688	0.11720	94.6%	5.6	0.55	345	0.223	0.046987	1.784	0.031012	1.890	0.004787	0.161	0.681	48.6	42.6	31.01	0.58	30.78	0.05
SGB09-007 (Carlini Tuff)																				
z12	0.574	0.24622	98.2%	17.0	0.37	1039	0.186	0.047117	0.580	0.034073	0.630	0.005245	0.078	0.670	55.2	13.8	34.02	0.21	33.72	0.03
z13	0.655	0.16886	97.9%	14.4	0.30	868	0.212	0.046971	0.701	0.033852	0.757	0.005227	0.085	0.694	47.7	16.7	33.80	0.25	**33.61**	**0.03**
z17	0.541	0.29113	96.6%	8.6	0.85	539	0.175	0.047063	1.031	0.033911	1.101	0.005226	0.095	0.755	52.4	24.6	33.86	0.37	**33.60**	**0.03**
z19	0.560	0.23839	97.0%	10.1	0.60	626	0.181	0.046996	0.895	0.033862	0.958	0.005226	0.089	0.742	49.0	21.3	33.81	0.32	**33.60**	**0.03**
z16	0.559	0.24819	96.9%	9.8	0.64	609	0.181	0.047149	0.929	0.033965	0.994	0.005225	0.091	0.743	56.8	22.1	33.91	0.33	**33.59**	**0.03**
z8	0.493	1.15770	99.4%	47.2	0.61	2921	0.159	0.046770	0.203	0.033688	0.245	0.005224	0.067	0.707	37.5	4.8	33.64	0.08	**33.59**	**0.02**
z10	0.552	0.32365	97.2%	10.5	0.78	656	0.178	0.046743	0.938	0.033658	1.002	0.005222	0.096	0.698	36.1	22.4	33.61	0.33	**33.58**	**0.03**
z14	0.707	0.14896	96.9%	10.0	0.39	599	0.229	0.047126	0.953	0.033933	1.020	0.005222	0.092	0.755	55.6	22.7	33.88	0.34	**33.58**	**0.03**
z18	0.567	0.24435	96.5%	8.4	0.74	525	0.183	0.046843	1.046	0.033720	1.117	0.005221	0.094	0.780	41.2	25.0	33.67	0.37	**33.57**	**0.03**
z9	0.559	0.52722	98.7%	24.1	0.55	1476	0.180	0.046698	0.383	0.033600	0.424	0.005218	0.071	0.643	33.8	9.2	33.56	0.14	**33.55**	**0.02**
z15	0.581	0.34708	95.9%	7.2	1.23	450	0.188	0.046994	1.249	0.033803	1.331	0.005217	0.106	0.785	48.9	29.8	33.76	0.44	**33.54**	**0.04**
RGB09-05 (Kay Tuff)																				
z11	0.837	0.26772	98.3%	19.6	0.37	1121	0.269	0.046926	0.500	0.040833	0.547	0.006311	0.072	0.694	45.5	11.9	40.64	0.22	40.56	0.03

z1	0.762	0.46994	98.1%	16.9	0.74	985	0.247	0.047283	0.561	0.039574	0.610	0.006070	0.074	0.699	63.6	13.4	39.41	0.24	39.01	0.03
z7	0.512	0.19947	95.9%	7.1	0.70	451	0.166	0.047178	1.201	0.038972	1.282	0.005991	0.103	0.806	58.3	28.6	38.82	0.49	38.51	0.04
z8	0.707	0.34475	98.2%	17.5	0.52	1038	0.228	0.047025	0.557	0.038809	0.607	0.005985	0.089	0.609	50.5	13.3	38.66	0.23	38.47	0.03
z14	0.593	0.21508	96.4%	8.5	0.65	523	0.193	0.047478	1.122	0.038514	1.194	0.005883	0.117	0.645	73.3	26.6	38.37	0.45	37.82	0.04
z5	0.863	0.20926	94.7%	6.0	0.96	353	0.279	0.047146	1.600	0.037936	1.702	0.005836	0.122	0.848	56.6	38.1	37.81	0.63	37.51	0.05
z10	1.105	0.12420	95.5%	7.5	0.48	414	0.363	0.047807	1.390	0.038050	1.480	0.005772	0.110	0.836	89.7	32.9	37.92	0.55	37.10	0.04
z3	0.672	0.17814	93.5%	4.6	1.02	286	0.217	0.046917	1.947	0.037250	2.068	0.005758	0.139	0.879	45.0	46.5	37.14	0.75	37.01	0.05
z4	0.731	0.15632	94.8%	5.9	0.71	357	0.237	0.047155	1.546	0.037424	1.645	0.005756	0.116	0.872	57.1	36.8	37.31	0.60	37.00	0.04
z13	0.739	0.15628	96.6%	9.1	0.46	543	0.240	0.047200	1.048	0.037434	1.122	0.005752	0.095	0.794	59.4	25.0	37.32	0.41	36.97	0.03
z9	0.716	0.29111	98.2%	18.0	0.43	1060	0.231	0.047034	0.543	0.037297	0.590	0.005751	0.078	0.648	50.9	12.9	37.18	0.22	36.97	0.03
z2	0.750	0.08902	93.1%	4.4	0.55	268	0.247	0.047904	2.152	0.037878	2.285	0.005735	0.151	0.892	94.6	50.9	37.75	0.85	36.86	0.06
z6	1.131	0.06078	84.4%	1.9	0.93	119	0.361	0.046403	5.735	0.036611	6.037	0.005722	0.335	0.906	18.6	137.6	36.51	2.17	**36.78**	**0.12**
z12	0.868	0.19362	96.5%	9.3	0.57	536	0.282	0.047288	1.071	0.037250	1.147	0.005713	0.092	0.830	63.8	25.5	37.14	0.42	**36.72**	**0.03**
SGB09-179 (Bed 10 Tuff)																				
z5	1.177	0.12787	91.8%	4.0	0.94	226	0.385	0.047734	2.551	0.040544	2.706	0.006160	0.179	0.874	86.1	60.5	40.35	1.07	39.59	0.07
z10	0.490	0.25491	96.5%	8.2	0.77	525	0.158	0.047059	1.139	0.039177	1.215	0.006038	0.098	0.801	52.2	27.2	39.02	0.47	38.81	0.04
z1	0.705	0.42607	97.3%	11.5	0.97	689	0.228	0.046976	0.774	0.037305	0.836	0.005760	0.071	0.884	48.0	18.5	37.19	0.31	**37.02**	**0.03**
z8	0.833	0.15020	92.9%	4.4	0.94	264	0.270	0.047277	2.204	0.037532	2.339	0.005758	0.155	0.880	63.2	52.4	37.41	0.86	**37.01**	**0.06**
z4	0.676	0.23409	95.8%	7.2	0.85	441	0.219	0.047082	1.234	0.037376	1.317	0.005757	0.102	0.823	53.4	29.4	37.26	0.48	**37.01**	**0.04**
z2	0.753	0.26116	95.8%	7.4	0.94	443	0.243	0.046910	1.251	0.037233	1.334	0.005757	0.104	0.810	44.7	29.9	37.12	0.49	**37.00**	**0.04**
z9	0.709	0.16118	92.7%	4.0	1.05	253	0.228	0.046871	2.241	0.037201	2.377	0.005756	0.158	0.871	42.6	53.5	37.09	0.87	**37.00**	**0.06**
z6	0.687	0.14319	93.3%	4.4	0.85	277	0.225	0.047667	2.212	0.037833	2.354	0.005756	0.147	0.964	82.8	52.4	37.71	0.87	**37.00**	**0.05**
z3	0.706	0.37960	97.3%	11.5	0.87	687	0.227	0.046715	0.812	0.037038	0.872	0.005750	0.092	0.691	34.7	19.4	36.93	0.32	**36.96**	**0.03**
z7	0.957	0.11598	92.3%	4.1	0.80	241	0.309	0.047029	2.525	0.037271	2.675	0.005748	0.173	0.874	50.7	60.2	37.16	0.98	**36.95**	**0.06**
SGB09-118 (Rosado Tuff)																				
z12	0.488	0.80580	99.2%	35.4	0.56	2200	0.153	0.048960	0.338	0.188263	0.380	0.027889	0.084	0.582	145.9	7.9	175.15	0.61	177.32	0.15
z14	0.549	0.25394	97.8%	13.8	0.46	855	0.176	0.048743	0.733	0.130497	0.790	0.019417	0.107	0.588	135.5	17.2	124.54	0.93	123.97	0.13
z9	0.538	0.75322	98.1%	16.0	1.19	989	0.172	0.048531	0.575	0.128431	0.632	0.019193	0.131	0.515	125.3	13.5	122.69	0.73	122.55	0.16
z11	0.710	0.14953	96.1%	7.9	0.50	479	0.230	0.047226	1.152	0.039098	1.232	0.006004	0.098	0.824	60.7	27.4	38.94	0.47	38.59	0.04
z13	0.690	0.06905	93.0%	4.3	0.43	266	0.229	0.048398	2.291	0.040029	2.430	0.005999	0.179	0.789	118.8	54.0	39.85	0.95	38.55	0.07
z6	0.511	0.44345	94.9%	5.7	1.95	366	0.165	0.046925	1.506	0.038757	1.603	0.005990	0.115	0.856	45.4	35.9	38.61	0.61	38.50	0.04
z7	0.846	0.21036	97.8%	14.7	0.39	843	0.273	0.047062	0.669	0.038819	0.723	0.005982	0.081	0.697	52.4	16.0	38.67	0.27	38.45	0.03
z10	0.796	0.09157	91.4%	3.5	0.71	216	0.256	0.046892	3.049	0.038612	3.217	0.005972	0.185	0.917	43.7	72.8	38.47	1.21	38.38	0.07
z2	0.823	0.05495	90.4%	3.1	0.48	194	0.276	0.048807	3.281	0.040062	3.454	0.005953	0.240	0.737	138.6	77.0	39.88	1.35	38.26	0.09
z8	0.695	0.11874	92.8%	4.1	0.75	259	0.224	0.046822	2.264	0.038229	2.401	0.005922	0.155	0.892	40.2	54.1	38.09	0.90	38.06	0.06
z15	0.758	0.07709	93.5%	4.6	0.44	284	0.249	0.047935	2.060	0.039074	2.186	0.005912	0.141	0.902	96.1	48.7	38.92	0.83	38.00	0.05
SGB09-037 (Simpson's Y Tuff)																				
z5	0.719	0.18192	93.1%	4.3	1.11	269	0.231	0.046935	2.102	0.040366	2.232	0.006238	0.145	0.901	45.9	50.2	40.18	0.88	40.09	0.06
z2	0.858	0.29754	95.2%	6.6	1.23	388	0.279	0.047311	1.408	0.040581	1.500	0.006221	0.110	0.851	64.9	33.5	40.39	0.59	39.98	0.04

z1	0.779	0.23598	94.9%	6.0	1.05	361	0.253	0.047352	1.510	0.040540	1.609	0.006209	0.126	0.802	67.0	35.9	40.35	0.64	**39.90**	**0.05**
z4	0.821	0.19873	96.2%	8.3	0.65	484	0.266	0.047221	1.143	0.040425	1.220	0.006209	0.098	0.807	60.4	27.2	40.24	0.48	**39.90**	**0.04**
z7	0.792	0.20642	95.8%	7.4	0.75	440	0.256	0.047149	1.250	0.040322	1.334	0.006202	0.102	0.832	56.8	29.8	40.14	0.52	**39.86**	**0.04**
z6	0.735	0.10470	94.5%	5.5	0.50	339	0.235	0.046655	1.984	0.039895	2.105	0.006202	0.145	0.838	31.6	47.5	39.72	0.82	**39.86**	**0.06**
z3	0.859	0.19000	94.9%	6.1	0.85	362	0.276	0.046909	1.527	0.040100	1.625	0.006200	0.115	0.860	44.6	36.5	39.92	0.64	**39.84**	**0.05**
z10	0.774	0.21346	94.3%	5.3	1.07	324	0.249	0.046926	1.730	0.040079	1.839	0.006194	0.129	0.857	45.5	41.3	39.90	0.72	**39.81**	**0.05**
z9	0.762	0.13108	91.6%	3.5	0.99	221	0.244	0.046588	3.093	0.039763	3.278	0.006190	0.196	0.949	28.1	74.1	39.59	1.27	**39.78**	**0.08**

Notes:

(a) z1, z2, etc. are labels for individual analyzed zircon grains treated by annealing and chemical abrasion [*Mattinson*, 2005]; bold labels denote analyses used in the weighted mean age calculations.

(b) Model Th/U ratio calculated from radiogenic $^{208}Pb/^{206}Pb$ ratio and $^{207}Pb/^{235}U$ date.

(c) Pb* and Pbc are radiogenic and common Pb, respectively. mol % $^{206}Pb^*$ is with respect to radiogenic, blank and initial common Pb.

(d) Measured ratio corrected for spike contribution and instrumental fractionation only. All analyses were spiked with the ET535 mixed tracer. An average Pb fractionation correction of 0.15 ± 0.03 (1σ) %/atomic mass unit was estimated from a large population of data obtained with the ET2535 mixed tracer.

(e) Ratios corrected for fractionation, spike contribution, common Pb, and initial disequilibrium in $^{230}Th/^{238}U$. All common Pb was assigned to procedural blank with a composition of $^{206}Pb/^{204}Pb$ = 18.60 ± 0.80%; $^{207}Pb/^{204}Pb$ = 15.69 ± 0.32%; $^{208}Pb/^{204}Pb$ = 38.51 ± 0.74% (1σ). $^{206}Pb/^{238}U$ and $^{207}Pb/^{206}Pb$ ratios are corrected for initial disequilibrium in $^{230}Th/^{238}U$ using a melt Th/U = 3.

(f) Errors are 2σ, propagated using algorithms of [*Schmitz and Schoene*, 2007].

(g) Calculations based on the decay constants of [*Jaffey et al.*, 1971]. $^{206}Pb/^{238}U$ and $^{207}Pb/^{206}Pb$ dates corrected for initial disequilibrium in $^{230}Th/^{238}U$ using a melt Th/U = 3.

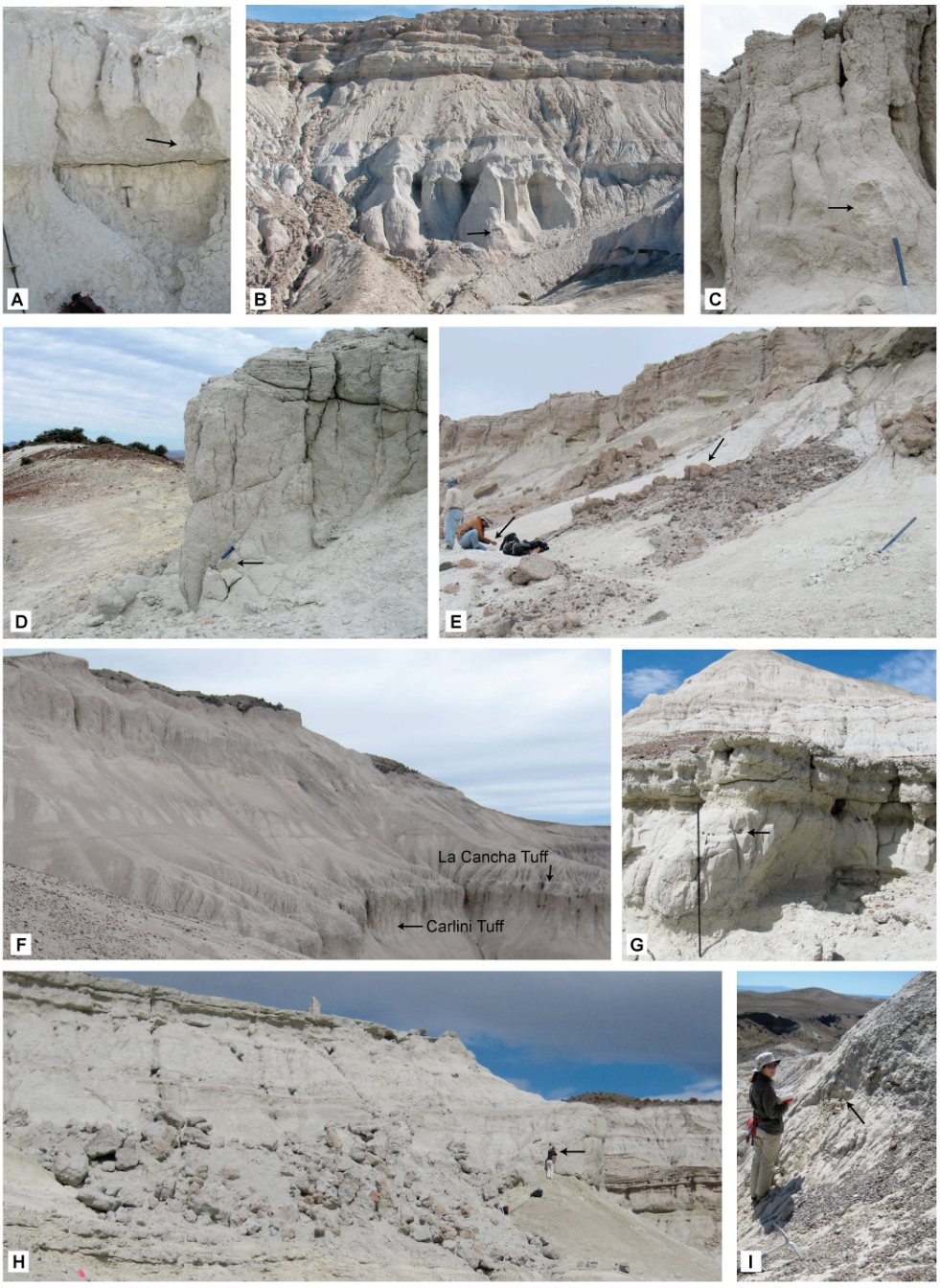

Figure A2.1. Photographs of tuffs collected from Gran Barranca. Black arrows indicate tuff collection sites, except for (F), La Cancha Tuff, which was collected from location where photograph was taken. A) Simpson's Y Tuff, Profile MMZ; B) Rosado Tuff, west of Profile J; C) Bed 10 Tuff, Profile A-2; D) Kay Tuff, Profile A-2; E) La Cantera Tuff (Profile A-2); F) La Cancha Tuff and Carlini Tuff, Profile M; G) Big Mammal Tuff, Profile A-1; H) Carbon Tuff, Profile MMZ; and I) CHW01-24.5 Tuff, Profile A-1.

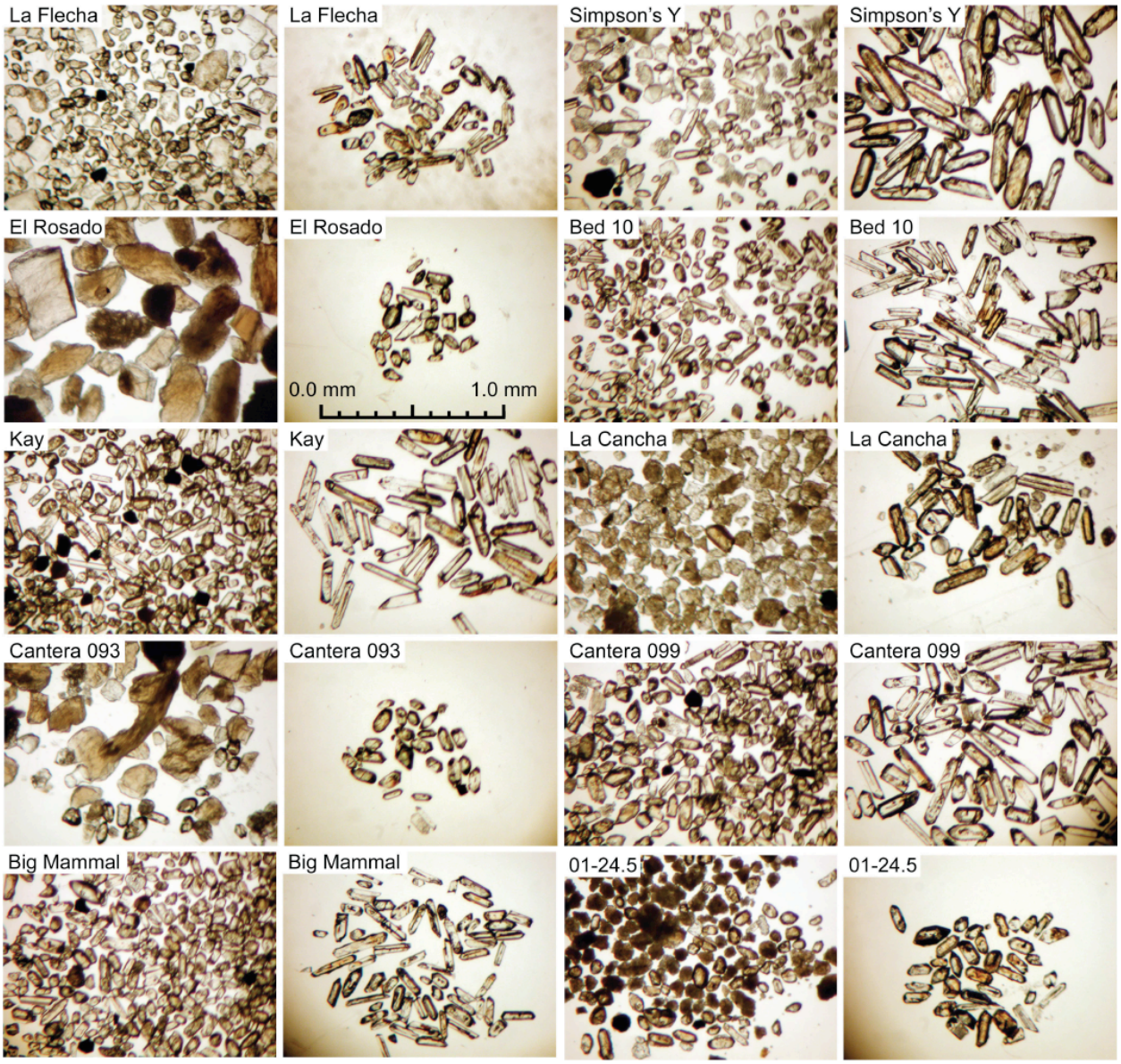

Figure A2.2. Photomicrographs of mineral separates from dated tuff horizons, southern Argentina, relevant to calibration of the South American Land Mammal Ages. Left image for each tuff is the remaining bulk material after picking zircons for annealing; right image for each tuff is remaining annealed zircons after removing c. 10-20 zircons for analysis. For the Rosado and La Cancha tuffs, nearly all zircons were picked from the bulk separate, so few or none occur in the bulk separate image. All images are at the same magnification, indicated by the scale for the Rosado Tuff annealed zircons.

REFERENCES CITED

Condon, D., Schoene, B., Bowring, S., Parrish, R., McLean, N., Noble, S., Crowley, Q., and Anonymous, 2007, EARTHTIME; isotopic tracers and optimized solutions for high-precision U-Pb ID-TIMS geochronology: Eos, Transactions, American Geophysical Union, v. 88, no. 52, Suppl., p. Abstract V41E-06.

Davydov, V. I., Crowley, J. L., Schmitz, M. D., and Poletaev, V. I., 2010, High-precision U-Pb zircon age calibration of the global Carboniferous time scale and Milankovitch-band cyclicity in the Donets Basin, eastern Ukraine: Geochemistry, Geophysics, Geosystems, p. 10.1029/2009GC002736.

Jaffey, A.H., Flynn, K.F., Glendenin, L.E., Bentley, W.C., and Essling, A.M., 1971, Precision measurement of half-lives and specific activities of ^{235}U and ^{238}U: Physical Review C, v. 4, p. 1889–1906.

Kramarz, A. G., and Bond, M., 2010, Colhuehuapian Astrapotheriidae (Mammalia) from Gran Barranca south of Lake Colhue Huapi, *in* Madden, R.H., Carlini, A.A., Vucetich, M.G., and Kay, R.F., *eds.,* The Paleontology of Gran Barranca: Evolution and Environmental Change through the Middle Cenozoic of Patagonia: Cambridge, UK, Cambridge University Press, p. 182–192.

Ludwig, K. R., 2003, User's Manual for Isoplot 3.00. , Berkeley, CA, Berkeley Geochronology Center, 70 p.

Mattinson, J. M., 2005, Zircon U-Pb chemical abrasion ("CA-TIMS") method: combined annealing and multi-step partial dissolution analysis for improved precision and accuracy of zircon ages: Chemical Geology, v. 220, p. 47-66.

Schmitz, M.D., and Schoene, B., 2007, Derivation of isotope ratios, errors and error correlations for U-Pb geochronology using ^{205}Pb-^{235}U-(^{233}U)-spiked isotope dilution thermal ionization mass spectrometric data: Geochemistry, Geophysics, Geosystems, v. 8, p. 1–20.

Appendix 2. Supplemental Data for Chapter III

Table A2.1. Burke Specimen Numbers

Species	Plant ID	Treatment	WTU Herb. #
CC	CC-01	120	389838
CC	CC-02	20	389839
CC	CC-03	60	389840
CC	CC-04	100	389841
CC	CC-05	100	389842
CC	CC-06	20	389843
CC	CC-07	20	389844
CC	CC-08	120	389845
CC	CC-09	60	389846
CC	CC-10	60	389847
CC	CC-11	100	389848
CC	CC-12	20	389849
CC	CC-13	100	389850
CC	CC-14	120	389851
CC	CC-15	60	389852
CC	CC-16	60	389853
CC	CC-17	100	389854
CC	CC-18	120	389855
CC	CC-22	120	389859
CC	CC-30	20	389868
PS	PS-01	20	390161
PS	PS-02	120	390162
PS	PS-03	120	390163
PS	PS-04	60	390164
PS	PS-05	100	390165
PS	PS-06	100	390166
PS	PS-07	60	390167
PS	PS-08	100	390168
PS	PS-10	20	390169
PS	PS-11	120	390170
PS	PS-12	20	390171
PS	PS-13	100	390172
PS	PS-14	60	390173
PS	PS-15	100	390174
PS	PS-16	120	389449
PS	PS-17	60	390175
PS	PS-18	20	390176
PS	PS-19	120	390177
PS	PS-25	20	390178
PS	PS-26	60	390179
SA	SA-01	20	390180
SA	SA-02	20	390272
SA	SA-03	100	392073
SA	SA-04	100	390274
SA	SA-05	120	390275
SA	SA-06	120	393856
SA	SA-07	120	390276

Species	Plant ID	Treatment	WTU Herb. #
SA	SA-09	100	390277
SA	SA-10	60	390278
SA	SA-11	20	390279
SA	SA-12	60	390280
SA	SA-13	20	390281
SA	SA-14	120	390282
SA	SA-15	100	390283
SA	SA-16	120	390284
SA	SA-17	100	390285
SA	SA-18	20	390286
SA	SA-19	60	390287
SA	SA-24	60	390288
SA	SA-32	60	390289
SS	SS-01	120	393802
SS	SS-02	100	393803
SS	SS-03	120	393804
SS	SS-04	120	393805
SS	SS-05	60	393806
SS	SS-07	100	393808
SS	SS-08	100	393809
SS	SS-09	60	393810
SS	SS-10	60	393811
SS	SS-11	20	393812
SS	SS-13	100	393813
SS	SS-14	60	393814
SS	SS-15	60	393815
SS	SS-16	120	393816
SS	SS-18	20	393818
SS	SS-19	100	393819
SS	SS-20	20	393820
SS	SS-21	120	393821
SS	SS-22	20	393822
SS	SS-32	20	393831
SV	SV-01	120	393836
SV	SV-02	100	393837
SV	SV-03	20	393838
SV	SV-04	120	393839
SV	SV-05	20	393840
SV	SV-06	60	393841
SV	SV-07	100	393842
SV	SV-08	60	393843
SV	SV-09	60	393844
SV	SV-10	100	393845
SV	SV-11	60	393846
SV	SV-12	100	393847
SV	SV-13	120	393848
SV	SV-14	120	393849
SV	SV-15	60	393850
SV	SV-16	120	393851
SV	SV-17	20	393852
SV	SV-18	20	393853
SV	SV-20	100	393854
SV	SV-27	20	393855

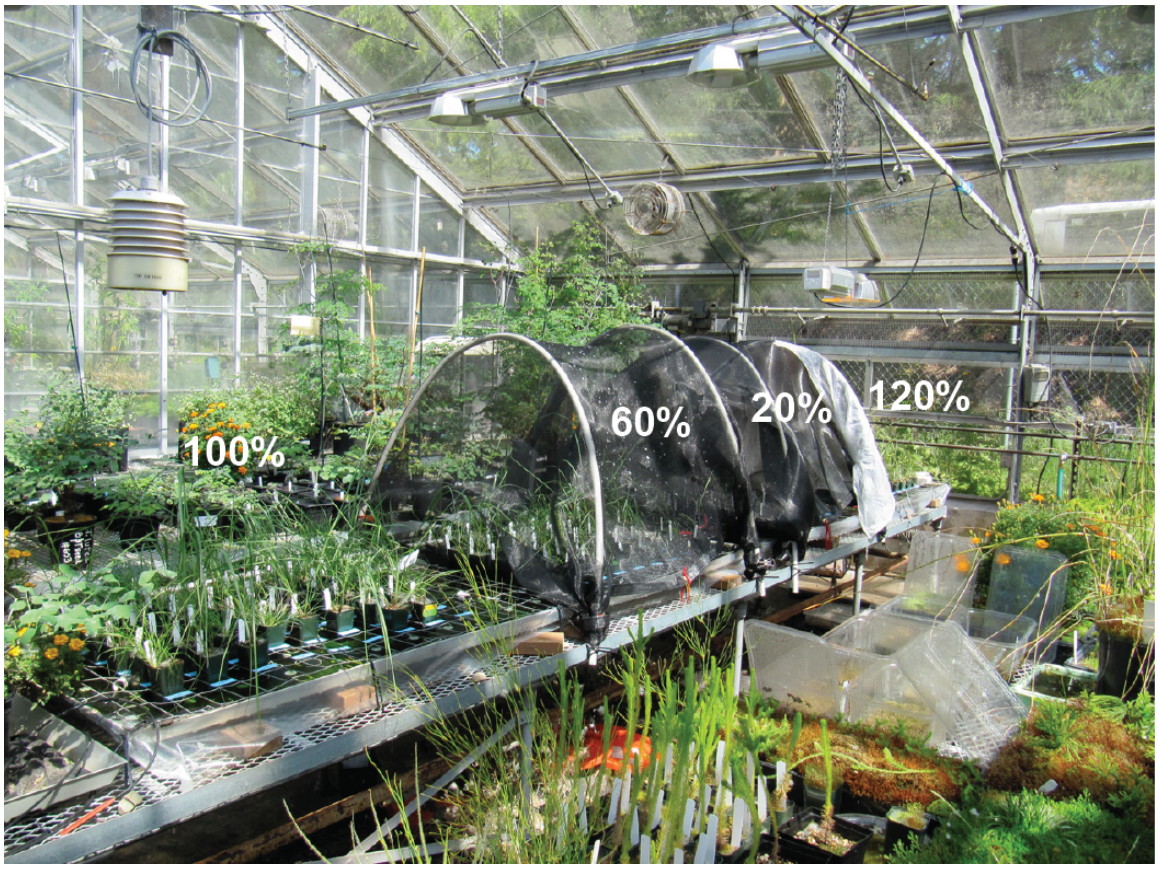

Figure A2.1. Picture of set up for growth experiment conducted in University of Washington Botany Greenhouse. Grasses growing under light treatments from left to right, 100% (control), 60%, 20%, 120% treatment with 400 watt high pressure sodium lamp. Grasses grown in 2.5" pots and placed in randomized grid within treatments.

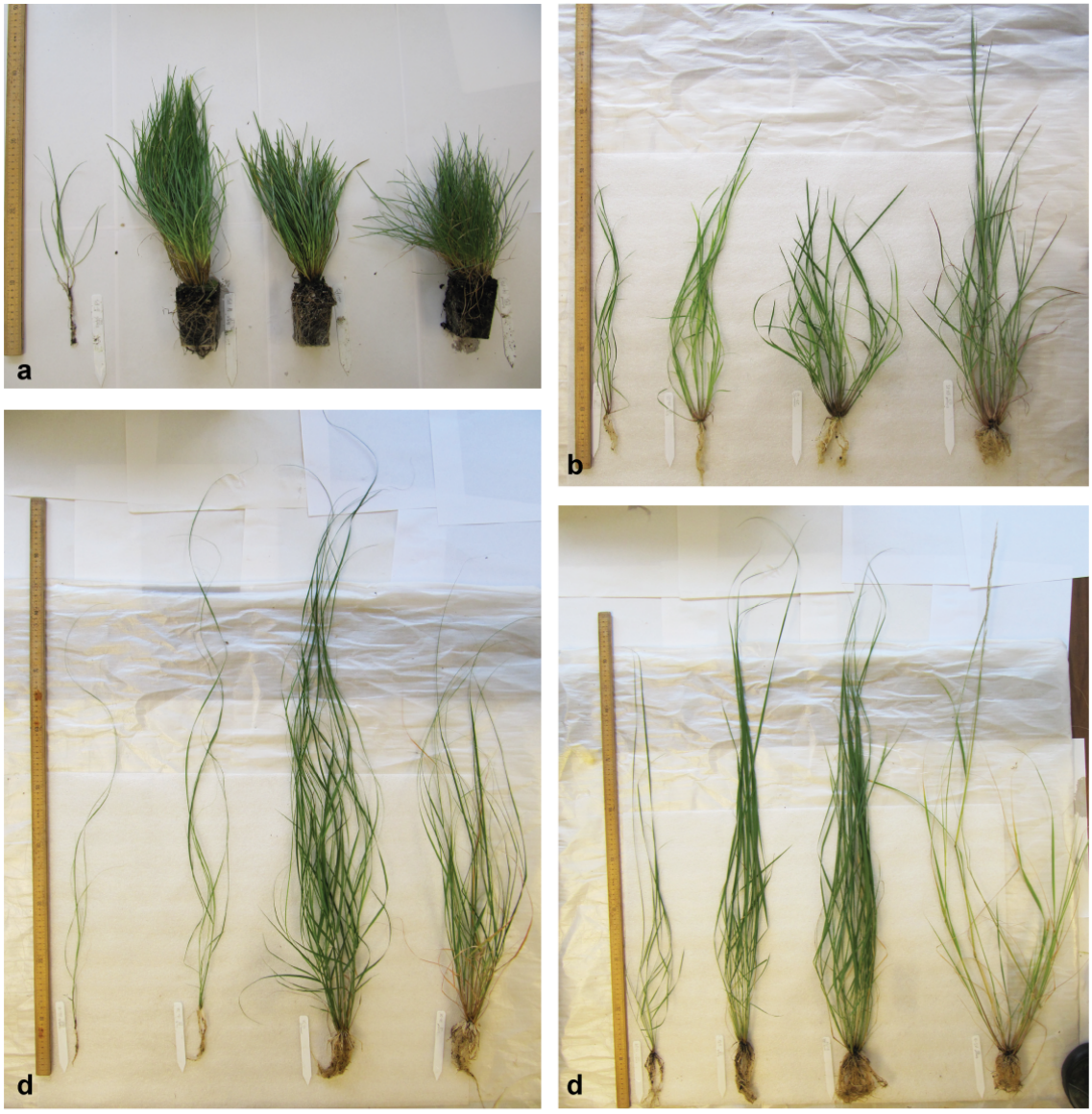

Figure A2.2. Example of grasses grown in shade treatments post-harvest; a) *Poa secunda*; b) *Schizachurium scoparium*; c) *Sporobolus asper*; d) *Stipa viridula*. From left to right in photographs treatment order is 20, 60, 100, 120% light treatments.

Appendix 3. Supplementary Data for Chapter IV

Table A3.1. Summary Data for Costa Rica soil samples.

Site No.	UWBM No.	Veg. type	Sample size	LAI 5[1]	Mean Area (um^2)	Area SD[2]	Area 95% CI[3]	Mean UI[4]	UI SD	UI 95% CI
RD001	PR08581	wet	54	2.95	367.84	342.41	91.33	1.44	0.14	0.04
RD007	PR08582	wet	74	3.88	258.14	281.77	64.20	1.40	0.14	0.03
RD008	PR08583	wet	65	2.79	781.74	494.18	120.14	1.44	0.18	0.04
RD010	PR08584	wet	71	2.37	790.12	419.55	97.59	1.39	0.14	0.03
RD011	PR08585	wet	40	2.73	874.80	586.95	181.89	1.43	0.13	0.04
RD013	PR08586	wet	42	2.75	924.08	758.48	229.39	1.44	0.15	0.05
RD014	PR08587	wet	31	2.53	628.09	311.33	109.60	1.51	0.22	0.08
RD016	PR08588	wet	36	3.09	1143.69	781.93	248.61	1.43	0.15	0.05
RD017	PR08589	wet	57	3.15	614.40	265.87	69.02	1.48	0.19	0.05
RD021	PR08590	wet	33	2.39	702.57	523.90	176.10	1.44	0.16	0.05
RD024	PR08591	wet	36	1.66	940.55	413.80	135.17	1.39	0.13	0.04
RD028	PR08592	wet	34	3.77	925.32	463.25	155.71	1.42	0.13	0.04
RD029	PR08593	wet	76	3.29	354.99	502.65	113.01	1.43	0.14	0.03
RD031	PR08594	wet	66	2.79	846.74	856.00	206.52	1.46	0.15	0.04
RD036	PR08595	wet	32	4.78	1330.47	1632.34	565.57	1.52	0.26	0.09
RD058	PR08596	wet	45	3.67	55.98	305.86	89.36	1.47	0.14	0.04
RD066	PR08597	wet	33	2.44	945.50	421.88	143.94	1.48	0.15	0.05
RD085	PR08598	wet	49	2.74	575.90	310.09	86.82	1.47	0.12	0.03
RD087	PR08599	wet	30	3.38	819.50	365.11	130.65	1.50	0.13	0.05
RD089	PR08600	dry	48	3.96	978.30	391.85	110.85	1.47	0.17	0.05
RD090	PR08601	dry	42	3.16	931.32	552.21	167.00	1.47	0.17	0.05
RD091	PR08602	dry	60	4.25	859.84	434.79	129.96	1.48	0.16	0.05
RD093	PR08603	dry	32	3.65	1026.69	395.75	139.31	1.46	0.16	0.05
RD096	PR08604	dry	40	2.98	733.63	364.73	113.03	1.50	0.17	0.05
RD099	PR08605	dry	30	3.35	785.28	292.74	104.76	1.47	0.17	0.06
RD100	PR08606	dry	47	2.84	1020.60	451.62	129.11	1.50	0.20	0.06
RD102	PR08607	dry	54	0.16	293.78	155.81	41.56	1.34	0.13	0.04
RD106	PR08608	dry	52	0.65	288.54	165.47	44.97	1.35	0.15	0.04
RD107	PR08609	dry	25	1.06	436.71	233.35	95.36	1.34	0.09	0.04
RD127	PR08610	dry	50	1.29	497.97	717.47	198.87	1.36	0.14	0.04
RD129	PR08611	dry	57	1.74	549.24	411.05	106.71	1.34	0.11	0.03
RD130	PR08612	dry	40	1.71	718.50	552.97	171.36	1.37	0.10	0.03
RD131	PR08613	dry	38	0.73	282.56	240.76	76.55	1.38	0.14	0.05
RD132	PR08614	dry	25	1.53	642.34	273.77	111.89	1.40	0.15	0.06
RD136	PR08615	dry	30	1.54	91.92	352.23	126.04	1.36	0.15	0.05
RD138	PR08616	dry	40	1.04	304.95	231.55	71.76	1.33	0.12	0.04
RD145	PR08617	dry	25	2.16	767.20	301.24	120.52	1.29	0.08	0.03
RD146	PR08618	dry	68	0.34	64.88	185.44	44.08	1.33	0.12	0.03
RD149	PR08619	montane	37	1.98	744.34	405.49	132.46	1.41	0.17	0.05
RD160	PR08620	montane	31	2.56	14.98	304.38	107.15	1.33	0.10	0.04
RD162	PR08621	montane	25	2.47	433.84	288.86	113.23	1.41	0.16	0.06
RD174	PR08622	montane	63	0.33	229.63	222.40	54.92	1.34	0.15	0.04
RD177	PR08623	montane	64	0.58	274.84	230.45	56.46	1.35	0.14	0.03
RD178	PR08624	montane	68	1.27	178.11	140.75	33.45	1.28	0.14	0.03
RD180	PR08625	montane	34	1.19	268.66	170.29	57.24	1.35	0.12	0.04

Notes: [1]LAI 5 = LAI calculated using 0-75° zenith angle, [2]SD=Standard Deviation, [3]95% Confidence Interval, [4]UI = Undulation Index (see Methods section below).

Table A3.2. Fossil sample data summary.

Sample No.	Stratum (Fm./Site)	Age (Ma)	Sample size	Mean PUI	Mean Area (um^2)	rLAI	Lower 95% PI[1]	Upper 95% PI[2]	Age Reference
ARG11-039	Río Mayo	11.78	47	1.39	679.32	2.16	0.74	3.58	Madden Pers Comm.
ARG12-105	Río Negro	13.40	16	1.32	1348.00	2.27	0.55	4.00	Kohn Pers Comm
ARG12-090	Collon Cura	13.70	37	1.35	754.00	1.76	0.30	3.23	Kohn Pers Comm
ARG12-088	Collon Cura	13.90	42	1.37	1325.31	2.67	1.04	4.31	Kohn Pers Comm
ARG12-083	Collon Cura	14.00	66	1.33	646.24	1.43	-0.03	2.90	Kohn Pers Comm
ARG12-079	Collon Cura	14.60	48	1.47	1155.49	3.53	2.06	5.00	Kohn Pers Comm
CHL11-001	Collon Cura	16.00	47	1.37	1099.00	2.46	0.93	3.99	Madden Pers. Comm
ARG09-065 (SGB09-281)	CH	20.36	85	1.36	735.00	1.91	0.46	3.35	Dunn et al., 2013
ARG09-051 (SGB09-275)	CH	20.89	49	1.35	690.00	1.74	0.29	3.19	Dunn et al., 2013
ARG10-001	CH	20.98	101	1.26	397.72	0.48	-1.04	1.99	Dunn et al., 2013
ARG10-003	CH	20.98	33	1.25	398.74	0.38	-1.14	1.91	Dunn et al., 2013
ARG10-005	CH	20.98	31	1.42	644.61	2.40	0.98	3.82	Dunn et al., 2013
ARG10-102	UPA	22.84	25	1.31	527.00	1.10	-0.37	2.57	Dunn et al., 2013
ARG09-027 (SGB09-224)	UPA	23.13	51	1.35	996.39	2.07	0.54	3.60	Dunn et al., 2013
ARG09-023 (SGB09-212)	UPA	23.45	65	1.28	782.87	1.08	-0.49	2.66	Dunn et al., 2013
ARG11-042	La Flecha	24.10	34	1.38	552.55	1.85	0.43	3.28	Schimtz pers comm
ARG09-006-SGB09-093	UPA	30.77	42	1.28	911.00	1.26	-0.36	2.88	Dunn et al., 2013
ARG09-054 (SGB09-172)	Vera	33.27	59	1.28	429.46	0.71	-0.78	2.20	Dunn et al., 2013
ARG09-184 (SGB09-136)	Vera	35.06	34	1.27	438.05	0.61	-0.90	2.11	Dunn et al., 2013
ARG10-094	LPA	36.80	33	1.32	916.00	1.66	0.11	3.21	Dunn et al., 2013
SGB09-315	LPA	37.41	68	1.31	973.00	1.71	0.14	3.28	Dunn et al., 2013
ARG09-029 (SGB09-292)	LPA	37.80	75	1.28	606.00	0.90	-0.63	2.42	Dunn et al., 2013
ARG09-021 (SGB09-117)	Rosado	38.00	47	1.21	553.43	0.17	-1.46	1.79	Dunn et al., 2013
ARG09-119 (SGB09-085)	Rosado	38.03	55	1.27	520.00	0.73	-0.79	2.24	Dunn et al., 2013
ARG09-007 (SGB09-105)	Rosado	38.10	41	1.26	483.00	0.52	-1.02	2.05	Dunn et al., 2013
ARG09-? (SGB09-325)	Gran Barranca	39.06	82	1.35	653.00	1.66	0.22	3.11	Dunn et al., 2013
ARG09-015 (SGB09-324)	Gran Barranca	39.06	87	1.30	650.00	1.17	-0.33	2.67	Dunn et al., 2013
ARG09-073 (SGB09-004)	Gran Barranca	39.86	67	1.27	656.00	0.86	-0.69	2.41	Dunn et al., 2013
ARG09-026 (SGB09-169)	Gran Barranca	39.86	50	1.29	635.00	1.05	-0.47	2.56	Dunn et al., 2013
ARG09-171 (SGB09-119)	Gran Barranca	39.86	64	1.36	776.00	1.97	0.52	3.42	Dunn et al., 2013
ARG09-076 (SGB09-120)	Gran Barranca	39.86	52	1.35	606.00	1.64	0.20	3.08	Dunn et al., 2013
ARG09-107-SGB09-041	Gran Barranca	39.86	28	1.40	1146.00	2.83	1.32	4.34	Dunn et al., 2013

ARG10-164	Gran Barranca	39.80	55	1.38	642.04	1.99	0.57	3.42	Dunn et al., 2013
ARG10-107	Gran Barranca	41.80	59	1.33	580.00	1.39	-0.07	2.84	Dunn et al., 2013
ARG10-108	Koluel-Kaike	44.00	60	1.39	679.00	2.16	0.74	3.58	Ré et al, 2010
ARG09-017 (SGB09-017)	Koluel-Kaike	44.00	66	1.44	713.60	2.67	1.25	4.09	Ré et al, 2010
ARG09-012 (SGB09-016)	Koluel-Kaike	44.10	73	1.43	1185.65	1.72	0.01	3.44	Ré et al, 2010
ARG10-178	Las Flores	48.90	66	1.39	1006.00	2.65	1.16	4.14	Kohn Pers Comm
ARG10-176	Las Flores	49.00	57	1.45	1655.00	3.96	2.28	5.64	Kohn Pers Comm
ARG10-173	Las Flores	49.10	65	1.38	1306.00	2.79	1.19	4.40	Kohn Pers Comm
ARG10-171	Las Flores	49.10	78	1.42	1537.29	3.51	1.86	5.17	Kohn Pers Comm

Notes:[1]Lower 95% Prediction Interval, [2]Upper 95% Prediction Interval.

METHODS

Over 200 samples of soil were collected from several locations in protected areas in Costa Rica where land use histories are known including OTS (Organization for Tropical Studies) sites La Selva and Parque Nacional Palo Verde, and sites within the Area de Conservación de Guanacaste including Parque Nacional Santa Rosa, Guanacaste, (Sector Cerro la Hacha), Rincón de la Vieja (Sector Las Pailas), and Puesto San Cristobol. Wet tropical forest soils were collected from La Selva, dry tropical forest soils from Santa Rosa, Guanacaste and Palo Verde, flooded forest soils from Palo Verde, and submontane forest samples from Rincon de la Vieja and Puesto San Cristobal (Fig. A3.1, Table A3.1).

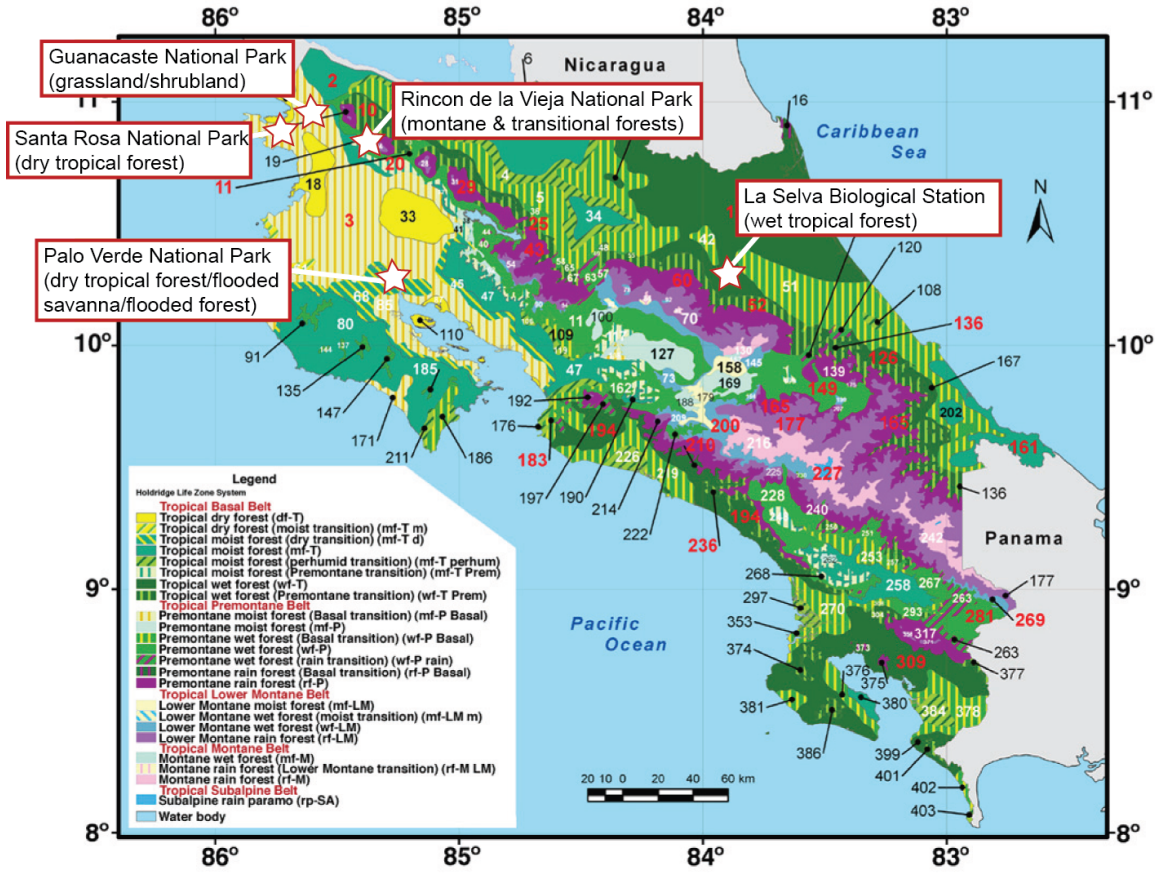

Figure A3.1. Map of sampling areas in Costa Rica along with Holdridge Life Zones. Modified from Kohlmann et al., 2010.

Sample sites were selected from undisturbed areas. Leaf litter was cleared from the sample sites and the top 1 cm of soil from a 10 x 10 cm area was collected. The resulting collection measured 250 ml in volume. For each collection site, hemispherical photographs were taken using a Nikon CoolPix 4500 camera with attached Nikon Fisheye Converter GC-E8 0.21x lens from a tripod 1 m from the ground. Sampling took place during cloudy days, or in mornings and evenings when the sun was not directly overhead and photographs were taken using the optimum exposure for each site (*1*). Effective Leaf Area Index (L_e) and % canopy openness were measured from the

photographs using Gap Light Analyzer (GLA), Version 2.0 imaging software (*2*) L_e is the product of L (the measured LAI) and Ω which is a clumping index resulting from the non-random distribution of element spatial positions such as needles on coniferous trees (*3*). For broad-leaved forests like those sampled in this study, clumping is less of concern and L_e is considered similar to L. Percent canopy openness is the percentage of open sky seen from beneath a forest canopy, which does not include the influence of surrounding topography, and LAI Ring 5 which is the effective leaf area index integrated over the zenith angle of 0-75°.

Soil samples were manually homogenized and 1 gram was measured for processing. Extraction of phytoliths was done using standard methods of (*4*) which involves carbonate removal using concentrated HCl, humic acid removal using a 10% KOH solution, organic removal using Schultzy's Solution (KCl+Nitric Acid) and removal of oxides with strong acid (equal parts of HCl and HNO_3). Sieving removed particles over 250 um in diameter, and a finer sieve (56 um diameter) was used to mechanically break up clays though all size fractions under 250 um were maintained as one sample. Heavy liquid extraction using zinc bromide.

For slide preparation, a subset of the sample was mounted on a slide and fixed in Cargille MeltMount™. Slides were scanned in their entirety at 400x magnification and the targeted epidermal phytoliths were located and photographed along slide transects. Measurements of cell area and perimeter were made using Adobe Photoshop Extended Version CS5. The Quick Selection Tool was used to outline the cell perimeters, and the relevant measurements of area and perimeter were recorded. In samples were epidermal phytoliths were rare, multiple slides were made to get at least 30 cells per sample.

There exists some overlap between wide grass long cells and those considered anticlinal epidermis of non-grass plants. Grass long cells were distinguished from other anticlinals by being two-thirds longer than wide and having an absence of undulations, or blunt ends on the short axis.

Undulation was quantified for each anticlinal phytolith using a unitless measure, the Undulation Index (UI) (*5*). UI is calculated as the circumference of the cell (Ce) divided by the circumference of a circle with the same area (Ae) as the cell (Co).

$$UI = \frac{Ce}{Co} = \frac{Ce}{2\pi\sqrt{\frac{Ae}{\pi}}}$$

Quantitative Analyses of Phytoliths-All analyses were done using R version 2.8.1 (*6*). For each site, mean phytolith undulation index (PUI) and phytolith area were calculated. The minimum sample size was determined to be 25 phytoliths/sample through bootstapping. Mean PUI and phytolith area for each sample were compared to L_e for each site using linear regressions. To develop a statistical model for predicting LAI, a multiple regression including both mean PUI and mean area was performed (mean PUI + Mean Area).

Calculating Errors of rLAI Estimates-The calculation of 95% prediction intervals (PI) follows Sokal and Rohlf (*7*).

Study Sites-

La Selva Biological Station, Heredia, Costa Rica (10°26'N, 83°59'W), elevation 35-137 m. Holdridge zone: Wet forest (evergreen forest of the Atlantic lowlands). Annual rainfall exceeds 2000 mm/year with an average of ~4000 mm/year. No month receives less than 100 mm ppt (*8*). Rainy season is June-July, and Nov-Dec (>400 mm per month). MAT ~26 °C (*8*). Mean Annual Daily temperatures between 18 and 24°C. Daily range in temperature is 6-12°C. August high temp is 27.1°C, Coolest in January 24.7°C. Forest canopies at La Selva are (like many old growth sites) a complicated mosaic of patches of different disturbance histories and canopy heights. Trees are the most important functional group (LAI 3.29) followed by palms (1.33) and lianas (0.73). Epiphytes, ferns and herbs account for only 11% of the total LAI. LAI values for tall forest sites do not differ from the dry season to the wet season, so LAI is constant throughout the year in this type of forest. Overall landscape LAI has been measured through destructive sampling as 6.00 +/- 0.32. Of that, trees, palms and lianas account for 89% of the total, and trees and lianas were 95% of the upper canopy (*9*)(Clark et al, 2008).

Area Conservacion de Guanacaste-NW Costa Rica

***Parque Nacional Santa Rosa* -** Holdridge Life Zone: semi-deciduous dry tropical forest. Elevation ~300m. Rainfall is seasonal, between April and November, averaging 1614 mm/year but ranging from 915 to 2558 mm/year with a pronounced dry season of 6-months with little to no precipitation (*10*). Mean annual temperature is 27°C with a range of 10°C. Warm month mean of temperature is ~33°C, and cold month mean is 21°C. Average temperatures vary between 32-36 °C (*11*). Dominant taxa in the area include *Quercus oleoides*, *Hymenaea courbail*, and *Manilkara zapota* and which are not synchronously deciduous (*10*). Samples were collected from early, intermediate and late stage successional plots (*12*). Early successional plots consisted of 1 canopy layer ~ 6 m average height, with many deciduous dicotyledonous taxa, shrubs and grasses. Intermediate successional plots consisted of 2 canopy layers averaging 10 m in height. These floras are dominated by fast growing deciduous species, lianas and shade tolerant species. Late successional floras have 2 layers of canopy averaging 30 m in height. They are dominated by evergreen species with an overlapping canopy in the Bosque Humedo. Maximum leaf fall occurs in April at the end of the dry season and maximal LAI values occur in November, though not all species shed their leaves entirely or at the same time. The change in leaf area index between the dry season and wet season is ~40% of the total. Our study was carried out in July when the forest had a continuous cover of leaves (*13*). Leaf litter studies indicate that the dominant and subdominant tree species and lianas are the most commonly represented taxa in forest leaf litter (*10*).

Parque Nacional Rincon de la Vieja is an active volcano and several of the Holdridge life zones can be found along its altitudinal gradient including tropical moist forest, premontane wet forest, premontane rain forest, and lower montane rain forest. Samples were collected on an elevational transect from 800 m -1500 m following

the Rio Colorado up the south slope of Rincon de la Vieja. Soils were also collected at ~800 m elevation around volcanic hot springs of the Sector Las Pailas.

Corredor Biológico Rincón Puesto San Cristobol - Lower montane and premontane wet forest corredor connecting Pacific and Atlantic forest.

Parque Nacional Guanacaste - Sector Cerro El Hacha - Open savanna with grasses and low shrubs growing on relict volcanic topography. The dominant grass is *Axonopus*. Managed as part of the Area de Conservación de Guanacaste.

LITERATURE CITED

1. Y. Zhang, J. M. Chen, J. R. Miller, Determining digital hemispherical photograph exposure for leaf area index estimation, *Agricultural and Forest Meteorology* **133**, 166–181 (2005).

2. G. Frazer, C. Canham, K. Lertzman, Gap Light Analyzer (GLA), Version 2.0: Imaging software to extract canopy structure and gap light transmission indices from true-colour fisheye photographs, users manual and program documentation, *Simon Fraser University,* (1999) (available at http://rem.sfu.ca/forestry/downloads/Files/GLAV2UsersManual.pdf).

3. J. M. Chen, T. a. Black, R. S. Adams, Evaluation of hemispherical photography for determining plant area index and geometry of a forest stand, *Agricultural and Forest Meteorology* **56**, 129–143 (1991).

4. D. R. Piperno, *Phytoliths: a comprehensive guide for archaeologists and paleoecologists* (AltaMira Press, New York, USA).

5. W. M. Kurschner, The anatomical diversity of recent and fossil leaves of the durmast oak (*Quercus petraea* Lieblein / *Q. pseudocastanea* Goeppert) - implications for their use as biosensors of palaeoatmospheric CO2 levels, *Review of Palaeobotany and Palynology* **96**, 1–30 (1997).

6. R Development Core Team (2008). R: A language and environment for statistical computing. R Foundation for Statistical Computing, Vienna, Austria. ISBN 3-900051-07-0, URL http://www.R-project.org.

7. R. Sokal, F. Rohlf, *Biometry* W. H. Freeman, Ed. (New York, ed. 3rd, 1995).

8. R. L. Sanford Jr, P. Paaby, J. C. Luvall, E. Phillips, Climate, geomorphology, and aquatic systems, *La Selva: ecology and natural history of a neotropical rain forest.* University of Chicago Press, Chicago, Illinois*, USA* , 19–33 (1994).

9. D. B. Clark, P. C. Olivas, S. F. Oberbauer, D. a Clark, M. G. Ryan, First direct landscape-scale measurement of tropical rain forest Leaf Area Index, a key driver of global primary productivity, *Ecology letters* **11**, 163–72 (2008).

10. R. Burnham, Stand Characteristics and Leaf Litter Composition of a Dry Forest Hectare in Santa Rosa National Park, Costa Rica, *Biotropica* **29**, 384–395 (2006).

11. D. Janzen, in *Caterpillars: Ecological and evolutionary constraints on foraging*, N. E. Stamp, T. M. Casey, Eds. (Chapman and Hall, New York, USA, 1993), pp. 448–477.

12. M. Kalácska *et al.*, Species composition, similarity and diversity in three successional stages of a seasonally dry tropical forest, *Forest Ecology and Management* **200**, 227–247 (2004).

13. M. Kalácska, J. C. Calvo-Alvarado, G. a Sánchez-Azofeifa, Calibration and assessment of seasonal changes in leaf area index of a tropical dry forest in different stages of succession, *Tree physiology* **25**, 733–44 (2005).